1998

Using the method of characteristics to predict transient flow phenomena

Richard Strunz
San Jose State University

INFORMATION TO USERS

This manuscript has been reproduced from the microfilm master. UMI films the text directly from the original or copy submitted. Thus, some thesis and dissertation copies are in typewriter face, while others may be from any type of computer printer.

The quality of this reproduction is dependent upon the quality of the copy submitted. Broken or indistinct print, colored or poor quality illustrations and photographs, print bleedthrough, substandard margins, and improper alignment can adversely affect reproduction.

In the unlikely event that the author did not send UMI a complete manuscript and there are missing pages, these will be noted. Also, if unauthorized copyright material had to be removed, a note will indicate the deletion.

Oversize materials (e.g., maps, drawings, charts) are reproduced by sectioning the original, beginning at the upper left-hand corner and continuing from left to right in equal sections with small overlaps. Each original is also photographed in one exposure and is included in reduced form at the back of the book.

Photographs included in the original manuscript have been reproduced xerographically in this copy. Higher quality 6" x 9" black and white photographic prints are available for any photographs or illustrations appearing in this copy for an additional charge. Contact UMI directly to order.

UMI

A Bell & Howell Information Company
300 North Zeeb Road, Ann Arbor MI 48106-1346 USA
313/761-4700 800/521-0600

Using the Method of Characteristics to Predict Transient Flow Phenomena

A Thesis

Presented to

The Faculty of the Department of Mechanical and Aerospace Engineering

San José State University

In Partial Fulfillment

Of the Requirements for the Degree

Master of Science

By

Richard Strunz

May, 1998

Thesis approved for the Department of Mechanical and Aerospace Engineering

F. J. Moody Date April 13, 1998

Dr. F.J. Moody, Thesis Advisor and Chairperson
General Electric, San José, California
SJSU, Department of Mechanical and Aerospace Engineering

Jose Maddren Date 4/13/98

Dr. J. Maddren, Reading Committee Member
SJSU, Department of Mechanical and Aerospace Engineering

Henry J. Pernicka Date 4/13/98

Dr. H.J. Pernicka, Reading Committee Member
SJSU, Department of Mechanical and Aerospace Engineering

APPROVED FOR THE UNIVERSITY

William Fisher Date 30 April 1998

Abstract

Using the Method of Characteristics
to Predict Transient Flow Phenomena

by Richard Strunz

Transient mass flows during the start-up phase of a rocket engine is studied, rocket instabilities explained, and preliminary thoughts for a computer program given for the prediction of the propellant mass flows at ignition. The analysis was done using the Method of Characteristics and applying the one-dimensional equilibrium thermochemistry code for a simplified combustion model. This work is the extension of the diploma thesis *Erstellung eines Fortran77-Programmes zur Simulation des Anfahrverhaltens eines Raketentriebwerks* of Daimler Benz Aerospace.

Acknowledgments

My special appreciation is devoted to my adviser Dr. F. J. Moody from whom I received abundant help, encouragement, and many suggestions. He kept my enthusiasm and inspiration alive so that I could accomplish the task. I also would like to mention Marianne Walker, who edited the work as well as Dr. H. Pernicka, who believed in me and gave me the opportunity to study at San José State University.

Finally, I would like to say thanks to Kai Eckert and Olivier de Bonn, who provided me with data of the rocket engine. It was also the lecture of Prof. Dr. A. Staudt at Fachhochschule Munich, who initiated my interest in thermodynamics and propulsion systems.

Richard Strunz, April 1998

Table of Contents

List of Figures

List of Tables

Nomenclature

A	Flow section area
A_t	Nozzle throat area
a,c	Speed of sound
c_F	Thrust coefficient
c^*	Characteristic exhaust velocity
c_p	Specific heat at constant pressure
c_d	Discharge coefficient
d	Pipe diameter
d_h	Hydraulic diameter
e	Specific internal energy
F	Thrust, Force
f_f	Fanning (small) friction factor, relative mass
f	Large friction factor
g	Gravity constant
H	Total enthalpy
h	Static enthalpy
I_{sp}	Vacuum specific Impulse
k	Wall roughness
L_r	Reference length
M	Molar mass
m	Mass
$\dot{m}$	Mass flow
P	Total pressure
p	Static pressure
P_w	Wetted perimeter
P_C	Chamber pressure
q	Heat transfer rate
q^*	Heat transfer rate per unit length
Re	Reynolds Number
T	Total temperature
t	Static temperature
V	Geometric volume
v	Flow velocity
v_p	Propagation velocity
x	Space variable
X	Quality
y	Geodetic height

Δp	Pressure loss
β	Thermal expansivity
Ψ	Total internal energy
κ	Thermal conductivity
μ	Fluid viscosity
π_i	Model coefficients
ρ	Density
τ	Time
τ_p	Propagation time
τ_d	Disturbance time
τ_w	Wall shear stress
υ	Specific volume
Θ	Angle between horizontal axis and flow direction
$\Re$	General gas constant

$( )_g$	Saturated gas
$( )_f$	Saturated liquid
$( )_{fg}$	Vaporization
$( )_{in}$	Inflowing quantity
$( )_{out}$	Outflowing quantity
$( )_{N_2O_4}$	Oxygen
$( )_{MMH}$	Fuel

Chapter 1: Introduction

Chapter one gives a short overview of rocket history and an introduction into rocket development problems.

The birth of rocket science can be attributed to Tsiolkovskii in 1883. He was a Russian teacher and rocket scientist. Two of his famous papers are *Free Space* published in 1883 and *Exploring Space with Devices* published in 1903. In the first paper, he realized that Newton's third law -- action equals reaction -- is the reason why rockets work. His second paper was focused on the theory of flight performance.

It took about another twenty-three years until the American scientist Robert Goddard could realize Tsiolkovskii's thoughts. The first liquid-fueled rocket was launched in Massachusetts on March 22, 1926. During the late '20s, German rocket enthusiasts founded a consortium known as Society for Space Travel (VfR). It was joined by Hermann Oberth and later by Wernher von Braun. In May 1931, the VfR launched a liquid-propelled rocket, which reached a height of 60 m.

At the same time, combustion instabilities were discovered in solid rocket motors as well as in liquid-propelled rocket engines. Engineers have been working on combustion instability since then. However, they could not make any significant progress until the '60s. Even now, combustion instabilities occur in practically all new rocket development programs.

One rocket development program is the European rocket Ariane 5 with its main stage engine *Vulcan* and upper stage engine *Aestus*. Both engines have a tendency towards combustion instability. Combustion instability can cause extreme vibration

forces or extreme heat transfer. The excessive vibration forces can break engine parts, and the heat transfer brings about the destruction of the cooling boundary layer of rocket chambers. The process of combustion in rocket chambers has therefore to be controlled by appropriate designs, cavity rings, and/or chamber dimensions. During the qualification tests of the upper stage engine *Aestus*, it was seen that the mass flow rates of the propellants were one of the significant factors of combustion instability; in particular, the mass flow rate ratio during the start-up phase.

A computer model was written for the upper stage engine *Aestus* at Daimler Benz Aerospace, which covered the transient phenomena using one-dimensional steady state equations. The program can calculate the mass flows at ignition up to a $3-\sigma$ value of about 4 %, even though, it did not include cavitation of the propellants in the injection elements, two-phase mixture flow, and/or a combustion chamber model able to capture moving shocks from the baseplate to the nozzle throat. However, the use of the program is limited because it was adjusted using measurement data. It took about one year to provide a running computer code and another half-year to adjust and validate the program.[25]

The aforementioned *Diploma* thesis plus the thought that more insight to the effect of mass flow rates on combustion instability could be obtained from improved theoretical models which capture the dominant phenomena led to the following objective for this thesis:

Transient mass flows are studied theoretically during the start-up phase of rocket engines using unsteady one-dimensional thermofluid mechanics equations. A simplified combustion model is included to help display the interactions between mass flow ratio, combustion, and system parameters.

Chapter two gives an introduction into rocket technology. It describes the main engine components of rocket engines. The emphasis is on liquid-propelled rockets.

Chapter three covers the development of liquid-propelled rocket engines. It includes different kinds of combustion instability, test facilities, and measurements.

Chapter four describes the test facility in Lampoldshausen, Germany. It also covers basic rules about measurements.

Chapters five and six are the core of this thesis. In these two chapters, the physical phenomena of transient mass flows in pipe systems are described and their mathematical treatment is shown. The filling interval is basically divided into two sections. One of the sections is the pipe system from the test facility tanks to the control valves. The other section is the rocket pipe system, starting from the control valves, via the injection system into the combustion chamber. The first flow section is described using one-dimensional unsteady thermofluid mechanics equations. The second section is governed by one-dimensional, homogeneous two-phase flow unsteady thermofluid mechanics equations.

Chapters seven and eight cover the numerical treatment of the problem. Numerical boundary conditions are defined as well as fundamentals of the numeric are given.

Chapter 2: Rocket Technology

The classification of rockets is described in this chapter to give a basic idea of rocket technology. Main components of rocket propulsion systems are explained, such as the propellant feed system, injection element, and nozzle extension.

2.1 Classification of Rockets

Rockets can be classified by the energy source used. In general, rocket propulsion techniques can be divided into chemical propulsion, nuclear propulsion, and electrical propulsion. The most useful technique is chemical-propelled rockets. The properties of the used propellant or the application of the rockets distinguish this technique into the following classification. Rocket propellants are used in all three phases (solid, liquid, and gaseous). Therefore, the nomenclature for the possible phases is solid-propelled, liquid-propelled, and cold-gaseous-propelled rockets. The three different phases can be used in a mixed form, too. For instance, the combination of the solid phase and the liquid phase is also called hybrid propulsion. The number of propellant types used also classifies rockets. The nomenclatures for more than one propellant are monergole, diergole, and triergole systems. Monergole systems use only liquid or solid propellant. Bipropellant systems consist of two propellants. Tripropellant systems use three different propellants; however, even though bi- and tripropellent have the highest specific impulse, they are not often used because it is a very expensive technology. An

additional classification criterion is the storability of the propellant such as earth-storable and space-storable.

2.2 Main Components of Liquid-Propelled Rockets

Any liquid-propelled rocket propulsion system can be divided into two main components; namely the propellant feed system and the rocket engine. Propellant feed systems can be subdivided into the pressurization system and the propellant tanks. Rocket engines consist of turbo-pumps, main valves, and a thrust chamber. The thrust chamber itself can be subdivided into an injector head, a combustion chamber, and a nozzle extension. Figure 2.1 depicts the definition of the subsystems and components of rocket engines. Figure 2.2 shows the classification of liquid-propelled rocket feed systems.

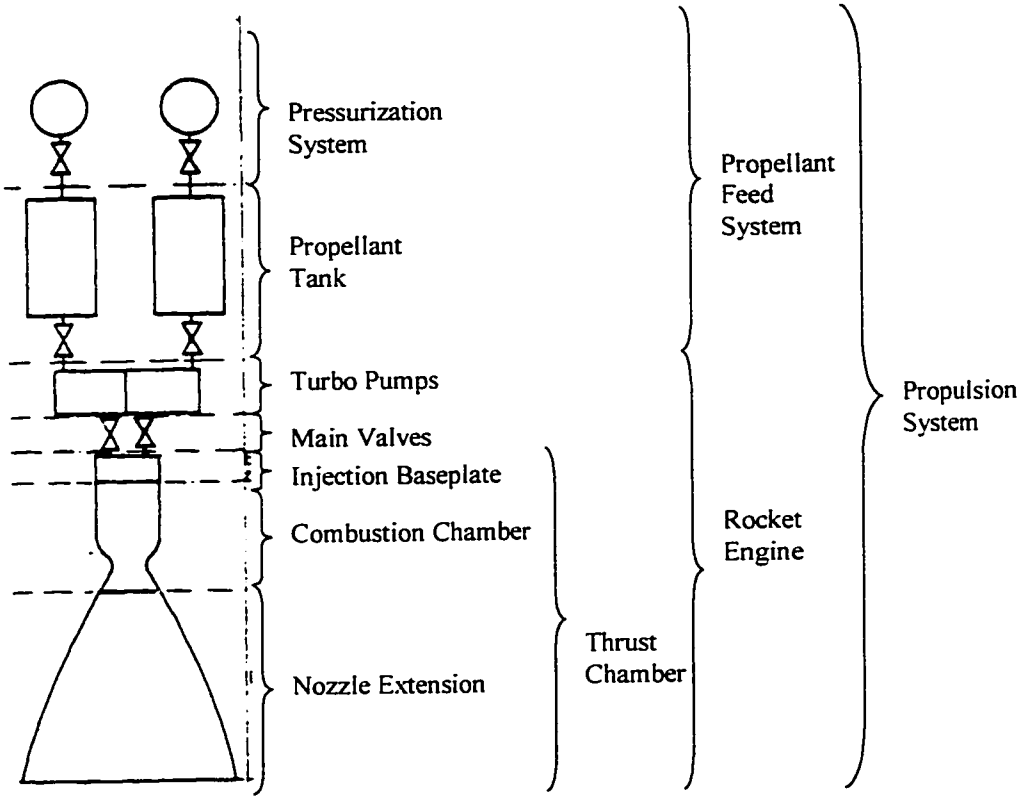

Figure 2.1: Definition of the Subsystems and Components of rocket engines[24]

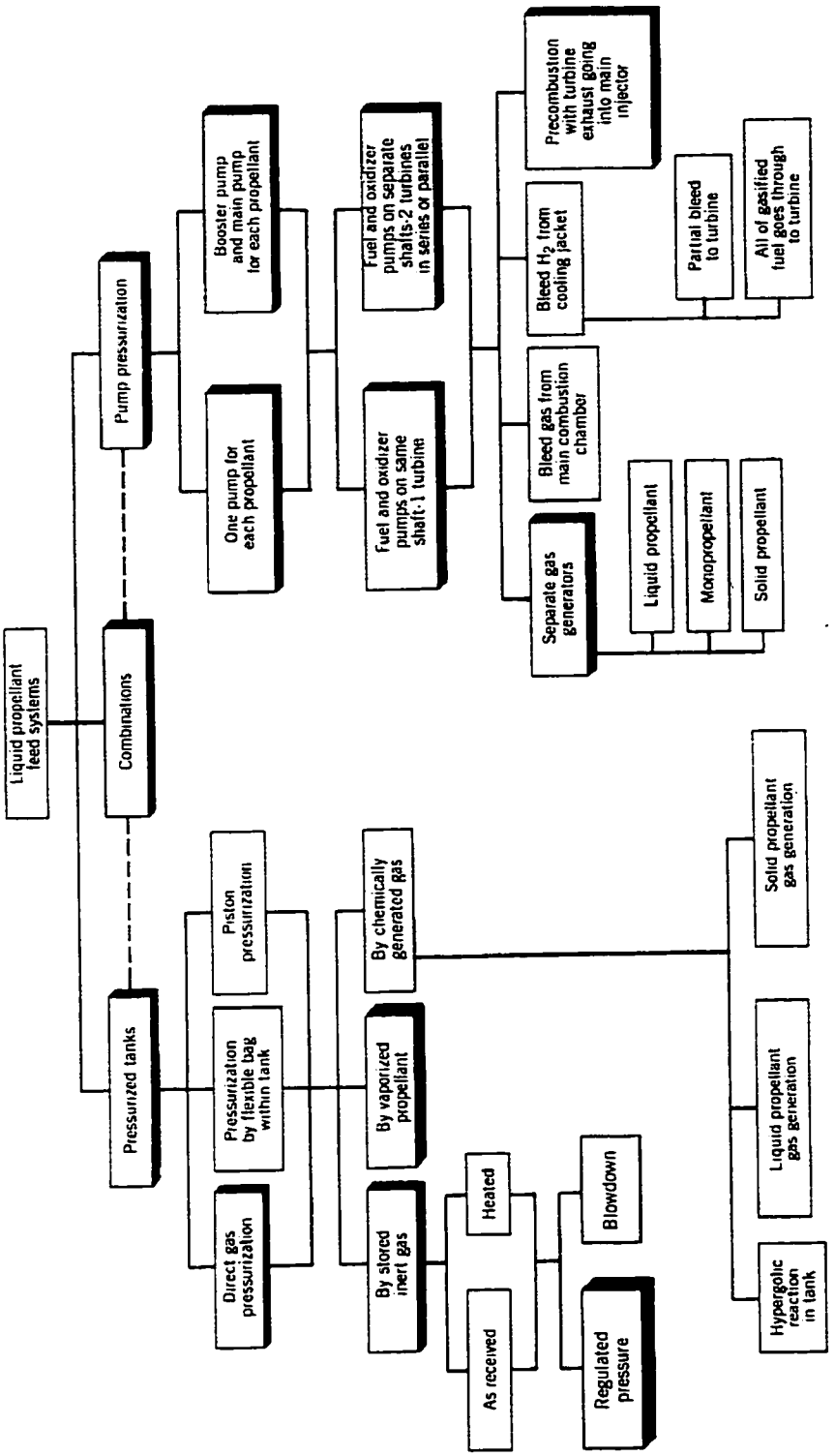

Figure 2.2: Classification of Liquid Propelled Rocket Engines[26]

The main purpose of the propellant system, with the subsystems pressurization system and propellant tank, is to supply the combustion chamber with an appropriate amount of propellant in order to get an optimized combustion. Generally, there are two means of feed systems, namely gas-pressurized and turbo-pump systems. The pressurized systems can be subdivided into cold-gas and hot-gas systems.

The turbo-pump system also provides the combustion chamber with a suitable amount of propellant. Turbo-pump systems can be divided into mainstream or closed cycle and side-stream or open cycles. The mainstream cycles provide a higher specific impulse providing the same chamber pressure because the working fluid from the turbine is injected into the combustion chamber to use the rest of the stored chemical energy of the propellant. In addition, the exhaust-products of the turbine are expanded through the full pressure ratio of the main nozzle whereas the exhaust-products from the turbine of open cycles are expanded through smaller nozzle, providing less thrust and therefore less specific impulse. Figure 2.3 shows the difference between the two cycles.

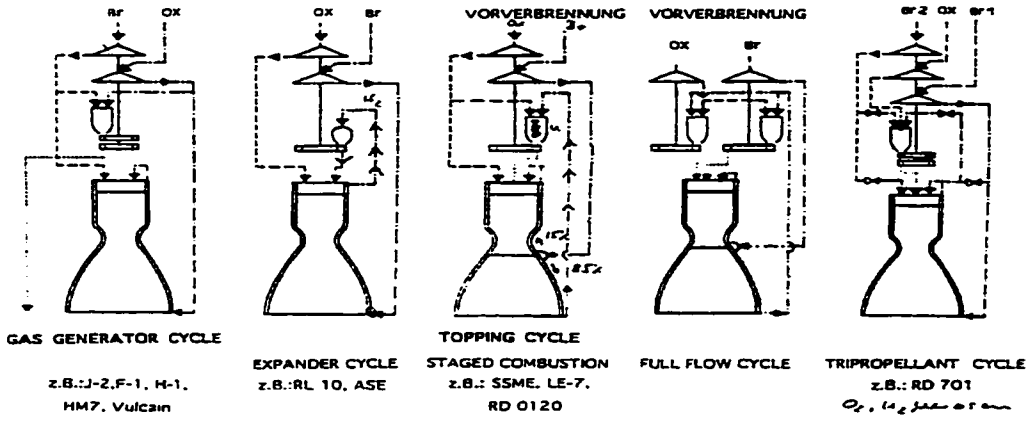

Figure 2.3: Turbo Pump Feed System Cycles[24]

Injector systems are very sophisticated and extremely important for the future of the propellants since they determine the degree of atomization of the propellant and the local mixture ratio of oxygen and fuel at the injector head in the combustion chamber. Figure 2.4 shows an injector system with distributor and injection baseplate.

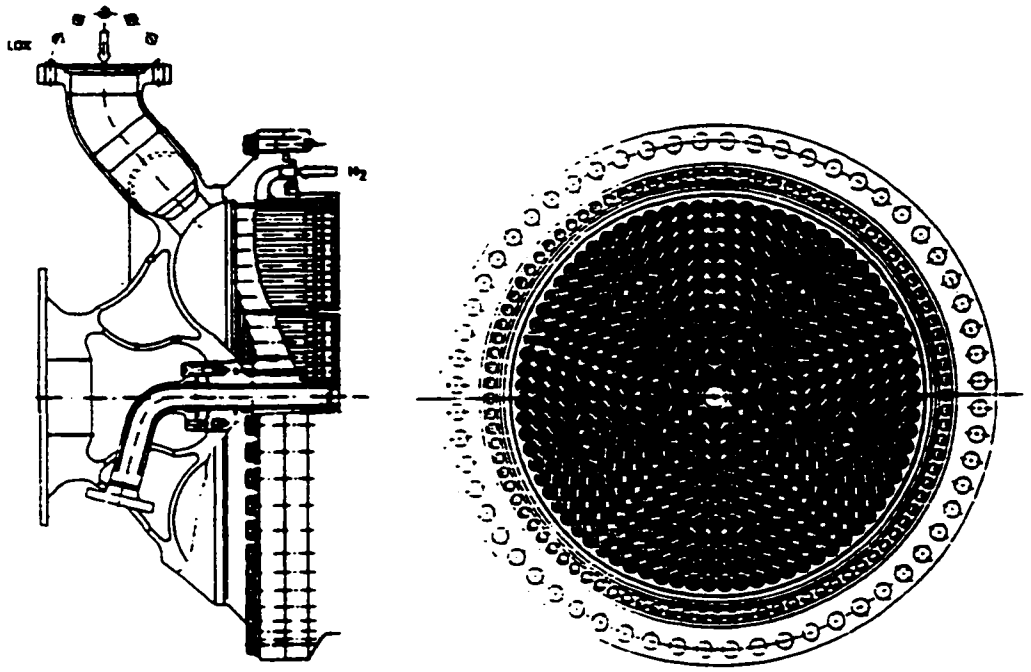

Figure 2.4: Distributor and Injection Head with Coaxial Injection Elements (HM60/MBB)[24]

Injector systems consist of a distributor (dome), which supplies a homogeneous propellant flow and the injection head, where the injection elements are located. The main purpose of the distributors is to reduce the flow velocity as low as possible. The distinctive designs of distributors are not very sophisticated, whereas the different designs of the injection elements is a science in itself. The two main features of injection

elements are to determine both the flow rate and the jet structure. Figure 2.5 shows an injection element of the upper stage engine *Aestus*.

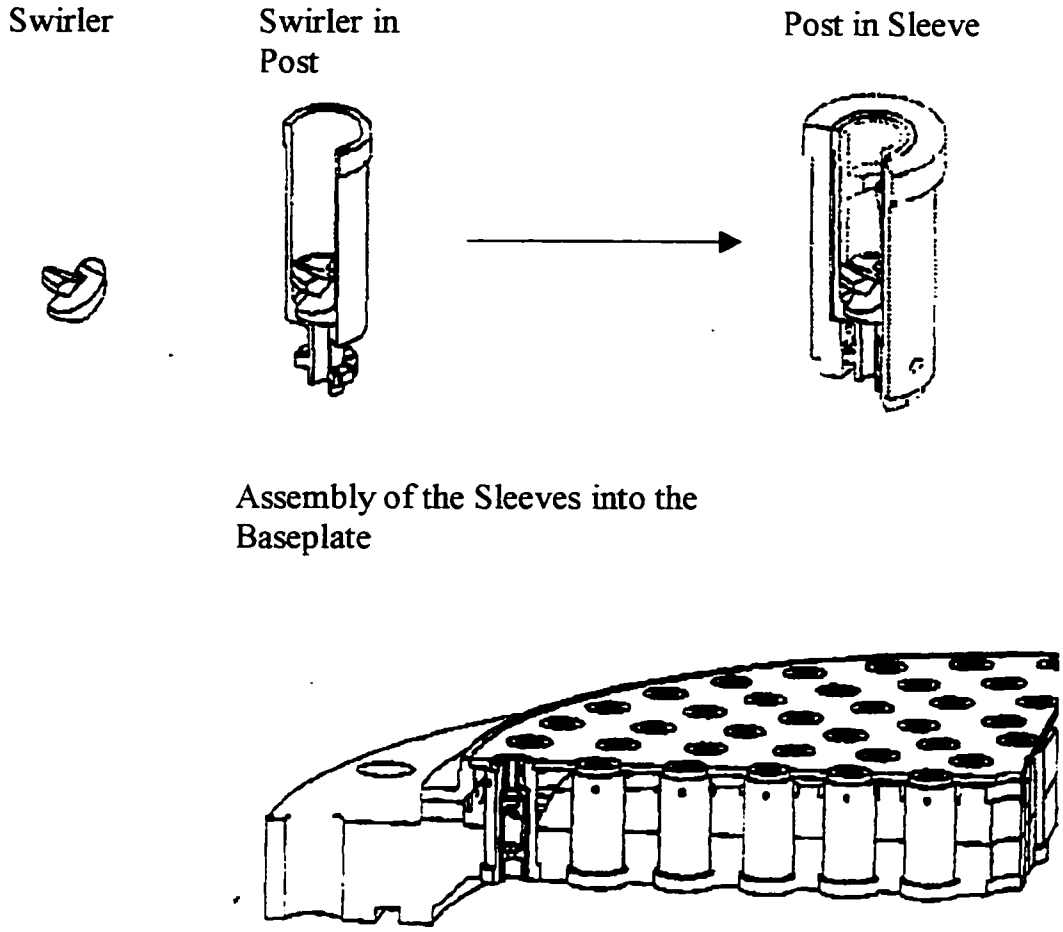

Figure 2.5: Assembly of the Injection Elements into Injection Head[24]

The combustion chamber's dimensions are determined by the measurement of the injector head to the nozzle throat. It is the heart of rocket engines because all physical and chemical processes take place here. These include vaporization, diffusion, heat transfer, combustion, and energy transfer from chemical to kinetic energy. As described above, the

injection elements provide a suitably atomized mixture. Depending on the propellant, the combustion process can take place in two different ways. If the propellants have no chemical affinity for each other in liquid phase, atomization and mixing take place in order to obtain an immediate vaporization of the liquids and creation of a homogeneous gaseous phase, ready for combustion. The other case is if the propellants have a chemical affinity (hypergolic propellant) for each other. This chemical exothermal reaction is used to vaporize the propellant, bringing about an immediate gaseous phase, and the self-igniting combustion, which also takes place immediately. Figure 2.6 shows the combustion chamber in integral construction. In addition, the combustion chamber wall provides the cooling system. The different kinds of cooling techniques are radiation, regenerative cooling, film cooling, and ablative cooling. More information about cooling techniques can be found in references [2,24,26].

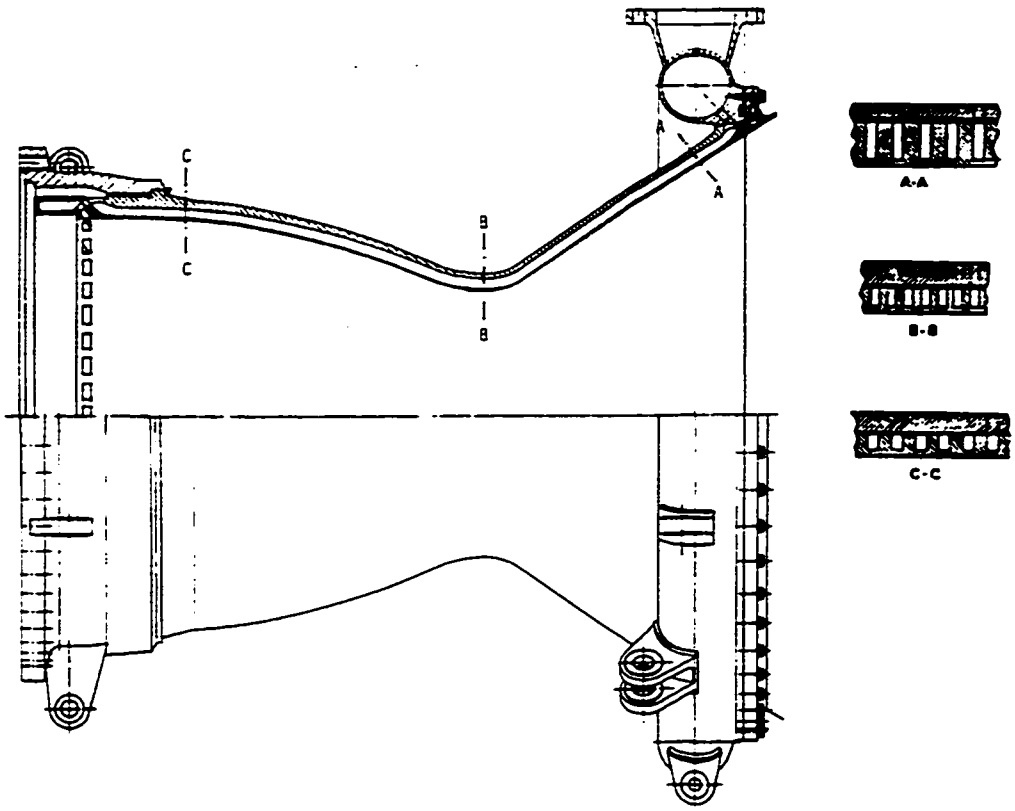

Figure 2.6: Combustion Chamber in Integral Construction[24]

The nozzle extension is used to further accelerate the combustion products after the nozzle throat. A very important property is the area ratio ε, which is the ratio of the exit area to the throat area. It basically determines if a nozzle is adapted or non-adapted to the ambient pressure. It is very important to find a high degree of adaptation because the better the adaptation the higher the specific impulse of the rocket. Figure 2.7 shows a nozzle extension with rectangular cooling channels.

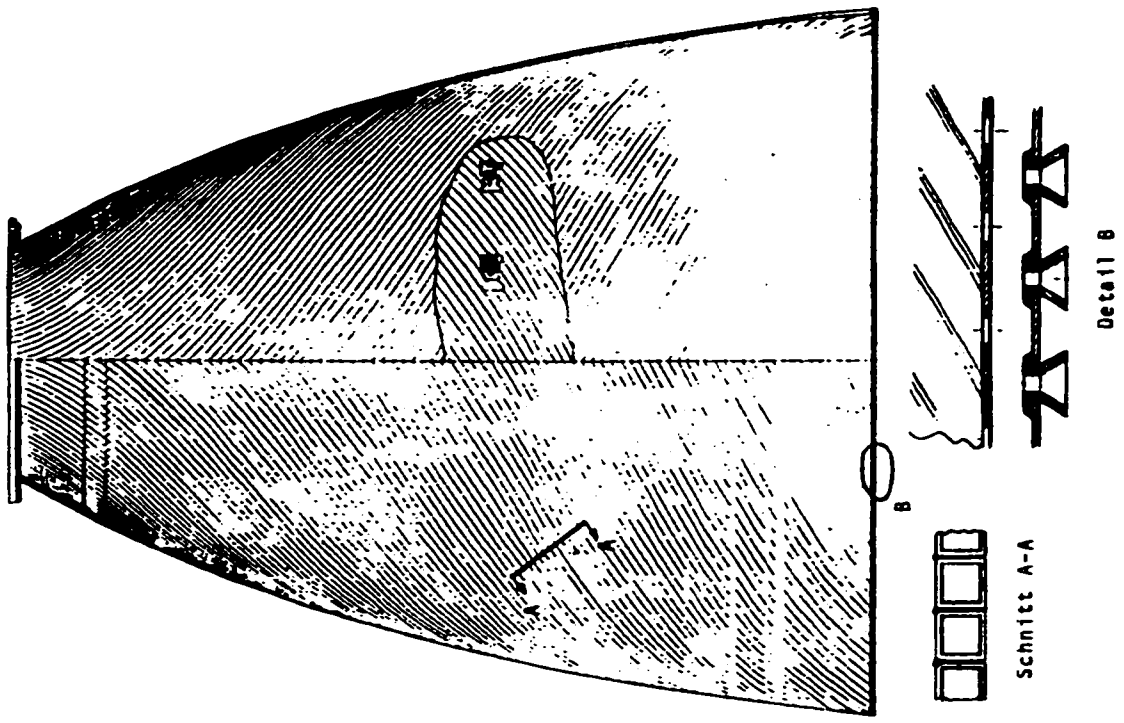

Figure 2.7: Nozzle Extension[24]

The reader can obtain more information about rocket propulsion systems in references [2,3,9,15,16,24,26,28].

Chapter 3: Rocket Engine Development

In this chapter, the development of a rocket propulsion system is discussed. The complex phenomena during the operation demand structured experimental techniques to avoid malfunctions of the rocket engine during its mission. The combustion is one possible source for a malfunction. It brings about high temperature profiles and combustion instabilities. Almost every new rocket engine development shows tendency to combustion instability. Combustion instability can lead to excessive forces as well as to destruction of the boundary layer, which is used to cool the combustion chamber wall. These phenomena have led to the development of special chamber designs and special testing procedures in order to avoid combustion instability.

3.1 Problems in Rocket Development – Combustion and Feed Line Instability

Names for certain instability modes are chugging, humming, groaning, motor-boating, organing, screaming, screeching, buzzing, squealing, POGO, and so on. These different descriptions basically cover two types of instabilities. The duller ones (deep sound) correspond to very noisy combustion which is characteristic of low-frequency instability (chugging). The second group has a sharper sound which is characteristic of high-frequency instability in the combustion chamber (screeching). A third instability is the POGO oscillation, which occurs in the feed line system[2].

Experimental studies showed that the main engine parameters influencing the low-frequency as well as the high-frequency instability are the characteristic combustion chamber length, the combustion chamber pressure, the injector head pressure drops, the

nature of the propellant, mixture ratio of the propellants, and the length of the oxygen and fuel feed lines.

3.1.1 POGO Oscillation

POGO oscillations are oscillations within the entire propulsion system during a flight due to resonance between structure, propellant flow and engine thrust. This physical phenomenon usually occurs when pumps are used (cavitation at the pump inlet). The frequency range is from 1 – 20 Hz. A possible solution is to detune the entire propulsion system with a gas cushion (cushion vessel) in the propellant feed system of the engine. The gas cushion can be regulated actively or passively. Figure 3.1 shows a POGO oscillation system.

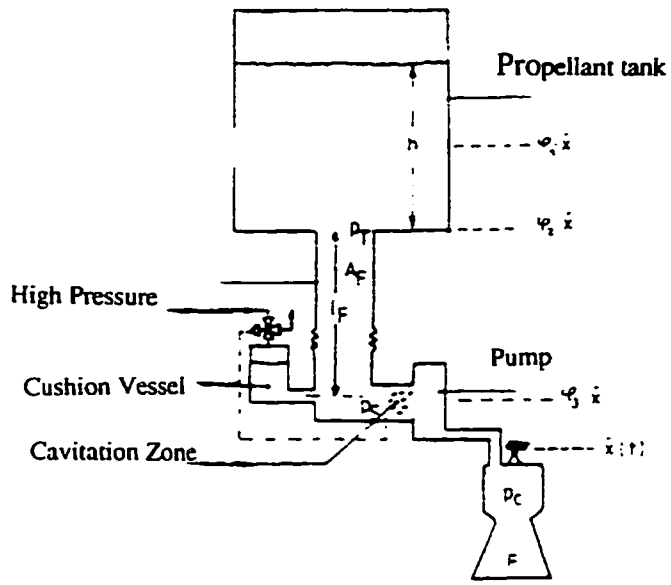

Figure 3.1: POGO Oscillation System[24]

3.1.2 Low-Frequency (LF) Oscillations

LF oscillations are hydraulic oscillations within the entire propulsion system due to resonance between the combustion chamber as an accumulator, the feed system, and the propellant tank; influenced through the ignition delay in the combustion chamber. The frequency range is between 20 Hz and 2000 Hz. A possible solution is to adjust the pressure loss (Δp injector) between the combustion chamber and the feed system. Additionally, the flow velocity in the pipe system should be as small as possible. Figure 3.2 shows an oscillation system with feed line coupled low-frequency (LF) oscillation.

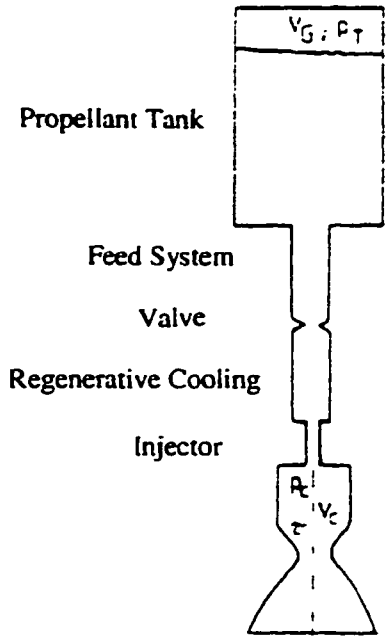

Figure 3.2: LF Oscillation – Chugging[24]

3.1.3 High-Frequency (HF) Oscillations

HF oscillations (screeching) are acoustic oscillations in the combustion chamber due to resonance between the acoustic eigenfrequencies of the combustion chamber (longitudinal, radial, tangential, and combined). The frequency range is 1 to 10 kHz.

The distinctive forms of HF oscillations can be determined from modified principle laws. Reference[30] shows the procedure on how to modify the three principle equations -- conservation of mass, conservation of momentum, and conservation of energy -- for transient motions in a two-phase mixture. The three modified equations are combined and the final equation for the wave equation written as

$$\nabla^2 p' - \frac{1}{\bar{a}^2} \cdot \frac{\partial^2 p'}{\partial \tau^2} = h + h_e \qquad (3\text{-}1)$$

where p' is the fluctuation pressure, $\bar{a}$ is the mean speed of sound, and the remaining h-terms on the right hand side are functions of density and velocity of the gas. Equation (3-1) is solved and natural modes are found. These natural modes reflect the pressure and velocity fields of the different forms of HF oscillations in combustion chambers. Figure 3.3 shows the different forms of HF oscillations in combustion chambers. More information on the derivation and instability analysis can be found in references[2,30].

One possible solution to avoid HF oscillations is to change the frequency of the system through the modification of the propellant preparation or through baffles. Baffles change the acoustic eigenfrequencies. In addition, the system can be damped (energy

absorption) through acoustic cavities. Figure 3.4 shows a baffle installation and Figure 3.5 shows the result.

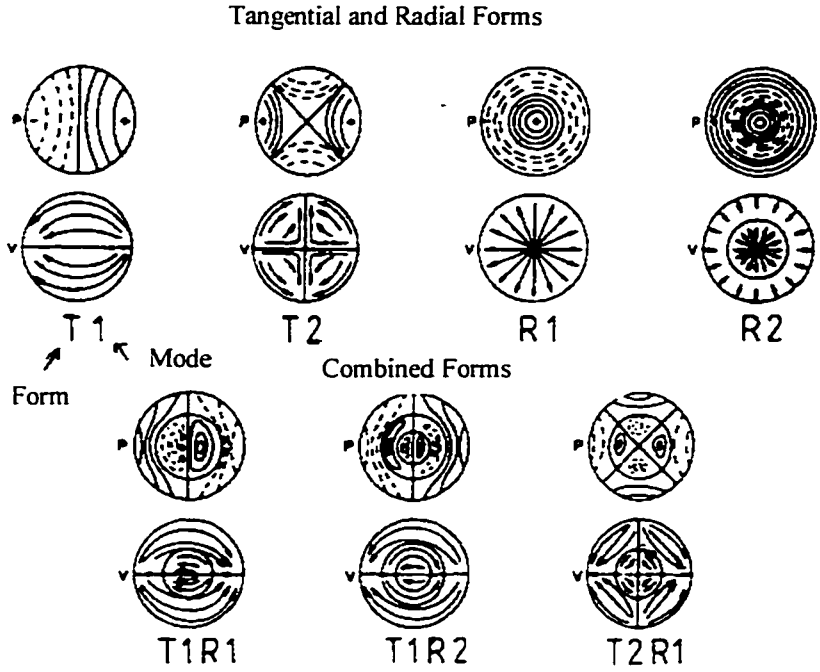

Figure 3.3: Oscillation Forms of HF Oscillations in Combustion Chambers[24]

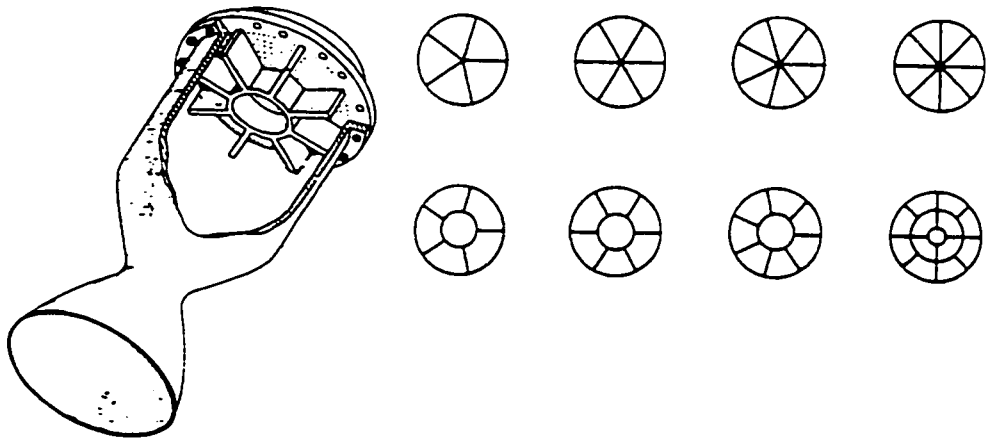

Figure 3.4: Baffles for the Modification of the Acoustic Eigenfrequencies of Combustion Chambers[24]

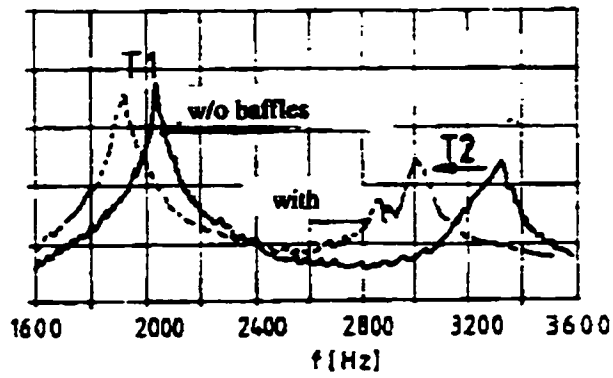

Figure 3.5: Modification of the Frequency due to Baffles[24]

3.1.4 Simulation and Analysis

Prior to 1972, liquid rocket combustion instability model development led to the publication *Liquid Propellant Rocket Combustion Instability*[30] from D. T. Harrje and F.H. Reardon. Linear and nonlinear acoustics equation were used as the main means to predict any combustion instability in rocket combustion chambers. These codes modeled injection; however, a mechanistic treatment of atomization was omitted. In addition, they did not have a "complete" combustion model. Numerical stability problems were also tremendous. The design tools for the '90s use a *Fourier time expansion*[30] and simple time-domain codes. These codes are able to determine stability margins and simulate the resulting oscillation. However, any of the approaches strongly rely on boundary conditions, such as injection, atomization rates at the injector face, and the mass flow in the feed lines. Unfortunately, the phenomena, which take place at injection and atomization, have not been fully understood yet. The transient mass flow through the feed system and the engine is of enormous importance, too.

Even today, the phenomena of combustion instability cannot be fully solved analytically. Tests still must be performed to ensure safe missions into space.

3.2 Main Parameters of Combustion Instability – LF Oscillation

One of the parameters for low-frequency combustion instability is the mixture ratio of the propellant at ignition. It was found that instability could be excited more easily at fuel-rich mixture ratios with colder hydrogen than at higher mixture ratios with warmer hydrogen.

Other parameters are the injection velocity ratio, momentum ratio, and contraction ratio of the injection elements. Generally, higher values of all these parameters support a stable combustion.

Two kinds of parameter can be tested: The operating parameters and the geometric parameters.

3.2.1 Influence of the Characteristic Length

The frequency of the disturbances decreases with an increase of the characteristic length for a same chamber pressure and injection pressure drop because the longer the characteristic length the longer it takes for the combustion gases to travel from the injection baseplate to the nozzle throat and back. Figure 3.6 shows the graphical result.

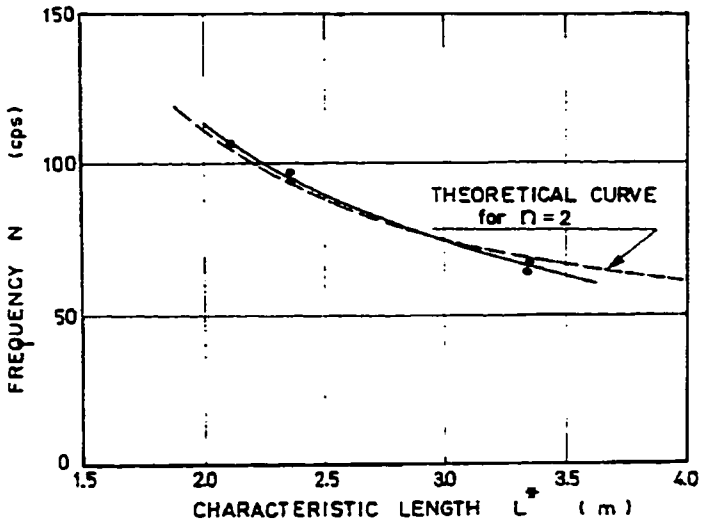

Figure 3.6: Relationship between Characteristic Length and Instability Frequency[2]

3.2.2 Influence of the Propellant

The nature of the propellants is a very important factor for low-frequency instability. Generally speaking, hypergolic propellants are more likely to produce a higher frequency with a lower amplitude than non-hypergolic propellant.

3.2.3 Influence of the Mixture Ratio

The equivalence mixture ratio is defined as

$$\Phi^* = \frac{\text{mass flow mixture ratio}}{\text{stochiometric mixture ratio}}$$

It has little effect on low-frequency instability. On the other hand, the stability depends highly on the mixture ratio. Figure 3.7 shows the influence of the equivalence ratio and Figure 3.8 shows the influence of the reciprocal mixture ratio; however, the exact influence of the propellant ratio has not been fully understood yet.

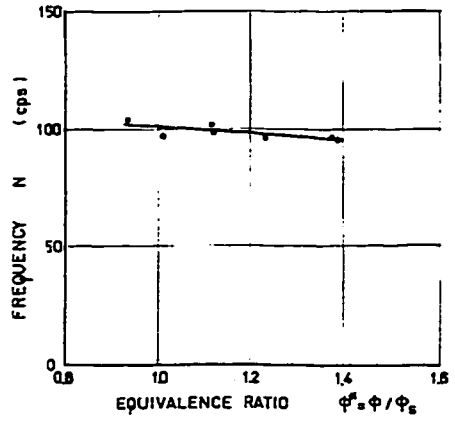

Figure 3.7: Influence of the Equivalence Ratio on LF Instability[2]

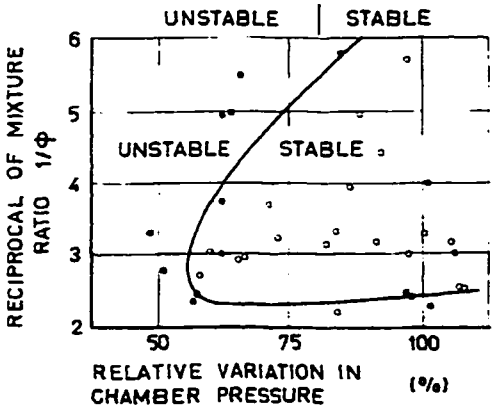

Figure 3.8: Influence of the Mixture Ratio[2]

3.3 Main Parameters of Combustion Instability – HF Oscillation

The most critical parameter for high-frequency combustion instability is the mixture ratio of the propellant at ignition. It was also found that that instability could be excited more easily at fuel-rich mixture ratios with colder hydrogen than at higher mixture ratios with warmer hydrogen. However, the real parameter has not been fully investigated: whether the higher temperature or the fuel-rich mixture is the responsible parameter. Combustion instability can be avoided using a low-mixture ratio and a sufficiently high hydrogen temperature. Other parameters are injection velocity ratio, momentum ratio, and contraction ratio of the injection elements. Generally, higher values of all these parameters support a stable combustion.

3.4 Rocket Engine Test Procedure and Test Facility

3.4.1 Test Procedure – Qualification Requirements

Rocket engines must be qualified before they can be used. Table 3.1 shows the qualification requirements.

Steps	*Examples*
Qualification of main sections	Operation check of injection elements, valves, and structural tests (static, and vibration)
Integration of the engine	Pressurization and sealing tests
Engine tests	Test performance using different ambient conditions (sea-level, vacuum)
Stage tests	Engine is in upper stage implemented and tested
Flight tests	Engine is implemented into the whole rocket and launched

Table 3.1: Qualification Requirements

The test procedure can vary from rocket development project to another. However, the engine tests are always performed using a test envelope around the optimized mixture ratio in order to determine the behavior of the engine parameter such as temperature of the nozzle, tendency of combustion instability, and the performance data. Figure 3.9 shows an envelope around the optimized mixture ratio of the upper stage engine Aestus. Each envelope point (LO, LM, MO, O, etc.) is tested at least once. Changing the total incoming mass flow of the propellants into the combustion chamber can produce the different combustion chamber pressures at the same mixture ratio.

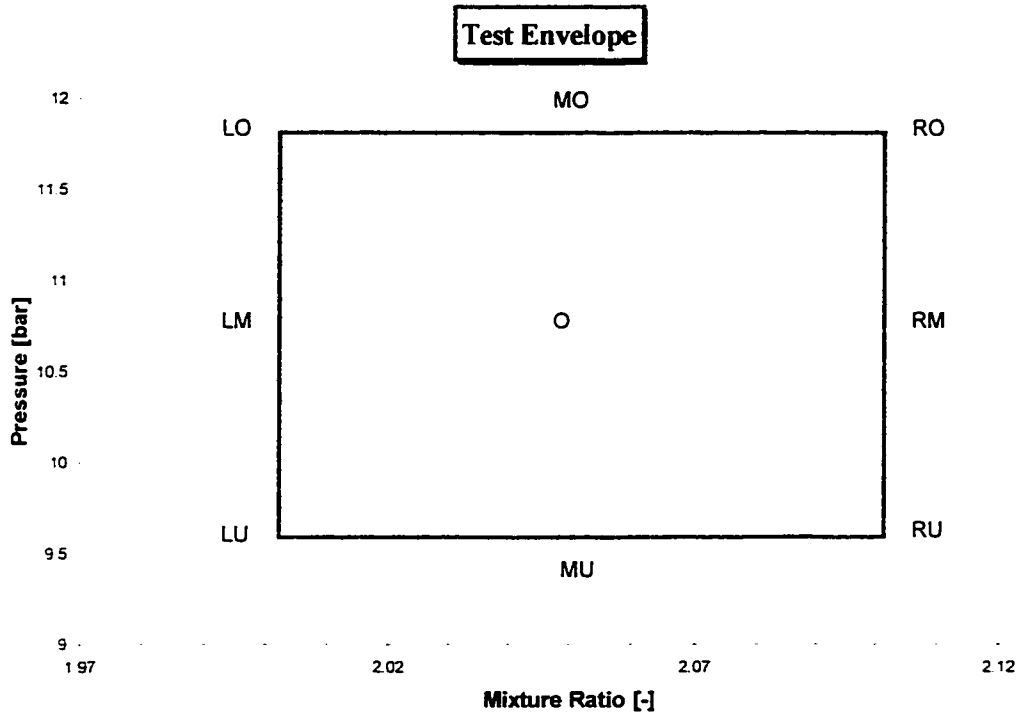

Figure 3.9: Test Envelope of the Upper Stage Engine Aestus

A test envelope can be used to determine the limits if the combustion at ignition is stable or not. Figure 3.8 was produced using a test envelope.

3.4.2 The Test Stand

The dimensions of test facilities depend on the qualification requirements, which can be distinguished into following groups:

- Fundamental research on rocket engines; the test stand is usually very small whereas the measurements are numerous
- Tests required for the development of a full-sized engine; parameter study is done in order to determine the actual performance of the engine; test stands should provide sea-level as well as vacuum conditions
- Test stands for a whole stage or rocket

Normally, the rocket engine test facility consists of a thrust bed with thrust chamber and nozzle extension, a shelter for the tanks, a shelter for personnel and control apparatus as well as measurement and recording equipment. The rocket engine can be mounted -- depending on the thrust level -- into the test stand either horizontally or vertically. Figure 3.10 shows a diagram of the arrangement and equipment of a test bed.

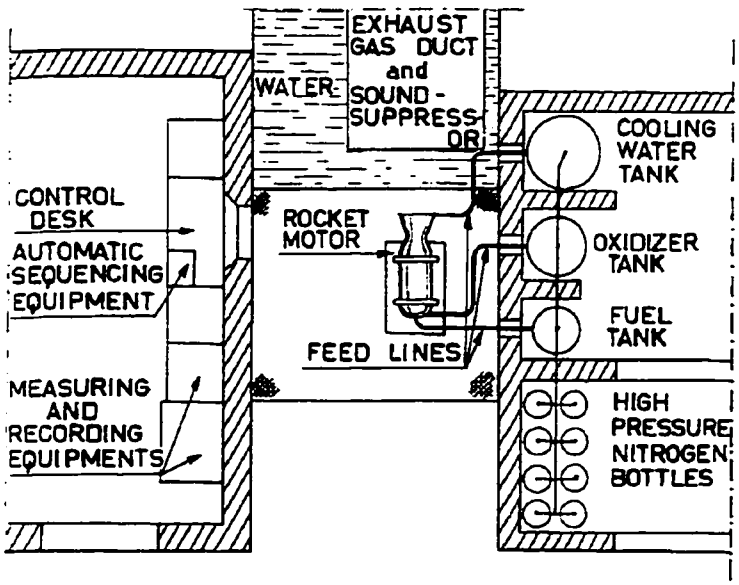

Figure 3.10: Diagram of a Test Bed[2]

Horizontal Stand

The lateral axis of the rocket engine is horizontal. The main disadvantage is the disposition of possible remains of liquid injected and not yet burned. The potential of an explosion is given. The advantages are an easy assembly of the engine and a very good measurement of the actual thrust. The horizontal solution is also used in the case of solid-propellant rocket motors. Figure 3.11 shows a burning rocket in a horizontal test stand.

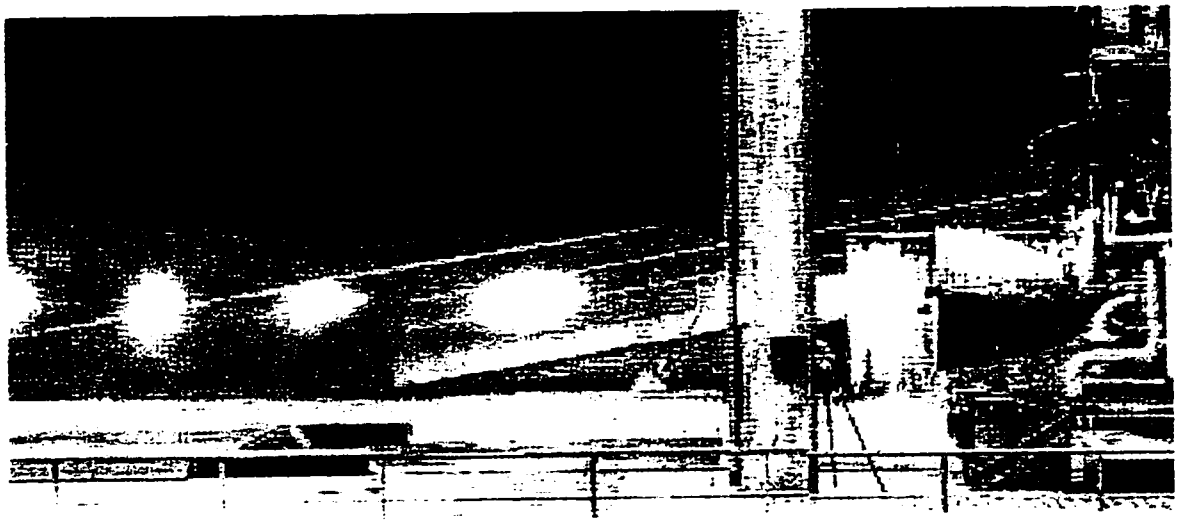

Figure 3.11: Horizontal Test Facility – Dasa Lampoldshausen, Germany[26]

Figure 3.11 shows also an overexpansion flow with regular reflection -- white spots in the figure -- of the exhaust gases. The reason for the overexpansion is that the nozzle is optimized for higher altitudes. At the current test configuration, the ambient pressure is greater than the nozzle exit pressure.

Vertical Stand

The lateral axis of the rocket engine is vertical. The disadvantage is that the engine must be mounted high enough above the ground in order to give adequate protection against erosion and high temperature of the combustion products. The main advantage is that the rocket engine is mounted similar to actual flight conditions. Figure 3.12 shows the upper stage engine *Aestus* mounted in the test bed.

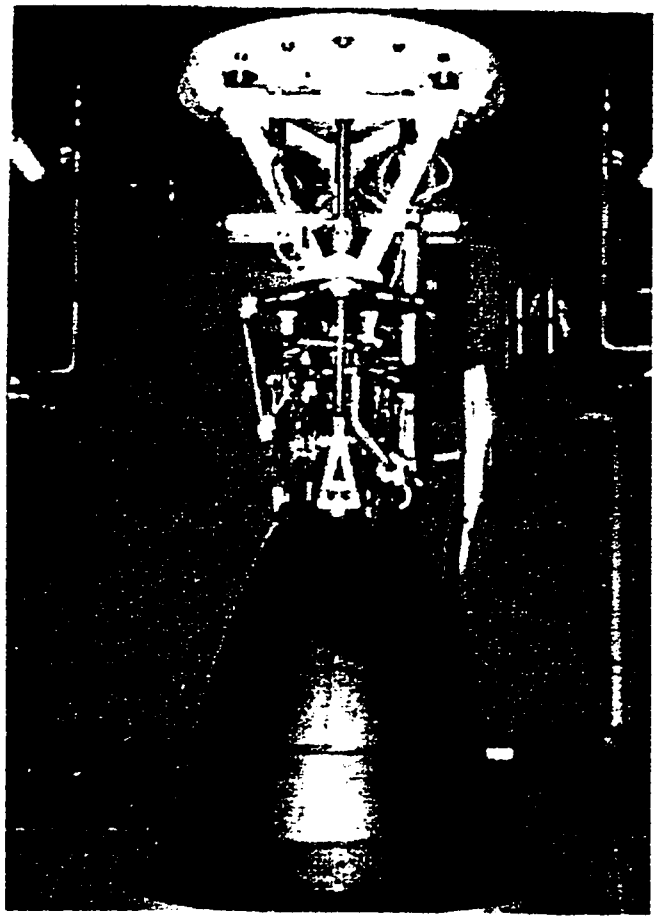

Figure 3.12: Vertical Test Facility, Dasa Lampoldshausen, Germany[25]

Figure 3.14 gives a sketch of the actual location of the engine implemented in the test facility in Lampoldshausen, Germany.

3.4.3 Test Facility – Dasa Lampoldshausen, Germany

A vacuum test facility located in Lampoldshausen, Germany is part of the German *Luft- und Raumfahrt Gesellschaft*. This test facility provides variable mass flow rates, vacuum condition up to 250 s, propellant temperatures of 273 K up to 313 K, and helium purging after operation. Table 3.2 gives the main data of the vacuum test facility.

Tank pressure range	17 – 30 bar	Propellant temperature	273 K – 313 K
Pressurizing fluid	N_2	Voltage	46 V – 59 V
Control pressure range	15 – 23 bar	Hydraulic pressure	75 +/- 5 bar
Control pressure medium	N_2 / He	Thrust measurement after	A5-NT-1921-2007-MBBO

Table 3.2: Test Facility Performance Data[25]

The principle of the vacuum simulation is explained using Figure 3.13 of the test facility P1.5 in Lampoldshausen, Germany.

A couple of hours before a test, the vacuum chamber (14) is evacuated using a mechanical pump until the pressure is 1 mbar. An oil-vapor pump (17) is used in order to drop the pressure to a value of 10^{-4} mbar. A couple of minutes before ignition of the engine (1), a vapor producer (10) is turned on whose vapor stream flows through two ejector stages (8) and (9) and produces a "pulling" pressure of about 12 mbar. Vapor production is supplied with propellants through the tanks (11) and (12) and with water through the test facility feed system. An additional nozzle (5) is turned on which is also in the vapor stream cycle. The described layout provides a constant vacuum pressure of 1.5 mbar after the valve (4) is opened. This pressure is constant throughout the whole

test. At the diffuser, the exhaust gases have reached the speed of sound. After the hot run, any kind of reverse flow is prevented through the impulse of the vapor stream. Limited re-ignition is possible during the same test. In the case of a malfunction from the vapor producer, the test can be aborted immediately without any destruction of the engine. A pre-programmed control program provides the appropriate steps. The engine is turned off and the valve (4) and flap (7) are closed.

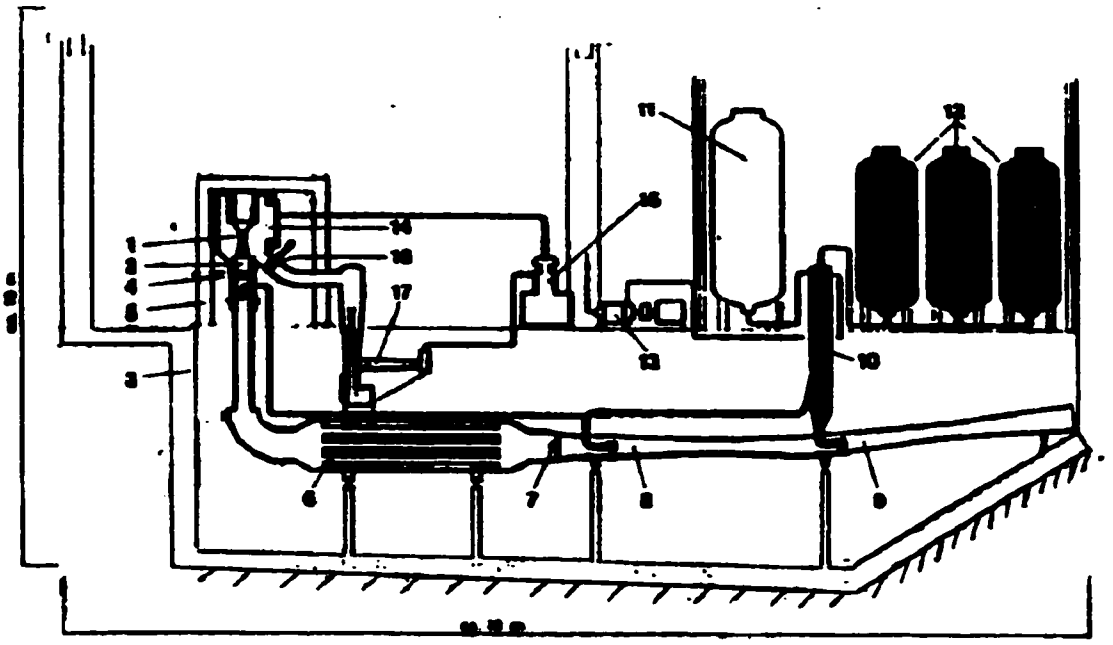

Figure 3.13: Scheme of the Test Facility P1.5 in Lampoldshausen, Germany[16]

Figure 3.14 shows the test facility P4.2 with its lift arm, the vacuum chamber, the exhaust fumes pipe system, and the exhaust fumes cooling system.

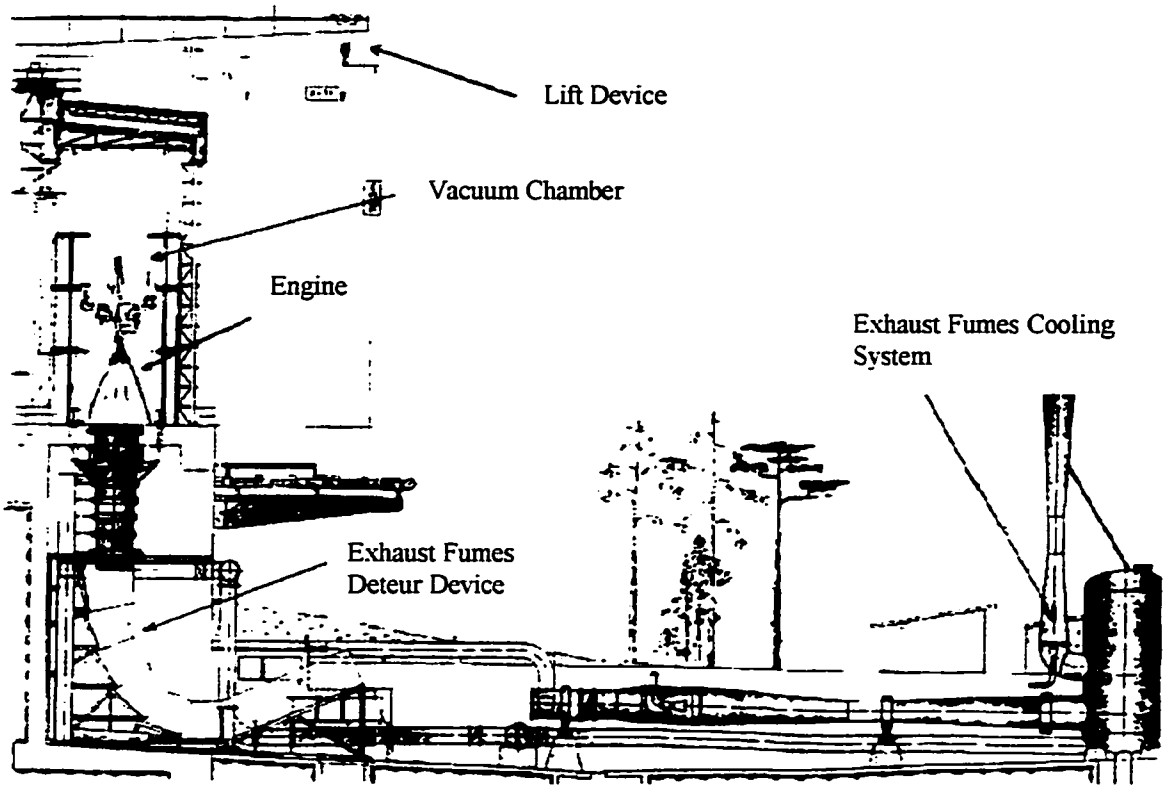

Figure 3.14: Scheme of the Test Facility P4.2 in Lampoldshausen, Germany[16]

3.4 Measurement

In rocket development, the most important physical quantities to be measured are: thrust, pressure, flow rates and temperature. Table 3.3 shows the main transducer nomenclature for the vacuum test of the upper stage engine Aestus.

Pressure:	PO205, PO206	@ Tank, ox
	PF205, PF206	@ Tank, fu
	PO106, PF106	@ control valve
	PT8	@ manifold
	PT9	@ dome (fuel)
	PT10	@ main valve (ox)
	PT12	@ chamber
	PT13	@ main valve (fu)

Table 3.3: Transducer Nomenclature

Thrust:	F	calculated
Mass Flows:	$x	calculated
Temperature:	TTxx	@ various locations

Table 3.3(cont'd): Transducer Nomenclature

The mean and the instantaneous measurements are of interest. From these values, the specific impulse, characteristic velocity, as well as the thrust coefficient can be determined.

$$I_{sp} = \frac{F}{\dot{m}} \qquad c^* = \frac{P_C \cdot A_t}{\dot{m}} \qquad c_F = \frac{F}{P_C \cdot A_t}$$

Measurement recording is made by a K8000 system from the company Kayser-Threde. The system records the data using 256 channels with a scanning frequency of 250 Hz and then stores the data digitally. Dynamical data are also stored on magnetic tape.

Figure 3.15 shows the transducer location on a diagram of the test facility P4.2 in Lampoldshausen, Germany. Figure 3.16 depicts the transducer location at the upper stage engine Aestus.

Additionally test facility dimensions can be found in the appendix A1.

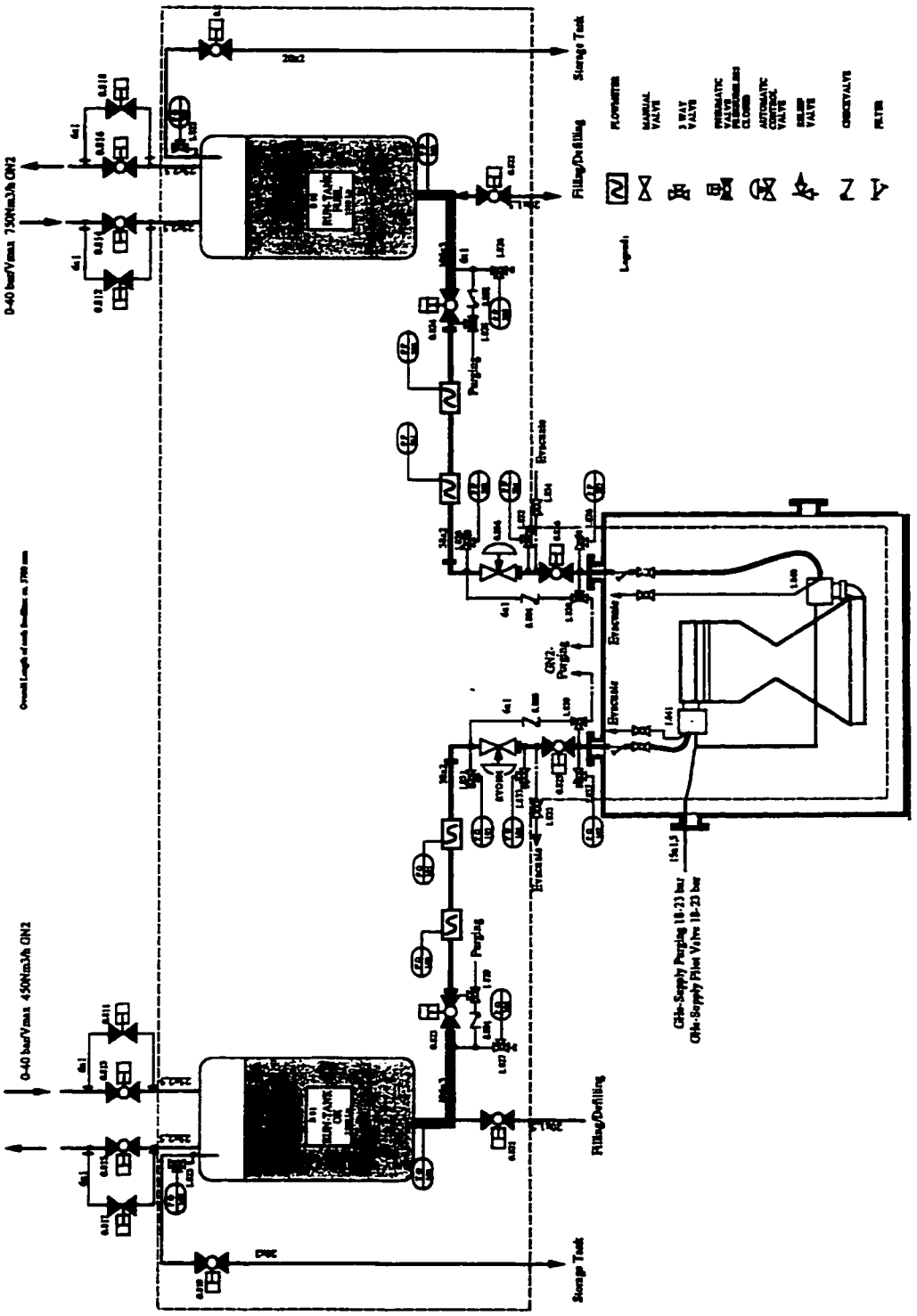

Figure 3.15: Transducer Location at P4.2[25]

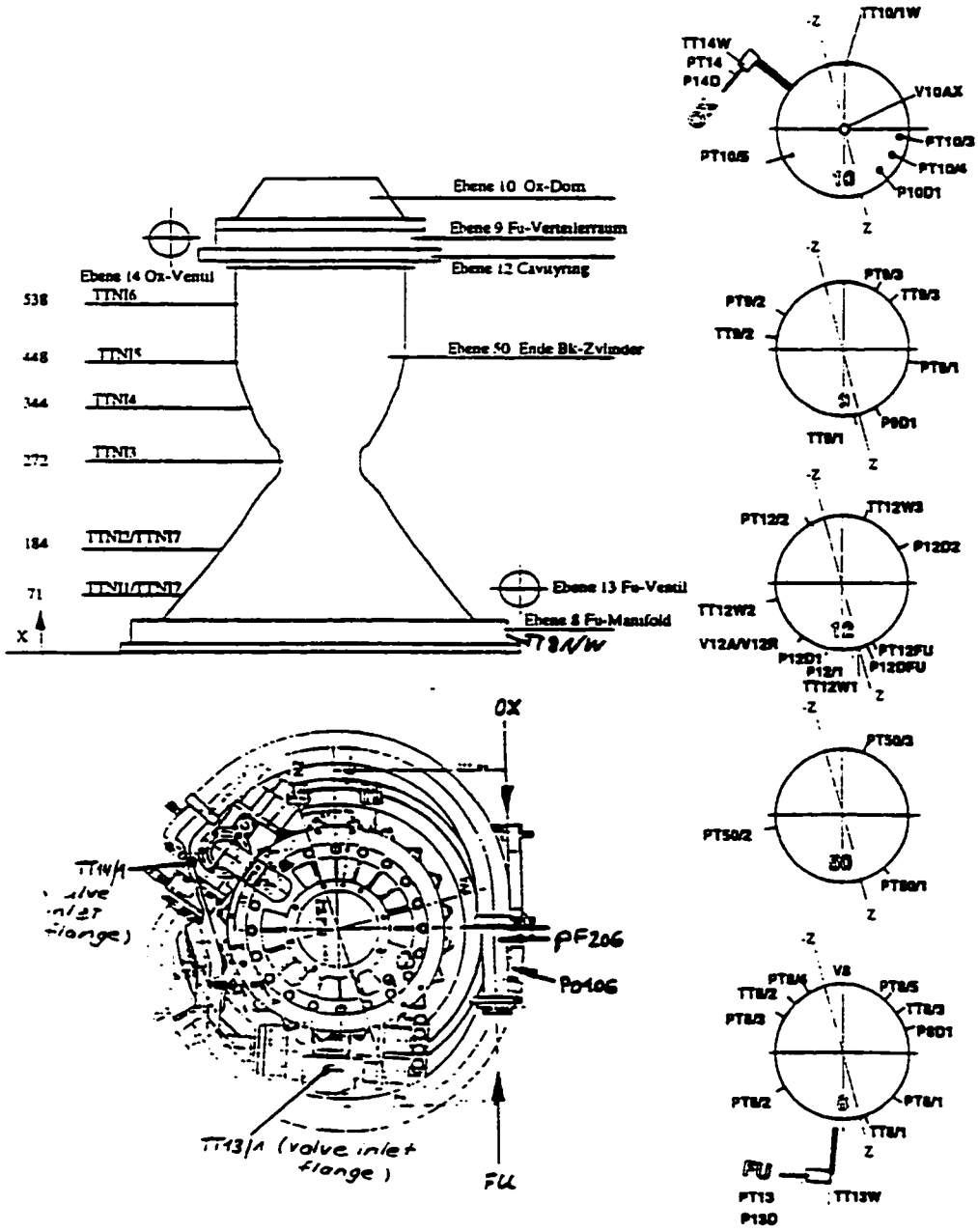

Figure 3.16: Transducer Location at the Upper Stage Engine Aestus[25]

Chapter 4: The Upper Stage Engine of the European Rocket Ariane 5 – Aestus (EPS)

The upper stage engine *Aestus* is introduced in this chapter to give a general overview of the history, development, and performance data of the rocket engine. The engine's operation is also included to provide a better understanding for the chapters following.

4.1 Historical Background

The upper stage engine (EPS) of the European rocket engine *Ariane 5* was developed in about eight years. The *Ariane 5* rocket finally had its maiden voyage on June 4, 1997. Unfortunately, the rocket had to be destroyed due to a malfunction of the control software. The upper stage engine was successfully ignited on its second flight on October 30, 1997.

The engine *Aestus* is the main propulsion system of the upper stage. While its maximum height is only 3.35 meters and its diameter only 3.9 meters, its four tanks can hold 10 tons of storable propellant (explaining the name EPS, Etagé a Propergols Stockables) as well as the gimbal-joined engine *Aestus*.

The engine was tested and qualified in 27 vacuum tests and about the same number of sea level tests. Approximately 1000 ignitions were performed during the test campaign. Even though the ignition phase of the engine was tested frequently, combustion instability still occurred. One vacuum test costs about 250.000 DM (US$ 140,000)[25].

4.2 Performance Data and Main Parts

EPS' engine -- *Aestus* -- is capable of delivering its payload into geo-stationary transfer orbit (GTO), sun-synchronized orbit (SSO), as well as the low earth orbit (LEO).

The engine belongs into the group of hypergolic rocket engines because of its propellant combination Nitrogen Tetroxide (N_2O_4) and Monomethylhydrazine (CH_3NHNH_2) also known as MMH. N_2O_4 is used as oxygen and MMH is used as fuel. Steady state combustion takes place at a propellant mixture ratio of 2.05 despite the fact that the stoichiometric mixture ratio is approximately 2.5 because the optimum mixture ratio either depends on a minimal total mass of the propellants or on a minimal volume of the stored propellants. In the case of the engine *Aestus*, the propellants have quiet distinctive densities. Namely, the density of MMH is about half the value of N_2O_4. More information about the determination of an optimized mixture ratio can be found in reference[24].

The engine consists mainly of the following parts: (a) A cardan and struts are used for the thrust vector control, and are also the interface between the engine and the upper stage unit where the payload is located. (b) The injector head with its coaxial impinging vaporization system, (c) A regenerative cooled combustion chamber and the nozzle extension, (d) Propellant valves, which are pneumatically controlled and Electro-mechanical actuators, which enables a movement in gear, and pitch direction, respectively.

The main performance data and geometric dimensions can be seen in Table 4.1. The complete listing of all data can be found in appendix A2.

Thrust in vacuum	28 kN	Expansion ratio	84
Specific impulse	324 s	Total length	2183 mm
Total mass flow	8.772 kg/s	Nozzle exit diameter	1315 mm
Mixture ratio	2.05	Total weight	120 kg
Chamber Pressure	10.8 bar	Re-ignition	Unlimited
Characteristic velocity	1684 m/s	Nominal operation length	1100 s

Table 4.1: Main Engine Data

Generally speaking, rockets consist of a combustion chamber and a nozzle extension as was mentioned earlier in chapter 2. The combustion chamber must be supplied with an appropriate propellant flow. The two propellants ignite in the chamber and the chemical energy is transferred into kinetic energy.

The upper stage consists of four propellant tanks, a feed system, and the rocket engine. Figure 4.1 shows a schematic sketch of the rocket engine. All four tanks are pressurized in order to obtain a constant mass flow in the two feed branches. At a given time interval, the two valves are opened and the propellants flow through the hydraulic system of the engine into the combustion chamber.

The oxygen flows into a dome at first, followed by the injector head. The injector head contains a complicated distribution system in order to obtain a homogeneous mass flow through 132 injection elements. The injection elements accommodate a swirler, which produces an angular momentum into the flow.

The valve for the fuel branch is opened slightly later to provide an oxidizer pre-flow in the chamber. The fuel flows through a manifold at first, fills it, and flows through rectangular cooling channels, which are located in the chamber wall, into the injector head. The mass flow continues through the injection elements, which have small lateral holes into the combustion chamber.

The two propellants are vaporized, atomized, and mixed due to the coaxial impinging system. The hypergolic propellants are mixed and combustion takes place immediately. A combustion coefficient of 98 % can be achieved due to an effective impinging system.

The combustion products are accelerated and reach sonic speed at the nozzle throat. Further acceleration takes place in the nozzle extension. The steady state thermodynamic values such as temperature and pressure are 3000 K and 10.8 bar, respectively.

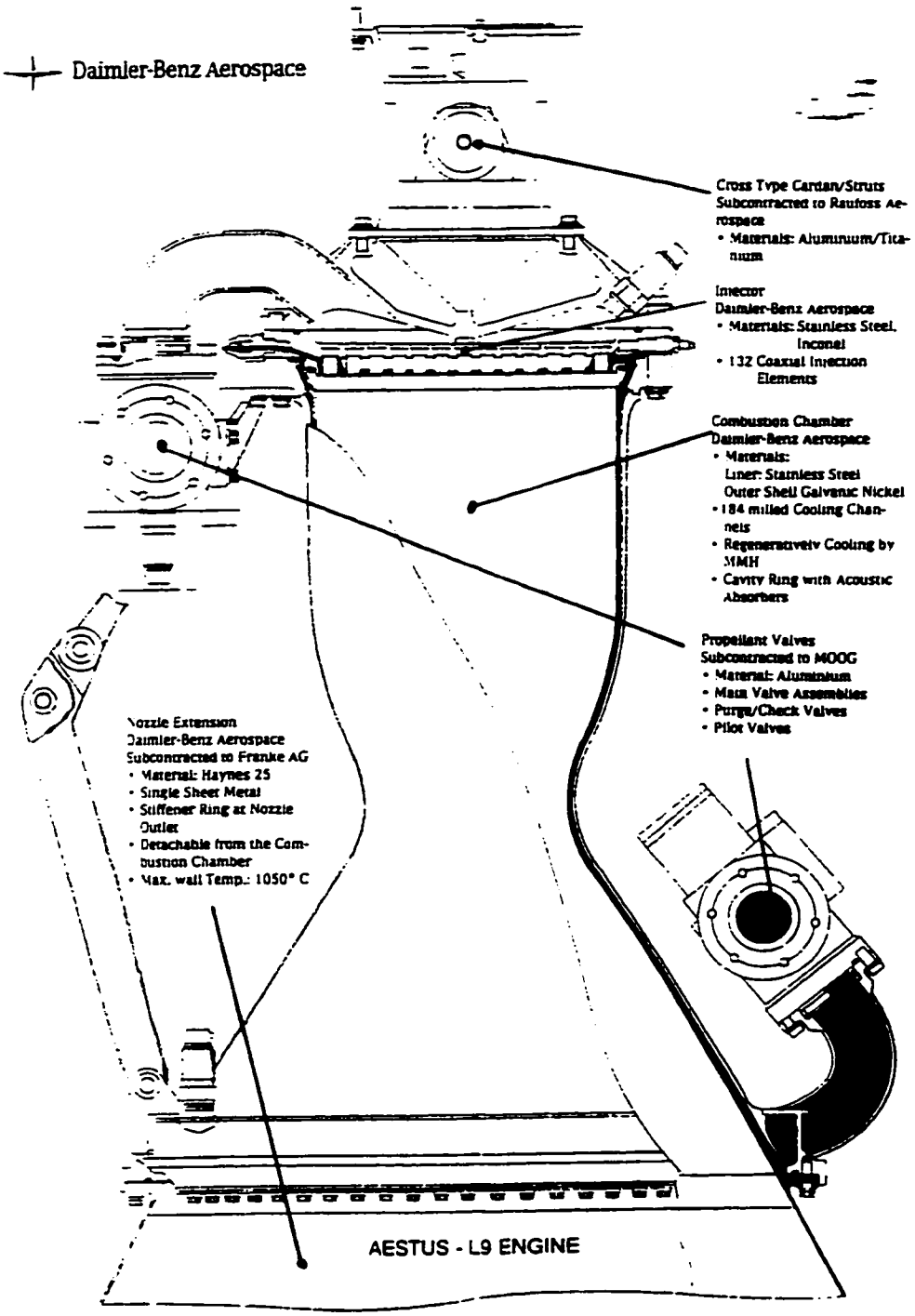

Figure 4.1: Schematic Sketch of the Upper Stage Engine Aestus[25]

Chapter 5: Description of the Transient Start-up Phase Using Vacuum Test Data of the Upper Stage Engine Aestus

Fundamental flow phenomena are described for unsteady thermofluid mechanics in rocket engine feed systems. The distinction between the three sections and their flow phenomena (1-D liquid flow, 1-D Two-Phase Flow, combustion) are discussed. Charts are presented because of their importance in understanding the complex relation between the hydraulic components of the engine.

In chapter 2, essential parts of rocket engines were described. The specific layout of the upper stage engine *Aestus* was discussed in chapter 3, and the test facility explained in chapter 4. Therefore, the engine feed system and the engine is assumed to be known. The following Figure 5.1 shows a diagram of the hydraulic components as well as the measurement instrumentation for a better understanding.

Generally speaking, the flow is a one-phase flow from the tanks to the main valves 1 and 2. After the main valves, the flow will become a two-phase flow due to the ambient vacuum pressure in the feed lines and engine after the main valves. Possible helium ingestion in the tanks has to be considered if the propellants were pressurized over a long time because of the phenomenon of diffusive mass transfer.

Combustion includes complex phenomena, which have not yet been clearly understood. The transient phase of ignition is still an unknown in rocket science. A general model is used to explain the different combustion zones.

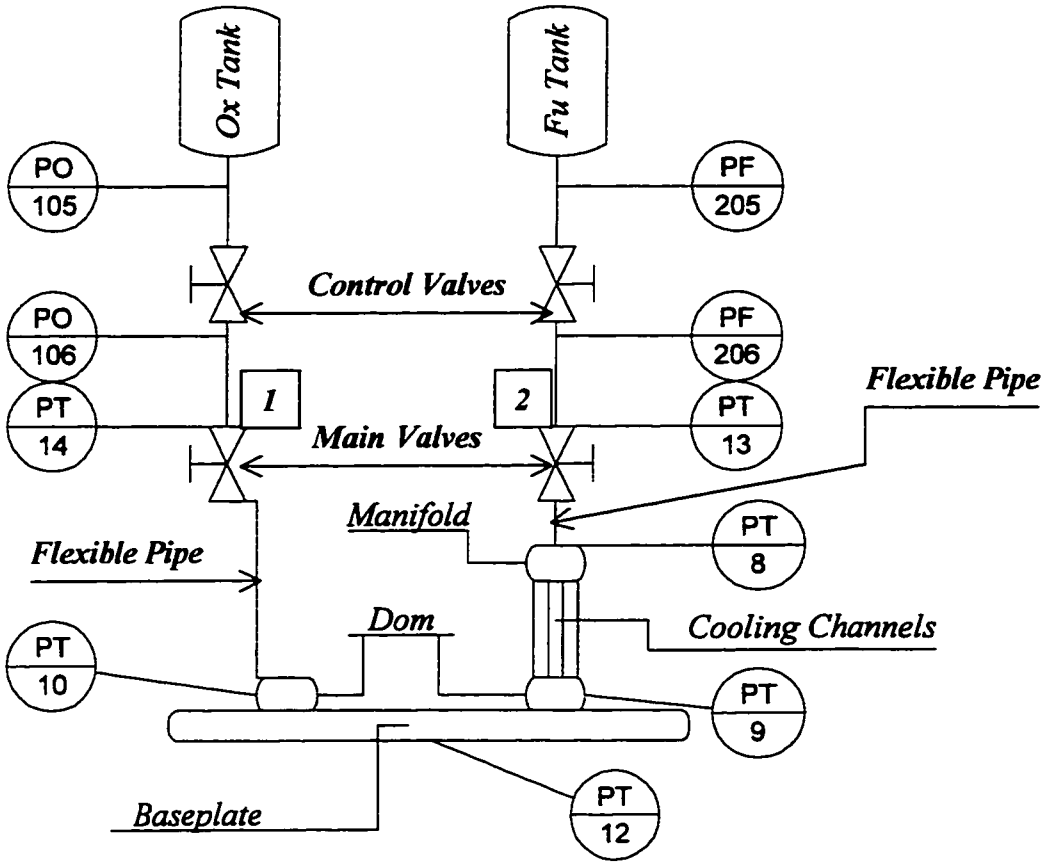

Figure 5.1: Diagram of the Flow System – Feed Line, Engine

5.1 Qualitative Description of the Start-up Phase

The transient start-up phase is packed with complex phenomena which have not yet been fully understood. However, the start-up phase is very important for the prediction of a stable combustion. Figure 5.2 shows a qualitative curve of the propellant mixture ratio during the start-up phase. It shows also regions where a tendency for unstable combustion is given. In order to understand Figure 5.2, Figures 5.3 and 5.4 must be taken into consideration. Figures 5.3 and 5.4 show typical plots for the transducers of

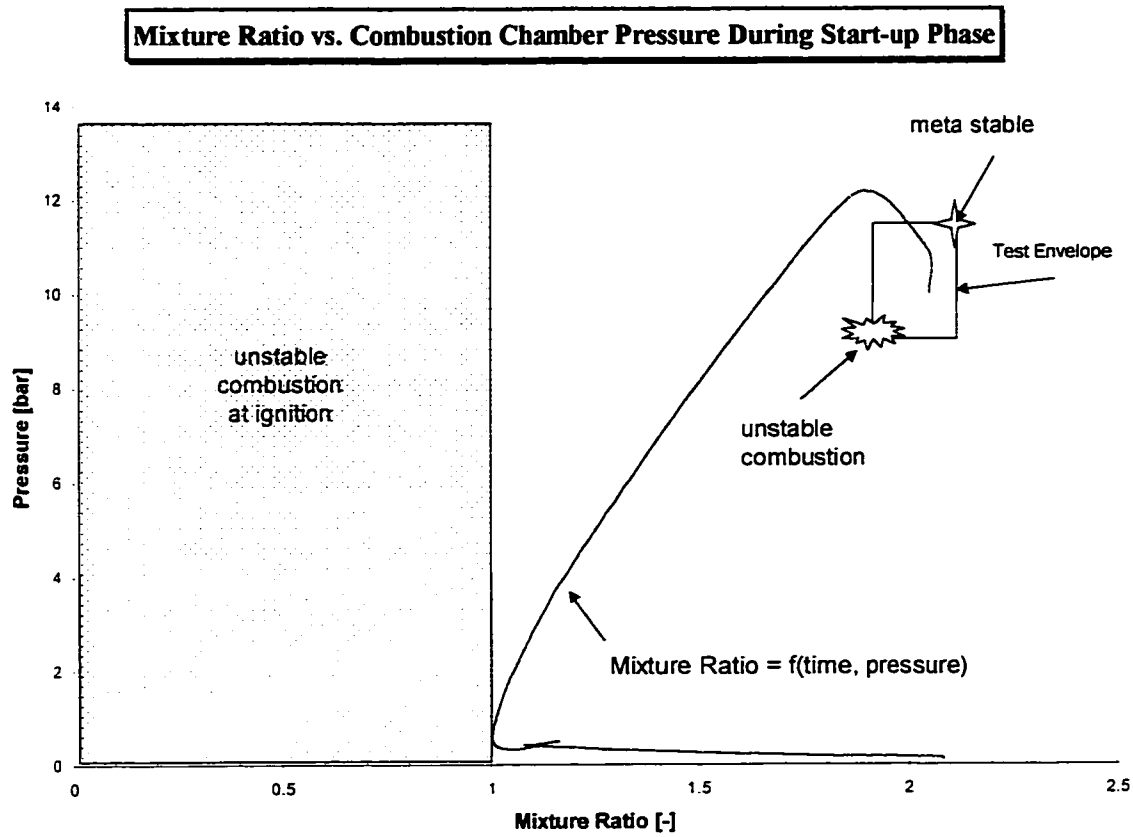

Figure 5.2: Mixture Ratio during the Start-up Phase

the valve strokes (Ox: DO113, Fu: DF213), as well as static pressure sensors at the tank exit (Ox: PO105, Fu: PF205), after the flow flux the regulator (control valve) (Ox: PO106_1, Fu: PF206_1), at the valve (Ox: PT14, Fu: PT13), at the dome (Ox: PT10, Fu: PT9), the manifold (Fu: PT8), and the static combustion chamber pressure (PT12).

For the following explanation of the transient mixture ratio, transducer curves $6, $7, and PT12 have to be considered. At the beginning of the transient start-up phase, the mixture ratio is infinity due to the oxygen pre-flow. The fuel begins to flow and the mixture ratio decreases. It is important for a stable combustion that the mixture ratio is not within the region left of a mixture ratio of 1.0 in Figure 5.2.

At a particular time (approximately at $\tau = 0.4\,\mathrm{s}$), both propellants are in the combustion chamber and ignite. The combustion pressure regulates the mixture ratio to a predicted value due to the pressure increase. The final operation mixture ratio is tested and verified during the vacuum tests of the rocket engine qualification in order to ensure a stable combustion.

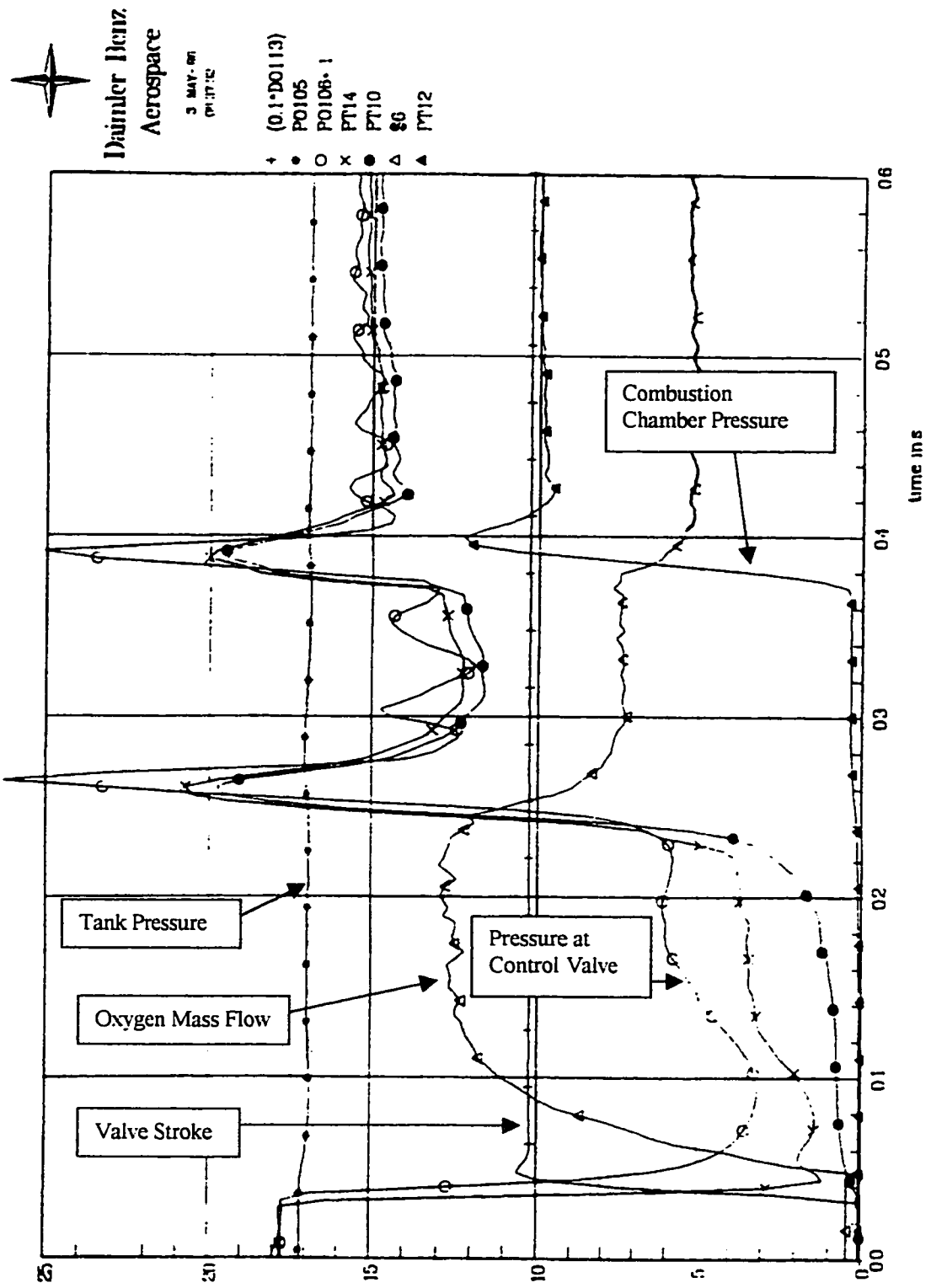

Figure 5.3: Transducer Curves – Oxygen Branch[25]

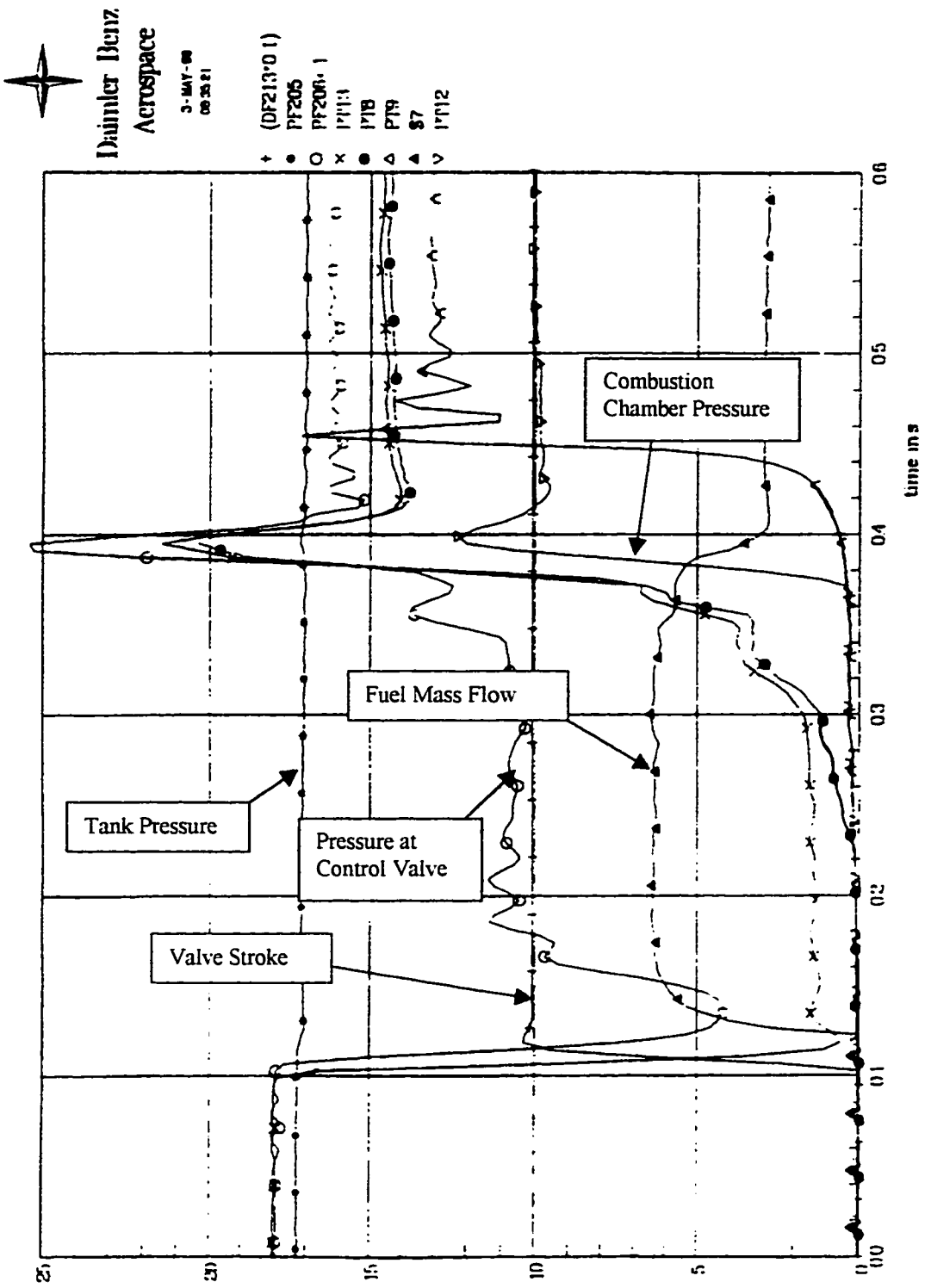

Figure 5.4: Transducer Curves – Fuel Branch[25]

The following explanation describes the filling process of the main engine components in detail. However, physical phenomena such as cavitation, bubble flow, and internal combustion are not included.

The transient start-up phase of a rocket engine -- especially with hypergole propellants -- occurs in a very short time interval; therefore, it is justifiable to consider the phenomenon within milliseconds. The reader will obtain only a qualitative understanding of the transient start-up phase.

The transient filling process of the feed system can be explained best using the following three equations.

$$\Delta p \propto \dot{m}^2 \tag{5-1}$$

$$\dot{m} = \rho \cdot v \cdot A \tag{5-2}$$

$$\underbrace{\frac{\rho}{2} \cdot v^2}_{\text{Dynamic Pressure}} + \underbrace{\rho \cdot \frac{\partial v}{\partial \tau} \cdot A_i \cdot \int \frac{dx}{A}}_{\text{Acceleration Pressure}} + \underbrace{p}_{\text{Static Pressure}} + \underbrace{\rho \cdot g \cdot y}_{\text{Geodetic Pressure}} = \underbrace{P}_{\text{Total Pressure}} \tag{5-3}$$

Equation (5-1) shows that the pressure loss Δp is directly proportional to the square of the flowing mass flux $\dot{m}$. Equation (5-2) is used to calculate the mass flow as a function of momentary density, momentary flow velocity, and area. In equation (5-3), the first term is equal to dynamic pressure and the second one to acceleration pressure. The last two correspond to static pressure, and geodetic pressure, respectively. The summation of all pressure terms lead to the total pressure of a fluid.

At the moment $\tau_0 = 0$, both of the propellants stand in front of the valves 1 and 2, i.e., the dynamic pressure and the acceleration pressure are zero. The static pressure

transducer PO106_1 (o), and PT14 (x) show the total pressure which is equal to the static pressure.

At the moment $\tau_1 = 50\,\text{ms}$, the oxygen valve 1 is opened and the fluid accelerates. The acceleration and dynamic pressure increase; therefore, the static pressure decreases at PO106_1. The increase of the dynamic pressures is due to the increase of the flow velocity in the hydraulic segment. The mass flow also increases because the area is constant and the density differs only slightly. The direct proportionality in equation (5-1) is justified.

At the moment $\tau_2 = 100\,\text{ms}$, the first pipe section is filled, and the oxygen mass flux flows into the oxygen dome. The dome can be considered as a large volume chamber which can be seen because the velocity decreases in this particular section. The dynamic and the acceleration pressure decrease; therefore, the static pressure PO106_1 increases again. The whole two-phase flow front is rapidly stopped, which explains the first pressure peak.

At the moment $\tau_3 = 260\,\text{ms}$, the oxygen dome is completely filled and the fluid flows into the base-plate (injector head). During this occurrence, the cross section area is suddenly changed, which can be seen through the transducer curves of PT10 (•), PT14 (x), and PO106_1 (o). The following oscillations can be explained through a springy fluid column. At this moment, the pressure in the oxygen base-plate is still below the vapor pressure of the oxygen; therefore, cavitation occurs in the injection elements. The flow resistance increases more, the flow velocity decreases and the static pressure achieves a

constant level. If equation (5-3) is applied, the decrease of the oxygen mass flux can be also explained.

In the meantime, the fuel valve is opened. The course of the pressure curves is different because of the distinctive hydraulic sections. At the moment $\tau_4 = 120\,\text{ms}$, the fluid column is moving towards the combustion chamber. The total pressure does not correspond to the static pressure PF206_1 (o) any longer. At the minimum, shortly after τ_4, the acceleration reaches a maximum. After the first filling section, the flow resistance increases and the fluid slows. The static pressure increases.

At the moment $\tau_5 = 180\,\text{ms}$, the fluid flows into the manifold. During the filling, the pressure remains constant. The constant mass flow can be explained again considering equation (5-1).

At the moment $\tau_6 = 220\,\text{ms}$, the fluid flows into the cooling channels; in the meantime, the manifold is completely filled, which can be seen at the transducer PT8 (•).

At the moment $\tau_7 = 340\,\text{ms}$, the fuel flows into the injector head, and the ignition immediately starts in the combustion chamber. The combustion chamber pressure can be considered as a counter-force versus the flow; therefore, the fluid is further slowed. During the ignition, the injector head is not completely filled, which can be seen at the transducer PT9 (Δ).

After the transient start-up phase, the combustion chamber pressure and pressures in the feed line are constant. The following section describes the combustion process more in depth.

5.2 Fundamentals of the Liquid Propellant Combustion Process

The combustion of rocket engine occurs in the combustion chamber. In order to understand the phenomena, it is appropriate to divide the chamber into coupled zones as shown in Figure 5.5.

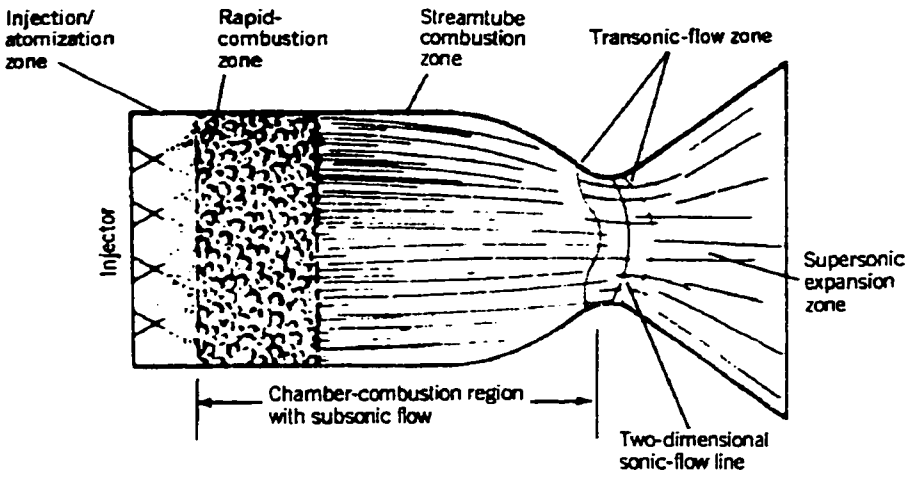

Figure 5.5: Division of Combustion Chamber into Zones for Analysis[26]

In general, rocket combustion chambers consist of an injector with many small injection elements (orifices), the chamber wall with or without cooling channels, and the conical nozzle throat. While the propellants are burning, the particles flow through discrete zones, namely, injection/atomization zones, rapid combustion zone, and stream tube combustion zone which can be influenced by the design of the injection orifices, the chamber geometry, the operation conditions, and the specific propellant combination.

Injection/Atomization Zone

At a velocity of approximately 7 to 60 m/s, liquid propellants are injected and vaporized through the base-plate. The appropriate injector design is very important for the following combustion because seemingly minor changes in designs have great influence on combustion instabilities. The distinctive designs are doublet impinging, triplet impinging, self-impinging, and shower head stream pattern, as well as hollow post and sleeve element, and variable injection area concentric tube injector. These different kinds of injectors manage the pressure drop or uncouple the chamber from the propellant feed system.

The propellants occur in both liquid and vaporized phases within the first zone. The chemical reactivity is small because the gases are relatively cold. Additionally, the vaporization is not yet completed because there are still fuel-rich and fuel-lean regions, which are not very reactive. However, local explosions occur due to combustion, which produce shock waves.

The shock waves travel to the nozzle throat. At the throat, the waves are reflected and travel back to the injection/atomization zone. During the startup phase of a rocket, the reflected waves can cause combustion instabilities.

Rapid Combustion Zone

In this zone, the propellants are highly reactive and combust at an increasingly higher temperature. The evaporation is completed and the propellants are further broken down into intermediate fractions, which increases the chemical reactivity tremendously. Besides the increase of the rate of heat, the local axial velocity is also increased by a

factor 100 or more. Farther down, the lateral velocities of the combustion products can be neglected compared to the high axial velocity.

The combustion is not a steady flow process. At one specific location, a rapid fluctuation in pressure, temperature, density, mixture ratio, and radiation emission can be observed with respect to time.

Stream Tube Combustion Zone

In this zone, the combustion reaction continues until the chemical equilibrium is reached. During this process, the combustion products provide some additional rate of heat. The axial velocity of the combustion products is approximately 200 to 600 m/s and it is accelerated to the speed of sound. Because of the high velocity, the residence time is very low compared to the time in the other two zones.

Transient Combustion

The transient combustion phenomena have not yet been fully understood. The zones -- injection/atomization, rapid combustion, stream tube combustion -- are basically the same; however, the influencing parameters for the size of each zone are still unknowns. Apparently, the injection velocity of the propellants not only has a significant influence on the size of the injection/atomization zone but also the different kinds of injection system determine the grade of atomization. Other influences are the mixture ratio during the start-up phase, the used propellant combination, temperature of the propellants, amount of ignitions (first or re-ignition), the combustion efficiency at ignition, etc. Further research needs to be done to specify certain influences on each other in order to predict combustion instability.

Chapter 6: Mathematical Formulation of the Governing Equations

In this chapter, the governing equations for the use in unsteady thermofluid mechanics are described. The means of verifying identity of propagative and bulk flow system responses is discussed for the determination of the proper mathematical equations for the transient physical flow phenomena. The governing equations are simplified using the means of normalization of unsteady flow systems. The final equations are numerically integrated by the technique *Method of Characteristics* (MOC).

6.1 Proof of Propagative and Bulk Flow

The physical phenomena in the feed lines have to be identified in order to obtain appropriate equations for the unsteady thermofluid mechanics in which the flow properties are continuous in both space and time. During the start-up phase of rocket engines, steep gradients or discontinuities in properties play an important factor. Proper analysis should cover property changes associated with acoustic and shock waves.

Propagation effects can be proven using the following procedure. It involves an estimation of the propagation time τ_p. The sources for system disturbances can be valve opening, abrupt change in dimensions, and/or ignition. The propagation time is defined as

$$\tau_p = \frac{L_r}{v_p}, \tag{6-1}$$

where L_r is the system reference length and v_p is the propagation speed or speed of sound in the system.

A criterion for bulk or propagative flow is given from reference[17]

Criterion for Bulk or Propagative Flows

Bulk flow if $\tau_p << \tau_d$ *; otherwise propagative flow* (6-2)

Propagation effects probably are not important in analysis When τ_p *is less than about* $0.1 \cdot \tau_d$

The following disturbance times are defined using the Figures 5.3 and 5.4 presented in chapter 5.

$$\tau_{d.valve} = 0.014\,s \qquad \tau_{d.dome} = 0.055\,s \qquad \tau_{d.ign} = 0.05\,s$$

The mean speed of sound for the oxygen and fuel branch is given using the following two empirical equations.

$$\text{NTO:}\quad a(t) = 2296\frac{m}{s} - 4.425\frac{l}{K}\cdot t \cdot 1\frac{m}{s} \tag{6-3}$$

$$\text{MMH:}\quad a(t) = 2711.6\frac{m}{s} - 3.903\frac{l}{K}\cdot t \cdot 1\frac{m}{s} \tag{6-4}$$

$$\text{NTO:}\quad a(293\,K) = 1000\frac{m}{s} \qquad \text{MMH:}\quad a(293\,K) = 1570\frac{m}{s}$$

Using equation (6-1) and the obtained values for the speed of sound, the proper propagation time can be calculated using a system reference length of approximately $L_r = 7\,m$ and a system reference temperature of 293 K.

$$\tau_p = \frac{L_r}{a(t)} \qquad \tau_p(NTO) = 0.0070\,s$$

$$\tau_p(MMH) = 0.0045\,s$$

The determining criterion for the analysis is the disturbance time of the valve stroke (opening) time $\tau_{d,valve}$. The two values of the propagation times, oxygen and fuel branch, due to the valve opening are used to determine if the filling process is a propagative flow or a bulk flow. Using the criterion (6-2), the assumption of a propagative flow can be made considering the fact that the propagation time is not less than about 0.1 of the disturbance time. However, a propagation flow analysis was assumed in order to capture moving shocks in the hydraulic feed lines to simulate POGO and low-frequency oscillations.

Oxygen branch: $\tau_p(\mathrm{NTO}) = 0.0070\,\mathrm{s}$ $\tau_{d,valve} = 0.014\,\mathrm{s}$ $\tau_p \approx 0.5 \cdot \tau_d$

Fuel branch: $\tau_p(\mathrm{MMH}) = 0.0045\,\mathrm{s}$ $\tau_{d,valve} = 0.014\,\mathrm{s}$ $\tau_p \approx 0.3 \cdot \tau_d$

6.2 One-Dimensional Thermofluid Systems

The mathematical derivation of one-dimensional thermofluid systems can be done after reference[17]. For a better understanding, Figure 6.1 shows a general model for the analysis of one-dimensional flow in hydraulic flow sections. The derivation includes an analysis where the flow area A can vary continuously in both space and time, heat transfer can occur from or to the walls, and heat conduction can also occur in the flow direction x. The fluid is arbitrary and friction effects are covered.

Using figure 6-1 (b), the mass conservation principle is applied for the stationary control volume (CV).

$$\frac{\partial \dot{m}}{\partial x} \cdot dx + \frac{\partial m}{\partial \tau} = 0 \qquad (6\text{-}5)$$

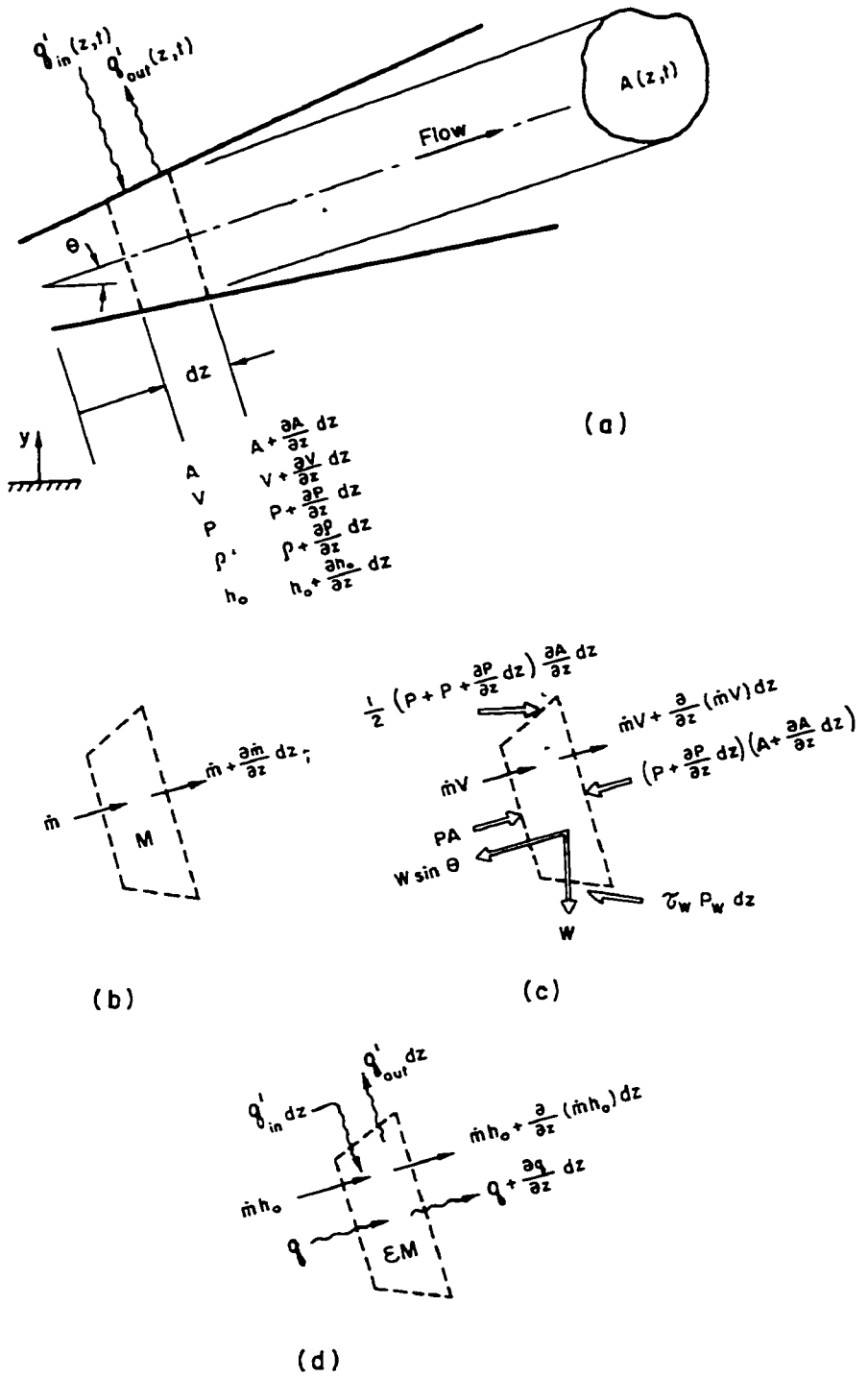

Figure 6.1: One-Dimensional Flow Model – (a) flow section, (b) mass conservation, (c) momentum, (d) energy conservation[17]

The momentum principle is applied using Figure 6-1 (c). The total force includes an average pressure force due to the varying flow section area with respect to space, the wall shear force, and a gravitational force.

$$F = -\left(A \cdot \frac{\partial p}{\partial x} \cdot dx + \tau_w \cdot P_w \cdot dx + m \cdot g \cdot \sin \Theta \right) \tag{6-6}$$

Shear stresses can be best explained using the analogy from strength of materials. The fluid fills the whole pipe and has a flow velocity; however, the fluid velocity equals zero at the contact area due to friction forces at the pipe wall. The fluid element is strained. The applied shear stress is then a function of the strain rate. The wall shear stress can be expressed using the Fanning, or small, friction factor f_F.

$$\tau_{w,steady} = f_F \cdot \frac{v^2}{2} \cdot \rho \tag{6-7}$$

In modern analysis; however, the large friction factor $f = 4 \cdot f_F$ is used. The equation governs only the steady state flow phenomenon; however, it is often permissible to also use it for transient analyses.

$$\tau_{w,steady} = \frac{f}{8} \cdot v^2 \cdot \rho \tag{6-8}$$

The value for the large friction factor f is taken from a plot of the Colebrook-White equation, also known as the Moody chart. However, the Colebrook-White equation requires an iterative solution and is not recommended for computer calculations. The following equation (6-9) can be used to express the large friction factor in an explicit form.

$$f = \frac{0.25}{\left[\log\left(\frac{k}{3.7 \cdot d} + \frac{5.74}{Re^{0.9}}\right)\right]^2}, \tag{6-9}$$

where k is the roughness value, d the pipe diameter, and Re the Reynolds number.

$$Re = \frac{\rho \cdot v \cdot L_r}{\mu} \tag{6-10}$$

Equation (6-9) provides a solution with similar accuracy to the Colebrook-White equation; however, the calculation is performed without iterations.

The rate of creation of momentum in the CV (6.1 c) is

$$ROC = \frac{\partial}{\partial x}(\dot{m} \cdot v) \cdot dx + \frac{\partial}{\partial \tau}(m \cdot v) \tag{6-11}$$

Using equation (6-5), equation (6-6), and expanding equation (6-11), the momentum principle can be written as equation (6-12).

$$\frac{\partial \dot{m}}{\partial x} \cdot dx = -\frac{\partial m}{\partial \tau} \qquad \text{from equation (6-5)}$$

$$\dot{m} \cdot \frac{\partial v}{\partial x} \cdot dx + \underbrace{v \cdot \frac{\partial \dot{m}}{\partial x} \cdot dx + v \cdot \frac{\partial m}{\partial \tau}}_{=0} + m \cdot \frac{\partial v}{\partial \tau} = ROC \qquad \text{from equation (6-9)}$$

$$m \cdot \frac{\partial v}{\partial \tau} + \dot{m} \cdot \frac{\partial v}{\partial x} \cdot dx = F \tag{6-12}$$

where F reflects equation (6-6).

The governing equation (6-13) for the energy principle can be derived using Figure 6-1 (d), which includes heating or cooling at the walls, heat conduction in the flow direction, and convected energy by mass flow.

$$\frac{\partial}{\partial x}(\dot{m}\cdot H)\cdot dx+\frac{\partial q}{\partial x}\cdot dx+\left(\dot{q}_{out}-\dot{q}_{in}\right)\cdot dx+\frac{\partial}{\partial \tau}(\Psi\cdot m)=0 \qquad (6\text{-}13)$$

Equation (6-13) is expanded, combined with equation (6-5), and the stagnation enthalpy replaced using $H=\Psi+\frac{p}{\rho}$.

$$\dot{m}\cdot\frac{\partial H}{\partial x}\cdot dx+\frac{p}{\rho}\cdot\frac{\partial \dot{m}}{\partial x}\cdot dx+\frac{\partial q}{\partial x}\cdot dx+\left(\dot{q}_{out}-\dot{q}_{in}\right)\cdot dx+m\cdot\frac{\partial \Psi}{\partial \tau}=0 \qquad (6\text{-}14)$$

Further replacements in equation (6-5), (6-11), (6-14) with the following expressions give the intermediate equations (6-15), (6-16), and (6-17).

$$\dot{m}=\rho\cdot v\cdot A \qquad \Psi=\frac{v^2}{2}+g\cdot y+e=H-\frac{p}{\rho}$$

$$m=\rho\cdot A\cdot dx \qquad q=-\kappa\cdot A\cdot\frac{\partial t}{\partial x}$$

$$V=A\cdot dx \qquad \frac{\tau_w\cdot P_w}{\rho\cdot A}=\frac{f\cdot v\cdot|v|}{2\cdot d_h}=\frac{f\cdot v\cdot|v|\cdot P_w}{8\cdot A}$$

Mass Conservation

$$\frac{\partial \rho}{\partial \tau}+v\cdot\frac{\partial \rho}{\partial x}+\rho\cdot\frac{\partial v}{\partial x}+\frac{\rho}{A}\cdot\left(\frac{\partial A}{\partial \tau}+v\cdot\frac{\partial A}{\partial x}\right)=0 \qquad (6\text{-}15)$$

Momentum Creation

$$\frac{\partial v}{\partial \tau}+v\cdot\frac{\partial v}{\partial x}+\frac{1}{\rho}\cdot\frac{\partial p}{\partial x}+\frac{f}{d_h}\cdot\frac{v\cdot|v|}{2}+g\cdot\sin\Theta=0 \qquad (6\text{-}16)$$

Energy Conservation

$$\frac{\partial H}{\partial \tau}+v\cdot\frac{\partial H}{\partial x}-\frac{1}{\rho}\cdot\frac{\partial p}{\partial \tau}-\frac{\kappa}{\rho}\cdot\left(\frac{\partial^2 t}{\partial x^2}+\frac{1}{A}\cdot\frac{\partial A}{\partial x}\cdot\frac{\partial t}{\partial x}\right)+\frac{\left(\dot{q}_{out}-\dot{q}_{in}\right)}{\rho\cdot A}=0 \qquad (6\text{-}17)$$

The stagnation enthalpy is replaced in equation (6-17) using following three equations for the total enthalpy, the static enthalpy, and the total differential of the static enthalpy, and further subsequent combination with (6-15) and (6-16) give the final equations (6-18) for the mass conservation and another intermediate equation (6-19) for the energy conservation.

$$H=\Psi+\frac{p}{\rho}=\frac{v^2}{2}+g\cdot y+h \qquad h=e+\frac{p}{\rho} \qquad dh=\left(\frac{1}{\rho}+\frac{c_p}{\beta\cdot\rho\cdot c^2}\right)\cdot dp-\left(\frac{c_p}{\beta\cdot\rho}\right)\cdot d\rho$$

$$\frac{\partial p}{\partial \tau}+v\cdot\frac{\partial p}{\partial x}+\rho\cdot c^2\cdot\frac{\partial v}{\partial x}+\rho\cdot c^2\cdot\left(\frac{\partial A}{\partial \tau}+v\cdot\frac{\partial A}{\partial x}\right)=\frac{\beta\cdot c^2}{c_p}\cdot F_I \qquad (6\text{-}18)$$

$$\frac{1}{c^2}\cdot\left(\frac{\partial p}{\partial \tau}+v\cdot\frac{\partial p}{\partial x}\right)-\left(\frac{\partial \rho}{\partial \tau}+v\cdot\frac{\partial \rho}{\partial x}\right)=\frac{\beta}{c_p}\cdot F_I \qquad (6\text{-}19)$$

Further combination of equation (6-19) with the following two thermodynamic property differential equations gives another useful equation (6-20) of the energy conservation.

$$dt=\left(\frac{1}{\rho\cdot\beta\cdot c^2}+\frac{\beta\cdot t}{\rho\cdot c_p}\right)\cdot dp-\frac{1}{\beta\cdot\rho}\cdot d\rho \qquad ds=\left(\frac{c_p}{\beta\cdot\rho\cdot t\cdot c^2}\right)\cdot dp-\left(\frac{c_p}{\beta\cdot\rho\cdot t}\right)\cdot d\rho$$

$$\frac{\partial t}{\partial \tau}+v\cdot\frac{\partial t}{\partial x}-\frac{\beta\cdot t}{\rho\cdot c_p}\cdot\left(\frac{\partial p}{\partial \tau}+v\cdot\frac{\partial p}{\partial x}\right)=\frac{1}{\rho\cdot c_p}\cdot F_I \qquad (6\text{-}20)$$

where

$$F_I=\kappa\cdot\left(\frac{\partial^2 t}{\partial x^2}+\frac{1}{A}\cdot\frac{\partial A}{\partial x}\cdot\frac{\partial t}{\partial x}\right)+\frac{f}{d_h}\cdot\rho\cdot\frac{v^3}{2}+\frac{\left(\dot{q}_{in}-\dot{q}_{out}\right)}{A} \qquad (6\text{-}21)$$

6.3 Normalization of Unsteady Flow Systems

The derived differential equations for one-dimensional flows in the previous section contain static pressure, velocity, and static temperature as dependent variables. Independent variables are time and space. These equations can be normalized and reduced for given system disturbances. The technique of normalization is therefore a powerful tool to reduce complex equations; however, important effects will be not dropped from the governing equations. Table 6.1 gives the normalized variables of the one-dimensional flow. Table 6.2 provides the model coefficients of the one-dimensional flow, and Table 6.3 shows the one-dimensional flow equations in a non-dimensional and dimensional form.

The normalization procedure involves a mathematical treatment of the independent variables space and time as well as the dependent variables pressure, velocity, and temperature.

The normalized time τ^* is expressed as the fraction of time τ and an estimated response time $\Delta\tau$.

$$\tau^* = \frac{\tau}{\Delta\tau} \tag{6-22}$$

The space variable is normalized with respect to the dimension of the considered region. Therefore, the length of the feed line would be the appropriate expected displacement L_r.

$$x^* = \frac{x}{L_r} \tag{6-23}$$

If the dependent variables appear in a derivative, they are normalized with respect to its estimated change

$$\Delta\Phi = \Phi_r - \Phi_i \tag{6-24}$$

where Φ_r is the expected maximum and Φ_i is the initial value.

The normalized form of dependent variables can be expressed as

$$\Phi^* = \frac{\Phi - \Phi_i}{\Delta\Phi} \tag{6-25}$$

Other parameters, which do not appear in derivatives of all governing equations can be expressed similarly as

$$\Psi^* = \frac{\Psi}{\Psi_r} \tag{6-26}$$

The normalized variables are substituted into the governing equations, which give non-dimensional groups (model coefficients). Depending on the magnitude of these model coefficients, the governing equations can be simplified by neglecting small terms. The reader can obtain more details in[17].

$p^* = \frac{p - p_i}{\Delta p}$	$c_p{}^* = \frac{c_p}{c_{pr}}$
$v^* = \frac{v - v_i}{\Delta v}$	$\rho^* = \frac{\rho - \rho_i}{\Delta \rho}$
$\beta^* = \frac{\beta}{\beta_r}$	$t^* = \frac{t - t_i}{\Delta t}$
$\kappa^* = \frac{\kappa}{\kappa_r}$	$\tau^* = \frac{\tau}{\Delta \tau}$
$x^* = \frac{x}{L_r}$	$q^* = \frac{q}{q_r}$
$d_h{}^* = \frac{d_h}{d_{hr}}$	$A^* = \frac{A}{A_r}$
$c^* = \frac{c}{c_r}$	

Table 6.1: Normalized Variables. One-Dimensional Flow[17]

$\pi_1 = \frac{\Delta p}{\rho_r \cdot c_r^2}$	$\pi_{10} = \frac{\beta_r \cdot \Delta p}{\rho_r \cdot c_{pr}}$
$\pi_2 = \frac{\Delta \tau \cdot \Delta v}{L_r}$	$\pi_{14} = \frac{f \cdot L_r}{d_h}$
$\pi_2^0 = \frac{v_i \cdot \Delta \tau}{L_r}$	$\pi_{15} = \frac{\beta_r \cdot L_r^2}{2 \cdot c_{pr} \cdot (\Delta \tau)^2}$
$\pi_3 = \frac{\Delta \rho}{\rho_r}$	$\pi_{16} = \frac{(\Delta \tau)^2 \cdot \sin \Theta}{L_r}$
$\pi_4 = \frac{\kappa_r \cdot \beta_r \cdot \Delta \tau \cdot \Delta t}{\rho_r \cdot L_r^2 \cdot c_{pr}}$	$\pi_{17} = \frac{q_r^* \cdot \Delta \tau}{\rho_r \cdot t_r \cdot A_r \cdot c_{pr}}$
$\pi_6 = \frac{\Delta p \cdot (\Delta \tau)^2}{\rho_r \cdot L_r^2}$	$\pi_{18} = \frac{L_r^2}{t_r \cdot c_{pr} \cdot (\Delta \tau)^2}$
$\pi_9 = \frac{\Delta t}{t_r}$	

Table 6.2: Model Coefficients. One-Dimensional Flow[17]

Mass Conservation *Non-Dimensional* (6-27 a)	*Dimensional* (6-27 b)
$\pi_1 \cdot \frac{1}{c^{*2}} \cdot \frac{\partial p^*}{\partial \tau^*}$ $+ \pi_1 \cdot \frac{1}{c^{*2}} \cdot \left(\pi_2 \cdot v^* + \pi_2^0\right) \cdot \frac{\partial p^*}{\partial x^*}$ $+ \pi_2 \cdot \left(\pi_3 \cdot \rho^* + 1\right) \cdot \frac{\partial v^*}{\partial x^*}$ $+ \left(\pi_3 \cdot \rho^* + 1\right) \cdot \frac{1}{A^*} \cdot \frac{\partial A^*}{\partial \tau^*}$ $+ \left(\pi_3 \cdot \rho^* + 1\right) \cdot \frac{1}{A^*} \cdot \left(\pi_2 \cdot v^* + \pi_2^0\right) \cdot \frac{\partial A^*}{\partial x^*}$ $= \frac{\beta^*}{c_p^*} \cdot F^*$	$\frac{1}{c^2} \cdot \frac{\partial p}{\partial \tau}$ $+ \frac{1}{c^2} \cdot v \cdot \frac{\partial p}{\partial x}$ $+ \rho \cdot \frac{\partial v}{\partial x}$ $+ \frac{\rho}{A} \cdot \frac{\partial A}{\partial \tau}$ $+ \frac{\rho}{A} \cdot v \cdot \frac{\partial A}{\partial x}$ $= \frac{\beta}{c_p} \cdot F$
Momentum Conservation *Non-Dimensional* (6-28 a)	*Dimensional* (6-28 b)
$\pi_2 \cdot \left(\pi_3 \cdot \rho^* + 1\right) \cdot \frac{\partial v^*}{\partial \tau^*}$ $+ \pi_2 \cdot \left(\pi_3 \cdot \rho^* + 1\right) \cdot \left(\pi_2 \cdot v^* + \pi_2^0\right) \cdot \frac{\partial v^*}{\partial x^*}$ $+ \pi_6 \cdot \frac{\partial p^*}{\partial x^*}$ $+ \frac{1}{2} \cdot \pi_{14} \cdot \left(\pi_3 \cdot \rho^* + 1\right) \cdot \left(\pi_2 \cdot v^* + \pi_2^0\right)^2$ $+ \pi_{16} \cdot \left(\pi_3 \cdot \rho^* + 1\right) = 0$	$\frac{\partial v}{\partial \tau}$ $+ v \cdot \frac{\partial v}{\partial x}$ $+ \frac{1}{\rho} \cdot \frac{\partial p}{\partial x}$ $+ \frac{f}{4} \cdot \frac{P_w}{A} \cdot \frac{\lvert v \rvert}{2} \cdot v$ $+ g \cdot \sin \Theta = 0$

Table 6.3: One-Dimensional Flow Equations[17]

Energy conservation	
Non-Dimensional (6-29 a)	*Dimensional* (6-29 b)
$\pi_9 \cdot (\pi_3 \cdot \rho^* + 1) \cdot c_p^* \cdot \frac{\partial t^*}{\partial \tau^*}$ $+ \pi_9 \cdot (\pi_3 \cdot \rho^* + 1) \cdot c_p^* \cdot (\pi_2 \cdot v^* + \pi_2^0) \cdot \frac{\partial t^*}{\partial x^*}$ $= \pi_{10} \cdot \beta^* \cdot (\pi_9 \cdot t^* + 1) \cdot \frac{\partial p^*}{\partial \tau^*}$ $+ \pi_{10} \cdot \beta^* \cdot (\pi_9 \cdot t^* + 1) \cdot (\pi_2 \cdot v^* + \pi_2^0) \cdot \frac{\partial p^*}{\partial x^*}$ $+ F^{**}$	$\rho \cdot c_p \cdot \frac{\partial t}{\partial \tau}$ $+ \rho \cdot c_p \cdot v \cdot \frac{\partial t}{\partial x}$ $= \beta \cdot t \cdot \frac{\partial p}{\partial \tau}$ $+ \beta \cdot t \cdot v \cdot \frac{\partial p}{\partial x}$ $+ F$
Function F	
Non-Dimensional (6-30 a)	*Dimensional* (6-30 a)
$\begin{Bmatrix} F^* \\ F^{**} \end{Bmatrix} = \begin{Bmatrix} \pi_4 \\ \pi_{11} \end{Bmatrix} \cdot \frac{1}{A^*} \cdot \frac{\partial}{\partial x^*} \cdot \left(\kappa^* \cdot A^* \cdot \frac{\partial t^*}{\partial x^*} \right)$ $+ \begin{Bmatrix} \pi_{13} \\ \pi_{17} \end{Bmatrix} \cdot \frac{\left(q_{in}^{**} - q_{out}^{**} \right)}{A^*}$ $+ \begin{Bmatrix} \pi_{14} & \pi_{15} \\ \pi_{14} & \pi_{18} \end{Bmatrix} \cdot \frac{(\pi_3 \cdot \rho^* + 1) \cdot (\pi_2 \cdot v^* + \pi_2^0)^3}{2 \cdot d_h^*}$	$F = \frac{1}{A} \cdot \frac{\partial}{\partial x} \cdot \left(\kappa \cdot A \cdot \frac{\partial t}{\partial x} \right)$ $+ \frac{\left(q_{in}^* - q_{out}^* \right)}{A}$ $+ \frac{f}{4} \cdot \frac{P_w}{A} \cdot \frac{\rho \cdot v^3}{2}$

Table 6.3 (contd.): One-Dimensional Flow Equations[17]

6.4 System Disturbances

The model coefficients in Table 6.1 include a selected space interval and response time for given phenomena of hydraulic systems. The following procedure explains how rapid pressure or velocity disturbances can be approximated using the waterhammer equation (6-31).

$$\Delta p = \rho_r \cdot c_r \cdot \Delta v \tag{6-31}$$

The density and temperature disturbance can be estimated using the following two equations (6-32) and (6-33).

$$\Delta \rho = \frac{1}{c_r^2} \cdot \Delta p \tag{6-32}$$

$$\Delta t = \frac{\beta_r \cdot t_0}{\rho_r \cdot c_{pr}} \cdot \Delta p \tag{6-33}$$

6.5 Application of the Derived Methods for the Determination of System Disturbances and Model Coefficients for the One-Dimensional Filling Process

6.5.1 Determination of the System Disturbances – Propagation Flow, Acoustic

The waterhammer equation (6-31) is used for the determination of the system disturbances as well as equation (6-32) and (6-33). In order to get an estimation of the velocity difference of the mass flow during the transient start-up phase, equation (6-34) as well as figure 5.2 and figure 5.3, respectively, are used. The pipe cross section is 36 mm and the density is calculated using the empirical equations (6-35) and (6-36) at a reference temperature of 293 K.

The liquid flow region is treated first.

$$\Delta v = \frac{\Delta \dot{m}}{\rho \cdot A} \qquad A = \frac{\pi}{4} \cdot d^2 \qquad A = 1.02 \cdot 10^{-3}\ m^2 \tag{6-34}$$

$$\rho_{N_2O_4}(t) = 2066\ K - 1.979 \cdot t - 0.0004826 \cdot t \tag{6-35}$$

$$\rho_{MMH}(t) = (1.15034\ K - 0.00093949 \cdot t) \cdot 1000 \tag{6-36}$$

$$\Delta v_{N_2O_4}(293\ K) = 1.3 \frac{m}{s} \qquad \Delta v_{MMH}(293\ K) = 1.2 \frac{m}{s}$$

Using these values and plugging them into the equation (6-31) provides an appropriate value for the pressure difference. Equations (6-32) and (6-33) are used successively in order to get the density and the temperature difference during the start-up phase.

$$\Delta p_{N_2O_4}(293\ K) \approx 18 \cdot 10^5\ Pa \qquad \Delta p_{MMH}(293\ K) \approx 46 \cdot 10^5\ Pa$$

$$\Delta \rho_{N_2O_4}(293\ K) \approx 1.8 \frac{kg}{m^3} \qquad \Delta \rho_{MMH}(293\ K) \approx 0.73 \frac{kg}{m^3}$$

The volume expansivity equals to zero for a liquid. Therefore, the temperature difference can be equated to zero.

$$\Delta t_{N_2O_4} = 0 \qquad \Delta t_{MMH} = 0$$

The two-phase region has to be treated differently because the volumetric expansivity approaches an infinite value for a saturated, bubble liquid-vapor mixture. However, it is seen that for a saturated, bubble liquid-vapor mixture following expression (6-37) has to be applied.

$$\frac{\beta}{c_p} = \frac{1}{\upsilon} \cdot \left(\frac{\partial \upsilon}{\partial h} \right)_p = \rho \cdot \frac{\upsilon_{fg}}{h_{fg}} \tag{6-37}$$

Expression (6-37) is evaluated in appendix A3. The two figures A3.1 and A3.2 show that the magnitude of the volumetric expansivity over the specific heat at constant pressure is very small. The maximal magnitudes are

$$\frac{\beta}{c_p}(N_2O_4) = 0.136$$

$$\frac{\beta}{c_p}(MMH) = -3.79 \cdot 10^{-3}$$

Using the normalization method and the Figures 5.3 and 5.4, a mass flow difference can be found for the oxygen of about 4 kg/s and for the fuel of about 1 kg/s, respectively. Recalling the definition of the normalization method: the expected maximum of the property has to be considered. Therefore, not only the mass flow difference has to be taken but also the density difference in order to get the velocity difference.

$$\Delta v = \frac{\Delta \dot{m}}{\Delta \rho \cdot A} \qquad A = \frac{\pi}{4} \cdot d^2 \qquad A = 1.02 \cdot 10^{-3}\ m^2 \tag{6-38}$$

The density of the two-phase region is very small in comparison to the liquid density. Therefore, the assumption to use the liquid density for the density difference can be made.

$$\Delta\rho_{N_2O_4}(t) = 2066\ K - 1.979 \cdot t - 0.0004826 \cdot t \tag{6-39}$$

$$\Delta\rho_{MMH}(t) = (1.15034\ K - 0.00093949 \cdot t) \cdot 1000 \tag{6-40}$$

$$\Delta v_{N_2O_4}(293\ K) = 2.64\ \frac{m}{s} \qquad \Delta v_{MMH}(293\ K) = 1.12\ \frac{m}{s}$$

Using these values, plugging them into the equation (6-31) provides an appropriate value for the pressure difference and the assumption of a decrease magnitude of the speed of sound. Equations (6-32) and (6-33) are used successively to obtain the density and the temperature difference during the start-up phase. The reference quality was chosen to be $x = 0.5$.

$$c_r \approx 100 \frac{m}{s} \quad \text{(assumption)}$$

$$\Delta p_{N_2O_4}(293\,K) \approx 0.00014 \cdot 10^5\ Pa \qquad \Delta p_{MMH}(293\,K) \approx 0.0000211 \cdot 10^5\ Pa$$

$$\Delta \rho_{N_2O_4}(293\,K) \approx 0 \qquad \Delta \rho_{MMH}(293\,K) \approx 0$$

$$\Delta t_{N_2O_4} \approx 0 \qquad \Delta t_{MMH} = 0$$

6.5.2 Determination of the Model Coefficients

The determination of the model coefficients takes into consideration the table 6.2 and the values for the system disturbances, calculated in the previous section. The two-phase region is captured with the same approach of finding the model coefficients in order to simplify matters. The approximated response time for the oxygen branch is $\Delta\tau_{N_2O_4} = 0.007\,s$ and for the fuel branch $\Delta\tau_{MMH} = 0.0045\,s$. The reference length is 7 meters. Table 6.4 gives the calculated model coefficients for the oxygen branch and Table 6.5 for the fuel branch, respectively.

$\pi_1 = 0.0035$	$\pi_{10} = 0.0035$
$\pi_2 = 0.0034$	$\pi_{14} =$ consider
$\pi_2^0 = 0$	$\pi_{15} = 0.499$
$\pi_3 = 0.0034$	$\pi_{16} = 0$
$\pi_4 = 0$	$\pi_{17} = 0$
$\pi_6 = 0.0035$	$\pi_{18} = 2.17$
$\pi_9 = 0.0034$	

Table 6.4: Calculated Model Coefficients for the Oxygen Branch

$\pi_1 = 0.0007$	$\pi_{10} = 0.0007$
$\pi_2 = 0.0007$	$\pi_{14} =$ consider
$\pi_2^0 = 0$	$\pi_{15} = 0.4435$
$\pi_3 = 0.0007$	$\pi_{16} = 0$
$\pi_4 = 0$	$\pi_{17} = 0$
$\pi_6 = 0.0007$	$\pi_{18} = 2.819$
$\pi_9 = 0.0007$	

Table 6.5: Calculated Model Coefficients for the Fuel Branch

The model coefficients for each branch are compared and all non-zero coefficients will be used for further analysis of the transient flow phenomena. Finally, the governing equations can be derived using table 6.3. It has to be taken into consideration that two distinctive flow phenomena occur, namely the flow of a simple compressible substance (SCS), and a saturated, bubble liquid mixture. Note that pressure and temperature are not independent in a multi-phase equilibrium system.

The final governing equations are solved by the method of characteristics in the following sections.

6.6 Solution by the Method of Characteristics (MOC)

6.6.1 Ideal Liquid

Mass Conservation

$$\frac{\partial p}{\partial \tau} + v \cdot \frac{\partial p}{\partial x} + \rho \cdot c^2 \cdot \frac{\partial v}{\partial \tau} + \rho \cdot c^2 \cdot \frac{1}{A} \cdot \frac{\partial A}{\partial \tau} + \rho \cdot c^2 \cdot \frac{1}{A} \cdot v \cdot \frac{\partial A}{\partial x} = \frac{c^2 \cdot \beta}{c_p} \cdot F_1 \qquad (6\text{-}41)$$

In the case of a rigid flow-section and an ideal liquid, Equation (6-41) can be further simplified to equation (6-42). A modified fluid-and-pipe speed of sound captures flexible pipes; see equation (6-43).

Requirement for rigid pipe: $\frac{\partial A}{\partial \tau} = 0$

Per definition for liquid phase: $\beta = 0$

$$\frac{\partial p}{\partial \tau} + v \cdot \frac{\partial p}{\partial x} + \rho \cdot c^2 \cdot \frac{\partial v}{\partial x} = -\rho \cdot \frac{1}{A} \cdot c^2 \cdot v \cdot \frac{\partial A}{\partial x} = F_2 \qquad (6\text{-}42)$$

$$c_{fp} = c \cdot \sqrt{\frac{1}{1 + \frac{d_{hyd} \cdot E}{Y_L \cdot \delta}}} \qquad (6\text{-}43)$$

where Y_L is the liquid elastic modulus. $Y_L = \rho \cdot c^2$

Momentum Creation

$$\frac{\partial v}{\partial \tau} + v \cdot \frac{\partial v}{\partial x} + \frac{1}{\rho} \cdot \frac{\partial p}{\partial x} = -\frac{f}{8} \cdot \frac{P_w}{A} \cdot v \cdot |v| = F_3 \qquad (6\text{-}44)$$

Energy Conservation

$$\frac{\partial t}{\partial \tau} + v \cdot \frac{\partial t}{\partial x} = \frac{\beta \cdot t}{\rho \cdot c_p} \cdot \frac{\partial p}{\partial \tau} + \frac{\beta \cdot t}{\rho \cdot c_p} \cdot v \cdot \frac{\partial p}{\partial x} + \frac{1}{\rho \cdot c_p} \cdot F_2 \qquad (6\text{-}45)$$

The equation (6-45) can be simplified in the same manner as it was done for the mass conservation ($\beta = 0$).

$$\frac{\partial t}{\partial \tau} + v \cdot \frac{\partial t}{\partial x} = \frac{1}{c_p} \cdot \frac{f}{8} \cdot \frac{P_w}{A} \cdot v^3 = F_4 \tag{6-46}$$

The total derivatives of the dependent variables pressure, velocity, and temperature are introduced. In addition, the equations (6-42), (6-44), and (6-46) are multiplied with unknown functions $\lambda_1, \lambda_2,$ and λ_3 and then added.

$$\frac{dp}{d\tau} = \frac{\partial p}{\partial \tau} + \frac{dx}{d\tau} \cdot \frac{\partial p}{\partial x} \qquad \frac{dv}{d\tau} = \frac{\partial v}{\partial \tau} + \frac{dx}{d\tau} \cdot \frac{\partial v}{\partial x} \qquad \frac{dt}{d\tau} = \frac{\partial t}{\partial \tau} + \frac{dx}{d\tau} \cdot \frac{\partial t}{\partial x}$$

$$\lambda_1 \cdot \frac{\partial p}{\partial \tau} + \lambda_1 \cdot v \cdot \frac{\partial p}{\partial x} + \lambda_1 \cdot \rho \cdot c^2 \cdot \frac{\partial v}{\partial x} + \lambda_2 \cdot \frac{\partial v}{\partial \tau} + \lambda_2 \cdot v \cdot \frac{\partial v}{\partial x} + \lambda_2 \cdot \frac{1}{\rho} \cdot \frac{\partial p}{\partial x} +$$
$$+ \lambda_3 \frac{\partial t}{\partial \tau} + \lambda_3 \cdot v \cdot \frac{\partial t}{\partial \tau} = \lambda_1 \cdot F_2 + \lambda_2 \cdot F_3 + \lambda_3 \cdot F_4 = F_5$$

$$\lambda_1 \cdot \frac{dp}{d\tau} - \lambda_1 \cdot \frac{dx}{d\tau} \cdot \frac{\partial p}{\partial \tau} + \lambda_1 \cdot v \cdot \frac{\partial p}{\partial \tau} + \lambda_1 \cdot \rho \cdot c^2 \cdot \frac{\partial v}{\partial x} +$$
$$+ \lambda_2 \cdot \frac{dv}{d\tau} - \lambda_2 \cdot \frac{dx}{d\tau} \cdot \frac{\partial v}{\partial x} + \lambda_2 \cdot v \cdot \frac{\partial v}{\partial x} + \lambda_2 \cdot \frac{1}{\rho} \cdot \frac{\partial p}{\partial x} +$$
$$\lambda_3 \cdot \frac{dt}{\partial \tau} - \lambda_3 \cdot \frac{dx}{d\tau} \cdot \frac{\partial t}{\partial x} + \lambda_3 \cdot v \cdot \frac{\partial t}{\partial x} = F_5$$

Collecting all the terms, we obtain equation (6-47).

$$\lambda_1 \cdot \frac{dp}{d\tau} + \lambda_2 \cdot \frac{dv}{d\tau} + \lambda_3 \cdot \frac{dt}{d\tau} + \underbrace{\left[-\lambda_1 \cdot \frac{dx}{d\tau} + \lambda_1 \cdot v + \lambda_2 \cdot \frac{1}{\rho} \right]}_{=0} \cdot \frac{\partial p}{\partial x} +$$
$$+ \underbrace{\left[\lambda_1 \cdot \rho \cdot c^2 - \lambda_2 \cdot \frac{dx}{d\tau} + \lambda_2 \cdot v \right]}_{=0} \cdot \frac{\partial v}{\partial x} + \underbrace{\left[-\lambda_3 \cdot \frac{dx}{d\tau} + \lambda_3 \cdot v \right]}_{=0} \cdot \frac{\partial t}{\partial x} = F_5 \tag{6-47}$$

The coefficients are set to zero to obtain two characteristic equations and one fluid particle path.

$$\begin{bmatrix} v-\frac{dx}{d\tau} & \frac{1}{\rho} & 0 \\ \rho\cdot c^2 & v-\frac{dx}{d\tau} & 0 \\ 0 & 0 & v-\frac{dx}{d\tau} \end{bmatrix}\cdot\begin{Bmatrix}\lambda_1\\ \lambda_2\\ \lambda_3\end{Bmatrix}=0 \qquad (6\text{-}48)$$

$$\left(v-\frac{dx}{d\tau}\right)\cdot\left(v-\frac{dx}{d\tau}\right)^2-c^2\cdot\left(v-\frac{dx}{d\tau}\right)=0$$

Case I (characteristics): $\left(v-\frac{dx}{d\tau}\right)=0 \qquad \lambda_3=0 \Rightarrow \qquad \frac{dx}{d\tau}=v\pm c$

Case II+III (fluid path): $\lambda_1=\lambda_2=0 \qquad \lambda_3\neq 0 \Rightarrow \qquad \frac{dx}{d\tau}=v$

Substituting the solutions for all cases into equation (6-48) gives the lambda relations for the right-traveling, left-traveling, and fluid path, respectively. The lambda values are substituted into equation (6-47) in order to get the final governing equations (6-49), (6-50), and (6-51) for the liquid fluid filled sections.

Right-traveling Characteristic:

$$\frac{dx}{d\tau}=v+c \qquad \frac{\lambda_2}{\lambda_1}=\rho\cdot c \qquad \lambda_3=0$$

$$dp+\rho\cdot c\cdot dv=-c^2\cdot\rho\cdot\frac{1}{A}\cdot v\cdot\frac{\partial A}{\partial x}\cdot d\tau-\rho\cdot c\cdot\frac{f}{8}\cdot\frac{P_w}{A}\cdot|v|\cdot v\cdot d\tau \qquad (6\text{-}49)$$

Left-traveling Characteristic:

$$\frac{dx}{d\tau} = v - c \qquad \frac{\lambda_2}{\lambda_1} = -\rho \cdot c \qquad \lambda_3 = 0$$

$$dp - \rho \cdot c \cdot dv = -c^2 \cdot \rho \cdot \frac{1}{A} \cdot v \cdot \frac{\partial A}{\partial x} \cdot d\tau + \rho \cdot c \cdot \frac{f}{8} \cdot \frac{P_w}{A} \cdot |v| \cdot v \cdot d\tau \qquad (6\text{-}50)$$

Fluid Path:

$$\frac{dx}{d\tau} = v \qquad \lambda_1 = \lambda_2 = 0 \qquad \lambda_3 \neq 0$$

$$dt = \frac{f}{8} \cdot \frac{P_w}{A} \cdot v^3 \cdot \frac{1}{c_p} \cdot d\tau \qquad (6\text{-}51)$$

6.6.2 Homogeneous Two-Phase Flow

A homogeneous model is assumed for the two-phase flow. This means that the molecular particle motion (temperature) is uniform throughout the flow region. In other words, the fluid properties are a mean value of the liquid and gaseous values. Using that assumption, a two-phase flow region can be predicted using the one-dimensional equations for mass, momentum, and energy conservation, respectively.

However, the properties -- pressure and temperature -- are dependent in the two-phase region. An intensive property -- the quality -- is introduced in order to distinguish a two-phase liquid-vapor mixture from one another. In the following derivation, pressure, velocity, and temperature are always taken as a mean value of the mixture.

The derivation of the governing equations can be done in a similar fashion; however, the volumetric expansivity is no longer zero. The following approach depicts only the difference between the liquid flow and the two-phase flow equations. The steps of the Method of Characteristics were performed in the same way.

The mass conservation principle is written for a stationary control volume as

$$\frac{\partial p}{\partial \tau}+v\cdot\frac{\partial p}{\partial x}+\rho\cdot c^2\cdot\frac{\partial v}{\partial x}+\rho\cdot c^2\cdot\frac{1}{A}\cdot\left(\frac{\partial A}{\partial \tau}+v\cdot\frac{\partial A}{\partial x}\right)=\frac{\beta\cdot c^2}{c_p}\cdot F_1 \qquad (6\text{-}52)$$

$$\text{where}\quad F_1=\kappa\cdot\left(\frac{\partial^2 t}{\partial x^2}+\frac{1}{A}\cdot\frac{\partial A}{\partial x}\cdot\frac{\partial t}{\partial x}\right)+\frac{f}{d_{hyd}}\cdot\rho\cdot\frac{v^3}{2}+\frac{\dot{q}_{in}-\dot{q}_{out}}{A}$$

Heat transfer and heat diffusion can be neglected. A flow area change can be captured by the modified sound speed. Hence, the mass conservation equation can be written in following form

$$\frac{\partial p}{\partial \tau}+v\cdot\frac{\partial p}{\partial x}+\rho\cdot c^2\cdot\frac{\partial v}{\partial x}=\frac{\beta\cdot c^2}{c_p}\cdot\left(\frac{f}{d_{hyd}}\cdot\rho\cdot\frac{v^3}{2}\right)-\rho\cdot c^2\cdot\frac{1}{A}\cdot v\cdot\frac{\partial A}{\partial x}=F_2 \qquad (6\text{-}53)$$

The momentum equation can be written as

$$\frac{\partial v}{\partial \tau}+v\cdot\frac{\partial v}{\partial x}+\frac{1}{\rho}\cdot\frac{\partial p}{\partial x}=-\frac{1}{2}\cdot\frac{f}{d_{hyd}}\cdot|v|\cdot v=F_3 \qquad (6\text{-}54)$$

The energy conservation principle is written as

$$\frac{\partial H}{\partial \tau}+v\cdot\frac{\partial H}{\partial x}-\frac{1}{\rho}\cdot\frac{\partial p}{\partial \tau}=0 \qquad (6\text{-}55)$$

The use of the energy conservation is most different to the single phase. The equation is not used to find the temperature or density; here, it is used to find the quality X.

The total enthalpy H is a sum of the specific kinetic energy, the specific potential energy, and the static enthalpy. The first two terms can be neglected; thus, the total enthalpy equals the static enthalpy.

$$H = \frac{v^2}{2} + g \cdot y + h \qquad => \qquad H = h \tag{6-56}$$

The final form of the energy conservation principle is written as

$$\frac{\partial h}{\partial \tau} + v \cdot \frac{\partial h}{\partial x} - \frac{1}{\rho} \cdot \frac{\partial p}{\partial \tau} = 0 \tag{6-57}$$

The entire flow phenomena are described by the three principle equations, namely mass, momentum, and energy, respectively. These three equations are a system of quasi-linear equations, where the dependent variables are static pressure, velocity, and static enthalpy, functions of space and time. They are expanded in such a way that the result provides uncoupled ordinary differential equation in terms of dp, dv, and dh.

The dependent variables are written using the total differential, solved for the partial with respect to time, and substituted into the equations (6-53), (6-54), and (6-57).

$$dp = \frac{\partial p}{\partial x} \cdot dx + \frac{\partial p}{\partial \tau} \cdot d\tau \qquad dv = \frac{\partial v}{\partial x} \cdot dx + \frac{\partial v}{\partial \tau} \cdot d\tau \qquad dh = \frac{\partial h}{\partial x} \cdot dx + \frac{\partial h}{\partial \tau} \cdot d\tau$$

The mathematical treatment is similar in order to obtain the characteristics and the fluid particle path. Finally, the following three equations can be found.

Right Traveling Characteristics

$$\frac{dp}{d\tau} + \rho \cdot c \cdot \frac{dv}{d\tau} = \left(\frac{\beta \cdot c^2}{c_p} \cdot \frac{f}{d_{hyd}} \cdot \rho \cdot \frac{v^3}{2} - \rho \cdot c^2 \cdot \frac{1}{A} \cdot v \cdot \frac{\partial A}{\partial x} - \rho \cdot c \cdot \frac{f}{d_{hyd}} \cdot \frac{1}{2} \cdot |v| \cdot v \right) \tag{6-58}$$

Left Traveling Characteristics

$$\frac{dp}{d\tau}+\rho\cdot c\cdot\frac{dv}{d\tau}=\left(\frac{\beta\cdot c^2}{c_p}\cdot\frac{f}{d_{hyd}}\cdot\rho\cdot\frac{v^3}{2}-\rho\cdot c^2\cdot\frac{l}{A}\cdot v\cdot\frac{\partial A}{\partial x}-\rho\cdot c\cdot\frac{f}{d_{hyd}}\cdot\frac{l}{2}\cdot|v|\cdot v\right) \quad (6\text{-}59)$$

Fluid Particle Path

$$-\frac{l}{\rho}\cdot\frac{dp}{d\tau}+\frac{dh}{d\tau}=0 \quad (6\text{-}60)$$

6.7 Flow Through Injection Elements

The two-phase jet is resolved into drops in the following three ways, namely, capillary resolution, oscillation, and atomization, which occur successively, as the velocity of the jet increases.

A swirl injection type is implemented in the upper stage engine's baseplate. The following Figure 6.2 shows the *Aestus* engine injection element.

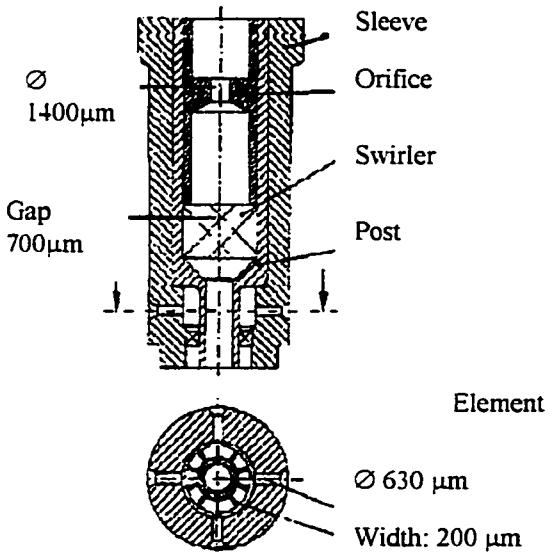

Figure 6.2: *Aestus* Engine Injection Element[25]

Oxygen flows through the orifice and decreases; however, it is still pushed through the swirler due to the upstream pressure in the oxygen dome. In the small auxiliary chamber, the fluid is calmed to obtain a continuous flow through the swirler. The purpose of the swirler is to bring the oxygen into rotation. After the swirler, the oxygen is filled into the conical sheet made up of fine droplets. The oxygen is pushed further; however, it does not fill the entire exit orifice because of the angular momentum due to the rotation.

The fuel flows through tiny lateral holes at the end of the sleeve. The atomization is due to the rapid flow velocity reduction and the extreme change in flow direction.

The propellants are atomized and ignited immediately in the combustion chamber.

One of the characteristic parameters involved here is the discharge coefficient. The discharge coefficient was determined experimentally; however, the following important facts should be kept in mind. The parameter is not a constant value but varies with the injection pressure drop (pressure in the dome versus pressure in the combustion chamber), the temperature, the nature of the liquid injected, and the geometry of the injector. The following values were experimentally determined:

Ox-Branch: $c_{d,ox} = 0.42$ with a reference area $A = 3.359 \cdot 10^{-4}\ m^2$ and reference pressure drop $\Delta p_{ref} = 5.98$ bar

Fu-Branch: $c_{d,f} = 0.468$ with a reference area $A = 2.64 \cdot 10^{-4}\ m^2$ and reference pressure drop $\Delta p_{ref} = 3.46$ bar

The incoming mass flow of the oxygen as well as the fuel into the combustion chamber can be calculated using the quasi steady state equation (6-60).

$$\dot{m}_{in,comb} = c_d \cdot A_{ref} \cdot \sqrt{2 \cdot \Delta p_{ref} \cdot \rho} \tag{6-61}$$

Equation (6-60) is used to provide the incoming mass flows for the combustion chamber model, described in the next section. Using the continuity equation and solving for the velocity provides the initial flow velocity in the chamber.

6.8 Simplified Combustion Model

The combustion model described here is using a modified approach of the paper AIAA-90-2299[23], which applies the Transient Performance Program (TTP) and Liquid Engine Transient Simulation (LETS) computer codes. The original approach employs a modified one-dimensional isentropic Saint-Vernaint Wantzel equation to obtain the mass efflux. In the described approach, transient principles are applied. The entire analysis relies on the one-dimensional equilibrium (ODE) thermochemistry code[23] or better known as Gordon-McBride code to determine the thermodynamic properties of the products of the combustion.

The chamber pressure can be determined using the ideal gas law

$$p = \frac{m \cdot \Re \cdot t}{V \cdot M} \tag{6-62}$$

where V, m, T, and M represent the volume of the combustion chamber, the mass, temperature, and molecular weight of the gaseous combustion products within the chamber, respectively.

Equation (6-61) is differentiated with respect to time to obtain the pressure variation.

$$\frac{dp}{d\tau} = \frac{\Re \cdot t}{M \cdot V} \cdot \frac{dm}{d\tau} + \frac{\Re \cdot m}{V \cdot M} \cdot \frac{dt}{d\tau} - \frac{\Re \cdot m \cdot t}{V} \cdot \frac{dM}{d\tau}$$

Note: The chamber volume is the geometric volume and $\Re$ the general gas constant; therefore, they do not need to be differentiated with respect to time. The terms in front of the time derivatives can be replaced using the equation of the ideal gas law. The intermediate equation (6-62) for the rate of combustion pressure is given as

$$\frac{dp}{d\tau} = \frac{p}{m} \cdot \frac{dm}{d\tau} + \frac{p}{t} \cdot \frac{dt}{d\tau} - \frac{p}{M} \cdot \frac{dM}{d\tau} \qquad (6\text{-}63)$$

The temperature and molecular weight of the combustion products are functions of the mixture ratio or fuel fraction and chamber pressure for combustion processes. Thus, writing the total derivatives for temperature, molecular weight, and substituting into equation above will give the final equation (6-65) for the rate of change of pressure due to the combustion of the incoming mass flows.

$$\frac{dt}{d\tau} = \left(\frac{\partial t}{\partial p}\right) \cdot \frac{dp}{d\tau} + \left(\frac{\partial t}{\partial f_f}\right) \cdot \frac{df_f}{d\tau} \qquad \frac{dM}{d\tau} = \left(\frac{\partial M}{\partial p}\right) \cdot \frac{dp}{d\tau} + \left(\frac{\partial M}{\partial f_f}\right) \cdot \frac{df_f}{d\tau} \qquad (6\text{-}64\ a/b)$$

$$\frac{dp}{d\tau} = \frac{\frac{p}{m} \cdot \frac{dm}{d\tau} + \frac{p}{t} \cdot \left(\frac{\partial t}{\partial f_f}\right) \cdot \frac{df_f}{d\tau} - \frac{p}{M} \cdot \left(\frac{\partial M}{\partial f_f}\right) \cdot \frac{df_f}{d\tau}}{\left[1 - \frac{p}{t} \cdot \left(\frac{\partial t}{\partial p}\right) + \frac{p}{M} \cdot \left(\frac{\partial M}{\partial P}\right)\right]} \qquad (6\text{-}65)$$

The equation (6-65) can be solved using relations for the mass balance and combustion thermodynamics.

The time rate of change of mass stored within the combustion chamber is defined as

$$\frac{dm}{d\tau} = \dot{m}_{in} - \dot{m}_{out} \tag{6-66}$$

where m is the mass held within the chamber at time t, and $\dot{m}_{in}$ and $\dot{m}_{out}$ are the influx and efflux of mass, respectively. The propellants enter the chamber independently and ignite immediately. When the transient begins, the sudden change in mass influx in the formation for a pressure or shock wave, which propagates through the chamber toward the throat of the nozzle. Therefore, the mass efflux can be calculated using the Methods of Characteristics to find the pressure and velocity of the combustion products particle. The mass efflux can be found applying the one-dimensional mass conservation. The initial conditions are defined by equation (6-61) for the velocity directly and by equation (6-65) for the pressure indirectly. It should be mentioned that the combustion chamber model does not take into considerations any ignition delays, which are common for hypergolic propellants.

The thermochemistry code requires knowledge of the relative masses of fuel and oxidizer, m_f and m_o, within the chamber. Defining the fuel fraction will provide the relative masses.

$$f_f = \frac{m_f}{m_f + m_o} = \frac{m_f}{m} \tag{6-67}$$

Equation (6-66) is expressed in a differential form

$$\frac{df_f}{d\tau} = \frac{1}{m}\cdot\frac{dm_f}{d\tau} - \frac{m_f}{m^2}\cdot\frac{dm}{d\tau} \tag{6-68}$$

It is assumed that the mass within the chamber is well mixed; therefore, the fuel fraction of the efflux is equivalent to that of the chamber. Thus, the mass of fuel within the chamber can be determined as

$$\frac{dm_f}{d\tau} = \dot{m}_{f,in} - f_f \cdot \dot{m}_{out} \tag{6-69}$$

Equations (6-66) and (6-69) are combined with equation (6-67) to express the fuel fraction variation as

$$\frac{df_f}{d\tau} = \frac{(1-f_f)\cdot \dot{m}_{f,in} - f_f \cdot \dot{m}_{o,in}}{m}. \tag{6-70}$$

The combustion reaction is controlled by the fuel fraction within the chamber, and to a lesser extent, the pressure of the propellant mixture. Given the values of the fuel fraction and pressure at time, the one-dimensional equilibrium (ODE) thermochemistry code will determine the products of combustion and the properties of the product gas. In particular, the reaction of flame temperature is given along with the molecular weight.

Furthermore, the combustion model assumes a gradual, one-dimensional filling of the combustion chamber with the combustion products. The filling process can be described best by the method of characteristics.

Writing the three principles for a steady control volume gives the equations for mass conservation, momentum creation, and energy conservation.

Mass Conservation

$$\frac{\partial p}{\partial \tau} + v \cdot \frac{\partial p}{\partial x} + \rho \cdot c^2 \cdot \frac{\partial v}{\partial x} = -\rho \cdot c^2 \cdot \frac{1}{A} \cdot \frac{dA}{dx} \cdot v + \frac{\beta \cdot c^2}{c_p} \cdot \Im \tag{6-71}$$

Momentum Conservation

$$\frac{\partial v}{\partial \tau}+v\cdot\frac{\partial v}{\partial x}+\frac{1}{\rho}\cdot\frac{\partial p}{\partial x}=-\frac{f\cdot P_w}{8\cdot A}\cdot|v|\cdot v-g\cdot\sin\Theta \tag{6-72}$$

Energy Conservation

$$\frac{\partial \rho}{\partial \tau}+v\cdot\frac{\partial \rho}{\partial x}-\frac{1}{c^2}\cdot\left(\frac{\partial p}{\partial \tau}+v\cdot\frac{\partial p}{\partial x}\right)=-\frac{\beta}{c_p}\cdot\Im \tag{6-73}$$

where

$$\Im=\frac{\left(\dot{q}_{in}-\dot{q}_{out}\right)}{A}+\frac{f\cdot P_w}{8\cdot A}\cdot\rho\cdot v^3$$

The three principle equations can be simplified applying following assumptions: Heat transfer, geodetic difference, and wall friction are negligible.

Mass Conservation

$$\frac{\partial p}{\partial \tau}+v\cdot\frac{\partial p}{\partial x}+\rho\cdot c^2\cdot\frac{\partial v}{\partial x}=-\rho\cdot c^2\cdot\frac{1}{A}\cdot\frac{dA}{dx}\cdot v \tag{6-74}$$

Momentum Creation

$$\frac{\partial v}{\partial \tau}+v\cdot\frac{\partial v}{\partial x}+\frac{1}{\rho}\cdot\frac{\partial p}{\partial x}=0 \tag{6-75}$$

Energy Conservation

$$\frac{\partial \rho}{\partial \tau}+v\cdot\frac{\partial \rho}{\partial x}-\frac{1}{c^2}\cdot\left(\frac{\partial p}{\partial \tau}+v\cdot\frac{\partial p}{\partial x}\right)=0 \tag{6-76}$$

Using the Method of Characteristics, the governing equations for the two characteristics and the fluid particle path can be found as

Right Traveling Characteristics

$$dp + \rho \cdot c \cdot dv = -\rho \cdot c^2 \cdot \frac{1}{A} \cdot v \cdot \frac{\partial A}{\partial x} \cdot d\tau \tag{6-77}$$

Left Traveling Characteristics

$$dp - \rho \cdot c \cdot dv = -\rho \cdot c^2 \cdot \frac{1}{A} \cdot v \cdot \frac{\partial A}{\partial x} \cdot d\tau \tag{6-78}$$

Fluid Particle Path

$$-\frac{1}{c^2} \cdot \frac{dp}{d\tau} + \frac{d\rho}{d\tau} = 0 \tag{6-79}$$

The assumption of a localized combustion has to be made if equations (6-77). (6-78), and (6-79) are used to determine the pressure and density of the combustion products. In reality, the propellants have still reactivity left. Recalling the combustion theory in chapter 5, the combustion takes place between the injector baseplate and the nozzle throat.

The main attempt of choosing such a combustion model was to establish an influencing boundary condition -- moving shock waves in the combustion chamber -- for the entire hydraulic system in order to get a fully coupled system.

Chapter 7: Fundamentals of the Numeric

The Method of Characteristics (MOC) provides the compatibility equation for the coupled partial differential equations of the system. Compatibility equations involve the unknown dependent variable, which holds only along the characteristic lines. One of the advantages of those equations is that they have one fewer dimension than the original partial differential equations. The governing equations depend on two dimensions, space and time, whereas the compatibility equations depend only on one dimension, which is along the characteristic direction.

Shocks are not covered by the MOC; however, the MOC captures shocks in form of steep pressure gradients over a couple of mesh points[17].

Numerical solution techniques involve three steps: Derivation of the governing equation, discretization (finite difference, finite volume, and finite element) of the computational domain (instead of the physical domain), basic derivation of the finite modules, types of solutions (explicit and implicit), and finally the stability analysis.

In the case of the one-dimensional Method of Characteristics, the stability analysis can be avoided for a proper choice of the discretization (time and space difference). It also uses an explicit solution method associated with Euler's method.

7.1 Finite-Difference Expression for Euler's Method[1]

In Euler's method, the derivative is expressed with a finite difference of first-order-accurate. The finite difference was derived uses a Taylor series expansion, where the truncation error was defined from the remaining terms on the right side.

$$\left(\frac{\partial u}{\partial x}\right)_{i,j} = \underbrace{\frac{u_{i+1,j}-u_{i,j}}{\Delta x}}_{\text{Finite Difference Representation}} \underbrace{-\left(\frac{\partial^2 u}{\partial x^2}\right)_{i,j}\cdot\frac{\Delta x}{2}-\left(\frac{\partial^3 u}{\partial x^3}\right)_{i,j}\cdot\frac{(\Delta x)^2}{6}+.....}_{\text{Truncation Error}} \qquad (7\text{-}1)$$

In equation (7-1), the lowest-order term in the truncation error involves the finite-difference to the first power; therefore, the finite-difference equation (7-2) is called first-order-accurate.

$$\left(\frac{\partial u}{\partial x}\right)_{i,j} = \frac{u_{i+1,j}-u_{i,j}}{\Delta x}+O(\Delta x) \qquad (7\text{-}2)$$

In this work, the variable u reflects the variable pressure, velocity, enthalpy, and density. The finite difference Δx reflects the time difference $\Delta\tau$.

7.2 Computational Mesh and Discretization of the Governing Equations[17]

The physical flow sections are divided into a computational mesh, which is divided into equal time and space increments. If the time and space increments are related with equation (7-3), the computation is always stable.

$$\Delta\Phi = c\cdot\Delta\tau \qquad (7\text{-}3)$$

The characteristic lines pass through general mesh points i, j; whereas the fluid particle path passes through point P shown in Figure 7.1.

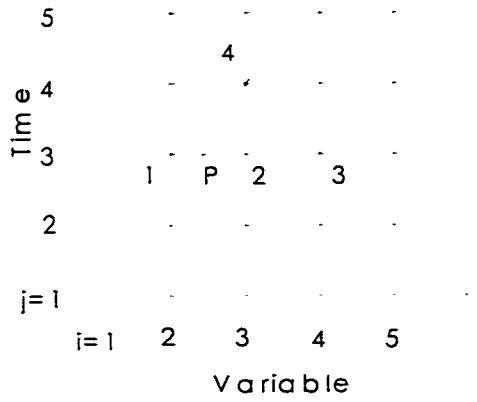

Figure 7.1: Computational Mesh

The next step is to replace the differentials in the compatibility equations with the finite difference equation (7-2) and to solve for the unknown properties at point P.

7.2.1 Discretization of the Compatibility Equation for the Liquid Flow Equations

The flow velocity does not exceed the speed of sound during the start-up phase; therefore, the following derivation is only done for non-critical (subcritical) flow. Values of the fluid properties at point P of Figure 7-1 is interpolated using mesh points 1, 2, and 3 as

$$\Phi_P = \Phi_2 + (\Phi_1 - \Phi_2) \cdot \frac{\Delta x_P}{\Delta x} \tag{7-4}$$

with

$$\frac{\Delta x_P}{\Delta \tau} = \frac{v_2}{c + v_2 - v_1} \qquad \text{and} \qquad \Phi = p, v, t, c \tag{7-5}$$

The finite difference forms of equations (6-49), (6-50), and (6-51) for computation of pressure, velocity, and temperature at point P become equations (7-6), (7-7), and (7-8).

$$(p_4 - p_1) + \rho_1 \cdot c_1 \cdot (v_4 - v_1) = \left(\underbrace{-c_1^2 \cdot \rho_1 \cdot \frac{1}{A_1} \cdot v_1 \cdot \left.\frac{dA}{dx}\right|_1}_{a_1} \underbrace{- c_1^2 \cdot \rho_1 \cdot \frac{f}{8} \cdot \left.\frac{P_w}{A}\right|_1 \cdot |v|_1 \cdot v_1}_{b_1} \right) \cdot d\tau \tag{7-6}$$

$$(p_4 - p_3) - \rho_3 \cdot c_3 \cdot (v_4 - v_3) = \left(\underbrace{-c_3^2 \cdot \rho_3 \cdot \frac{1}{A_3} \cdot v_3 \cdot \left.\frac{dA}{dx}\right|_3}_{a_3} \underbrace{+ c_3^2 \cdot \rho_3 \cdot \frac{f}{8} \cdot \left.\frac{P_w}{A}\right|_3 \cdot |v|_3 \cdot v_3}_{b_3} \right) \cdot d\tau \tag{7-7}$$

$$(t_4 - t_P) = \frac{f}{8} \cdot \left.\frac{P_w}{A}\right|_P \cdot v_P^3 \cdot \left.\frac{1}{c_p}\right|_P \cdot d\tau \tag{7-8}$$

with $$t_P = t_2 + (t_1 - t_2) \cdot \frac{v_2}{c + v_2 - v_1} \tag{7-9}$$

$$v_P = v_2 + (v_1 - v_2) \cdot \frac{v_2}{c + v_2 - v_1} \tag{7-10}$$

$$c_{p,P} = c_{p,P}(t)$$

Equations (7-6) and (7-7) are solved simultaneously for point P. to obtain equations (7-11) and (7-12).

$$v_4 = -\frac{1}{\rho_1 \cdot c_1 + \rho_3 \cdot c_3} \cdot \begin{bmatrix} (a_3 + b_3 - a_1 - b_1) \cdot d\tau + (p_3 - p_1) + \\ + (-\rho_1 \cdot c_1 \cdot v_1 - \rho_3 \cdot c_3 \cdot v_3) \end{bmatrix} \tag{7-11}$$

$$p_4 = a_1 \cdot d\tau + b_1 \cdot d\tau + p_1 - \rho_1 \cdot c_1 \cdot v_4 + \rho_1 \cdot c_1 \cdot v_1 \tag{7-12}$$

with $a_1 = -c_1^2 \cdot \rho_1 \cdot \frac{1}{A_1} \cdot v_1 \cdot \left.\frac{dA}{dx}\right|_1$ $\qquad a_3 = -c_3^2 \cdot \rho_3 \cdot \frac{1}{A_3} \cdot v_3 \cdot \left.\frac{dA}{dx}\right|_3$

$b_1 = -\rho_1 \cdot c_1 \cdot \frac{f}{8} \cdot \left.\frac{P_w}{A}\right|_1 \cdot |v|_1 \cdot v_1$ $\qquad b_3 = -\rho_3 \cdot c_3 \cdot \frac{f}{8} \cdot \left.\frac{P_w}{A}\right|_3 \cdot |v|_3 \cdot v_3$

It should be mentioned that all thermodynamic and fluid dynamic properties are liquid phase properties.

7.2.2 Discretization of the Compatibility Equation for the Homogeneous Two-Phase Flow Equations

Using the same procedure as described for the liquid phase flow, the flow properties for the two-phase flow, using the equations (6-58), (6-59), and (6-60) from previous chapter 6.4.3, can be calculated as

$$\begin{aligned} p_4 = {} & \frac{\beta_1 \cdot c_1^2}{c_{p,l}} \cdot \frac{f}{d_{hyd}} \cdot \rho_1 \cdot \frac{v_1^3}{2} \cdot d\tau - \rho_1 \cdot c_1^2 \cdot \frac{1}{A} \cdot v_1 \cdot \left.\frac{\partial A}{\partial x}\right|_1 \cdot d\tau - \\ & - \rho_1 \cdot c_1 \cdot \frac{f}{d_{hyd}} \cdot \frac{1}{2} \cdot |v|_1 \cdot v_1 \cdot d\tau - \rho_1 \cdot c_1 \cdot (v_4 - v_1) + p_1 \end{aligned} \tag{7-13}$$

$$v_4 = \frac{1}{(\rho_1 \cdot c_1 + \rho_3 \cdot c_3)} \cdot \left[\begin{array}{l} \frac{\beta_1 \cdot c_1^2}{c_{p,1}} \cdot \frac{f}{d_{hyd}} \cdot \rho_1 \cdot \frac{v_1^3}{2} \cdot d\tau - \rho_1 \cdot c_1^2 \cdot \frac{1}{A} \cdot v_1 \cdot \left. \frac{\partial A}{\partial x} \right|_1 \cdot d\tau \\ - \rho_1 \cdot c_1 \cdot \frac{f}{d_{hyd}} \cdot \frac{1}{2} \cdot |v|_1 \cdot v_1 \cdot d\tau \\ - \frac{\beta_3 \cdot c_3^2}{c_{p,3}} \cdot \frac{f}{d_{hyd}} \cdot \rho_3 \cdot \frac{v_3^3}{2} \cdot d\tau + \rho_3 \cdot c_3^2 \cdot \frac{1}{A} \cdot v_3 \cdot \left. \frac{\partial A}{\partial x} \right|_3 \cdot d\tau \\ + \rho_3 \cdot c_3 \cdot \frac{f}{d_{hyd}} \cdot \frac{1}{2} \cdot |v|_3 \cdot v_3 \cdot d\tau + \rho_1 \cdot c_1 \cdot v_1 \\ \rho_3 \cdot c_3 \cdot v_3 + p_1 - p_3 \end{array} \right] \quad (7\text{-}14)$$

$$h_4 = \frac{1}{\rho} \cdot (p_4 - p_P) + h_P \quad (7\text{-}15)$$

with

$$h_P = h_2 + (h_1 - h_2) \cdot \frac{v_2}{c + v_2 - v_1} \qquad p_P = p_2 + (p_1 - p_2) \cdot \frac{v_2}{c + v_2 - v_1} \quad (7\text{-}16a/b)$$

The following properties are calculated using the solutions of previous time steps.

$$\frac{\beta}{c_p} = \frac{1}{\upsilon} \cdot \left(\frac{\partial \upsilon}{\partial h} \right)_p = \frac{1}{\upsilon} \cdot \frac{\upsilon_{fg}}{h_{fg}} \qquad \upsilon_{fg} = \frac{1}{\rho_{fg}}$$

$$\rho = \frac{\rho_g \cdot \rho_f}{x \cdot \rho_f + \rho_g \cdot (1 - x)} \qquad h_{fg} = \frac{h_g \cdot h_f}{h_g - h_f} \qquad \rho_{fg} = \frac{\rho_g \cdot \rho_f}{\rho_g - \rho_f}$$

The quality x can be found from the static enthalpy of the mixture.

$$x = \frac{h - h_f}{h_g - h_f} \quad (7\text{-}17)$$

The corresponding temperature of the mixture is calculated from the empirical equation (7-18).

$$t = 0.18441 \cdot p_S^3 - 157.6 \cdot p_S^2 + 45128 \cdot p_S - 4325700 \tag{7-18}$$

The speed of sound for a two-phase mixture can be expressed as

$$c = \sqrt{-\upsilon \cdot \frac{\left(\frac{dh}{dt}\right)_S}{\left(\frac{d\upsilon}{dt}\right)_S}} \tag{7-19}$$

where

$$\left(\frac{dh}{dt}\right)_S = \frac{1}{\rho_f} \cdot \frac{dp_S}{dt} + \frac{1}{t} \cdot (h - h_f) \tag{7-20}$$

$$\left(\frac{d\upsilon}{dt}\right)_S = \frac{d}{dt}\frac{1}{\rho_f} - \frac{1}{h_{fg} \cdot \upsilon_{fg}} \cdot \left(\frac{dh_f}{dt} - \frac{1}{\rho_f} \cdot \frac{dp_S}{dt}\right) + \frac{d}{dt} \cdot \left(\frac{h - h_f}{h_{fg} \cdot \rho_{fg}}\right) \tag{7-21}$$

It should be mentioned that all thermodynamic and fluid dynamic properties are expressed for a homogeneous, two-phase-flow phenomena.

7.2.3 Discretization of the Compatibility Equation for the Simplified Combustion Chamber Model

The points for the numerical mesh can be calculated similarly to the previous two sections. Only subcritical flow needs to be considered because the products of combustion are accelerated up to the speed of sound until the nozzle throat. At the nozzle throat, the speed of sound is reached.

$$p_4 = -\rho_1 \cdot c_1^2 \cdot \frac{1}{A} \cdot v_1 \cdot \left.\frac{\partial A}{\partial x}\right|_1 \cdot d\tau - \rho_1 \cdot c_1 \cdot (v_4 - v_1) + p_1 \tag{7-22}$$

$$v_4 = \frac{1}{(\rho_1 \cdot c_1 + \rho_3 \cdot c_3)} \cdot \left[\begin{array}{l} \left(-\rho_1 \cdot c_1^2 \cdot \frac{1}{A} \cdot v_1 \cdot \left.\frac{\partial A}{\partial x}\right|_1 + \rho_3 \cdot c_3^2 \cdot \frac{1}{A} \cdot v_3 \cdot \left.\frac{\partial A}{\partial x}\right|_3 \right) \cdot d\tau \\ + \rho_1 \cdot c_1 \cdot v_1 + \rho_3 \cdot c_3 \cdot v_3 + p_1 - p_3 \end{array} \right] \quad (7\text{-}23)$$

$$\rho_4 = \frac{1}{c^2} \cdot (p_4 - p_P) + \rho_P \quad (7\text{-}24)$$

with

$$\rho_P = \rho_2 + (\rho_1 - \rho_2) \cdot \frac{v_2}{c + v_2 - v_1} \qquad p_P = p_2 + (p_1 - p_2) \cdot \frac{v_2}{c + v_2 - v_1}$$

$$c = \sqrt{\frac{\chi \cdot p_1}{\rho_1}}$$

The heat ratio χ can be obtained from the one-dimensional equilibrium (ODE) thermochemistry code. It should be mentioned that all variables are expressed for the combustion products.

7.3 Appropriate Numerical Boundary Conditions[17]

Characteristic boundary conditions are obtained from simultaneous solution of the left and right traveling equations (compatibility equations) with quasi-steady state boundary conditions such as the Bernoulli or the Darcy-Weisbach equation. The left end of the hydraulic segments corresponds to the minimum index i. the right end corresponds to the maximum, respectively. Velocities are defined positive to the right.

7.3.1 Ideal Nozzle at Left End – Tank Inlet

$$v_{i,j} = -c_{i+1,j-1} + c_{i+1,j-1} \cdot \sqrt{1 + \frac{2 \cdot v_{i+1,j-1}}{c_{i+1,j-1}} - \frac{2}{\rho_{i+1,j-1} \cdot c_{i+1,j-1}^2} \cdot \left(p_{i+1,j-1} - p_{tank}\right)} \tag{7-25}$$

$$p_{i,j} = p_{i+1,j-1} + \rho_{i+1,j-1} \cdot c_{i+1,j-1} \cdot \left(v_{i,j} - v_{i+1,j-1}\right) \tag{7-26}$$

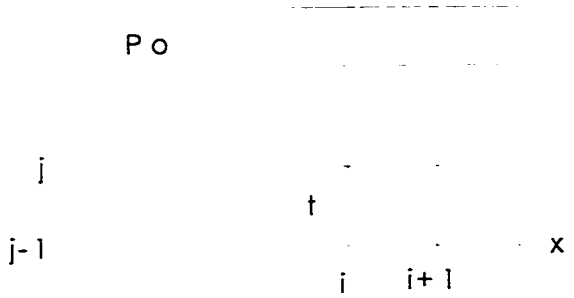

7.3.2 Ideal Nozzle at Right End – Dome Inlet

$$v_{i,j} = c_{i-1,j-1} - c_{i-1,j-1} \cdot \sqrt{1 - \frac{2 \cdot v_{i-1,j-1}}{c_{i-1,j-1}} - \frac{2}{\rho_{i-1,j-1} \cdot c_{i-1,j-1}^2} \cdot \left(p_{i-1,j-1} - p_{tank}\right)} \tag{7-27}$$

$$p_{i,j} = p_{i-1,j-1} - \rho_{i-1,j-1} \cdot c_{i-1,j-1} \cdot \left(v_{i,j} - v_{i-1,j-1}\right) \tag{7-28}$$

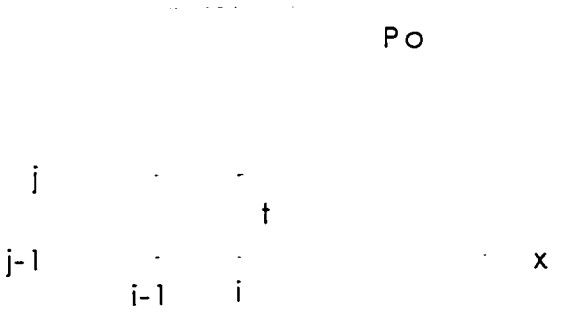

7.3.3 Orifice, Curved Pipe, Filter, Control Valves - Right or Left Flow

Test for direction of flow:

$$p_{i-1,j-1} - p_{i+2,j-1} + \rho_{i-1,j-1} \cdot c_{i-1,j-1} \cdot \left(v_{i-1,j-1} + v_{i+2,j-1}\right) \begin{cases} \geq 0 & \text{rightward} \\ < 0 & \text{leftward} \end{cases} \tag{7-29}$$

$$v_{i,j} = v_{i+1,j} = \begin{Bmatrix} - \\ + \end{Bmatrix} \frac{2 \cdot c_{i-1,j-1}}{K_L} \begin{Bmatrix} + \\ - \end{Bmatrix} \frac{2 \cdot c_{i-1,j-1}}{K_L} \cdot \sqrt{1 \begin{Bmatrix} + \\ - \end{Bmatrix} \frac{2 \cdot c_{i-1,j-1}}{K_L} \cdot \left(v_{i-1,j-1} + v_{i+2,j-1}\right) \begin{Bmatrix} + \\ - \end{Bmatrix} \frac{K_L}{2 \cdot \rho_{i-1,j-1} \cdot c_{i-1,j-1}^2} \cdot \left(p_{i-1,j-1} - p_{i+2,j-1}\right)} \tag{7-30}$$

$$p_{i,j} = p_{i-1,j-1} - \rho_{i-1,j-1} \cdot c_{i-1,j-1} \cdot \left(v_{i,j} - v_{i-1,j-1}\right) \tag{7-31}$$

$$p_{i+1,j} = p_{i+2,j-1} - \rho_{i+2,j-1} \cdot c_{i+1,j-1} \cdot \left(v_{i+1,j} - v_{i+2,j-1}\right) \tag{7-32}$$

In the above equations, the upper sign in the braces reflect a rightward flow, the lower sign for rightward flow.

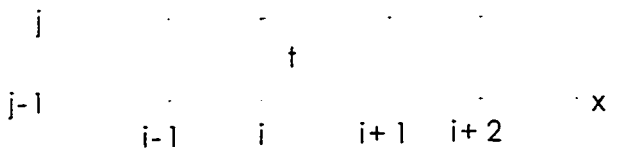

7.3.4 Ideal Pipe Branch Boundary – Manifold, Injection Elements

The ideal multiple branch theory provides a pressure-velocity boundary condition for each branch in a waterhammer analysis. Using Kirchhoff's law that all incoming velocities are negative and all outward velocities are positive from the attachments, the mass conservation for incompressible liquid provides one boundary condition.

$$\sum_{n=1}^{N} A_n \cdot V_n = 0 \tag{7-33}$$

The quasi-steady state pressure-velocity relationship between any two branches can be expressed by the following equation (7-34)

$$p_n - p_m = \left(b_n \cdot v_n^2 + b_m \cdot v_m^2\right) \cdot \frac{\rho}{2} \tag{7-34}$$

where pressure losses due to geometric dimensions are incorporated by the coefficients b_n, and b_m. Generally, dynamic pressure terms are negligible in waterhammer analysis; therefore, another boundary condition is given by equation (7-35).

$$p_1 \approx p_2 \approx .... \approx p_n \approx p_N = p \tag{7-35}$$

In order to obtain appropriate numeric boundary conditions, equations (7-33), (7-34), and (7-35) are substituted with the characteristic equations.

The following two equations can be found for the boundary condition of branches.

$$p = p_{n,j} = \frac{\sum_{n=1}^{N} A_n \cdot \left(p_{n_0,j-1} - \rho \cdot c \cdot v_{n_0,j-1}\right)}{\sum_{n=1}^{N} A_n} \tag{7-36}$$

$$v_{n,j} = v_{n_0,j-1} + \frac{1}{\rho \cdot c}\left(p - p_{n_0,j-1}\right) \tag{7-37}$$

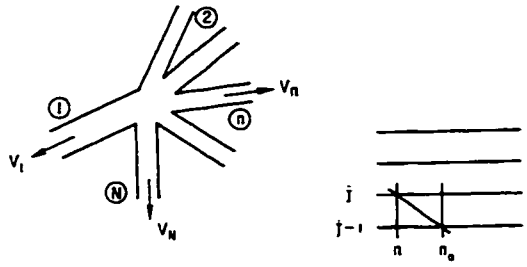

Note: Each velocity component has a positive sign per definition if outward. The subscript n_0 designates the next mesh point with index i+1 outward from the branch in segment n. whereas subscript n is denoted for the boundary mesh point i in each segment n.

Chapter 8: Preliminary Thoughts for the Computer Program

This chapter covers preliminary thoughts for a computer program to govern transient mass flows using the derived equations of this work. The chapter gives a short introduction into programming, followed by thoughts on how the segments can be divided to simulate the filling process of the initially empty pipes.

8.1 Introduction into Programming

Programming solving is not only an art in that it requires a good deal of imagination, ingenuity, and creativity, but it is also a science in that it uses certain techniques and methodologies. The program-development progress can be identified in at least five steps.

1. Problem analysis and specification
2. Data organization and algorithm design
3. Program coding
4. Execution and testing
5. Program maintenance

Only the first two steps are covered in this work. The problem analysis and specification is basically covered in chapters three, four, five, six, and seven. Data organization and algorithm design will be captured within this chapter. The following three steps will be done soon.

The second step can be subdivided into two concurrent steps.

1. Determine how to organize and store the data in the problem
2. Develop procedures to process the data and produce the required output

8.2 Procedure to Cover Transient Filling Process

The used procedure -- Method of Characteristic -- is best applied if the discretization is evenly sized. The prediction of the time steps can be obtained from the stability criterion (7-3).

$$\Delta\tau = \frac{\Delta x}{c}$$

The speed of sound is given from the empirical equations (6-3) and (6-4). The discrete space size can be any appropriate length. It could be seen that the smallest segment should be divided into 10 discrete steps. The other segments are then divided using the given space step size of the smallest segment. Each mesh point therefore obtains a unique number within the entire system. The time step is then calculated from the stability criterion.

The described approach has no drawbacks on liquid filled sections. However, unfilled pipes must be treated differently. Generally speaking, the filling rate is transient throughout the entire start-up phase. Therefore, no actual step size can be predicted. However, the general rule to divide the smallest section into 10 steps should be applied again to simplify matters. Thus, the calculation should include a sub-if construct within the main if construct for filling the discrete space step size.

Moreover, the whole flow process should be calculated as a coupled system to obtain a complete system response. Therefore, a general discretization should look like the one depicted in Figure 8.1.

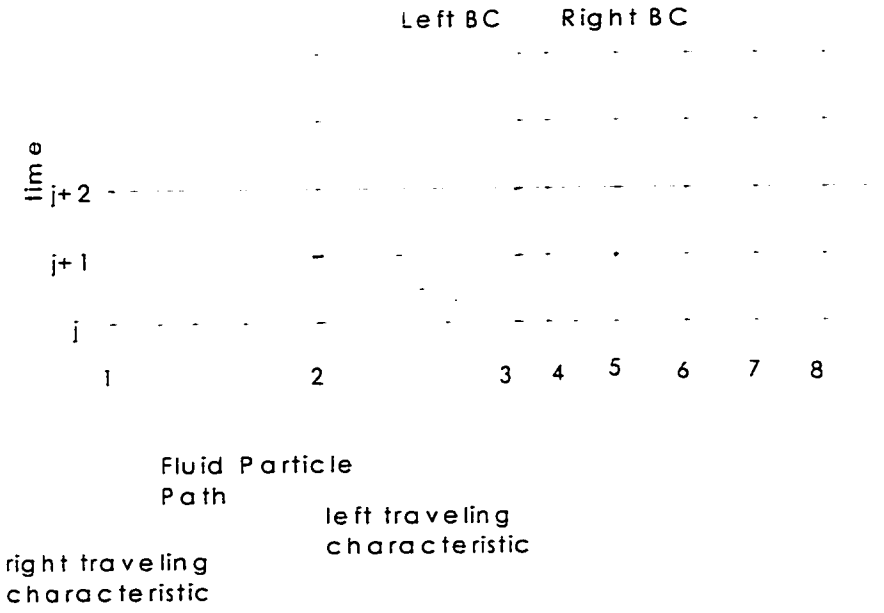

Figure 8.1: General Discretization of Flow Sections

Once the actual sizes of the space steps are determined, the entire system should be numbered. The Figure 8.1 shows the difference between the liquid flow section and the two-phase section expressed by the distinctive slopes of the characteristic lines.

The following Figure 8.2 depicts a small section of figure 8.1 in order to explain the numerical approach of calculating the non filled sections. Firstly, the left boundary condition of the unfilled section is coupled with the right boundary condition of the liquid filled section. At time j, the fluid starts to fill the hydraulic section with two-phase mixture. The mass flow rate of the mixture is determined by the local density, velocity, and area.

$$\dot{m} = \rho \cdot v \cdot A \tag{8-1}$$

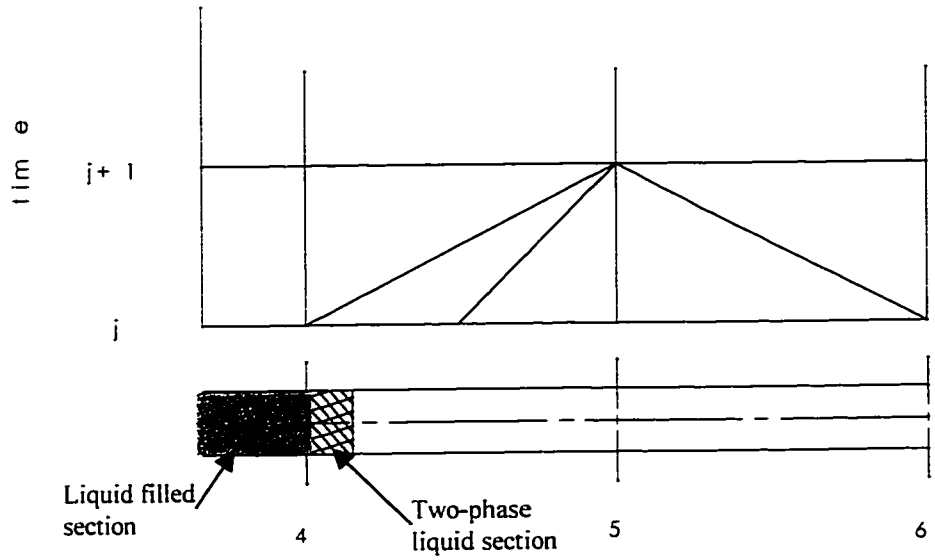

Figure 8.2: Filling Process of Unfilled Sections

The flow section between 4 and 5 is limited from the geometric volume V. Equation (8-1) can be used to find the differential volume of the incoming mixture.

$$dV = v(x,\tau) \cdot A(x) \cdot d\tau \tag{8-2}$$

If dV is smaller than the incremental geometric volume more calculations need to be done until the incoming total volume equals the geometric volume between 4 and 5.

The next step is to decide at what moment the liquid column will enter the section to be filled. The options are that the liquid column will enter when the section is half filled or if the section is completely filled. There may be a possibility to adjust the computer program with time variables.

Chapter 9: Conclusion

This thesis has described a short introduction into rocket science, rocket test facilities, and an approach for calculating transient mass flows in test facility feed lines and rocket engine parts. The approach uses the numerical technique Method of Characteristics for solving the governing partial differential equations for the transient flow phenomena. This paper also includes a combustion chamber model, which is able to calculate moving shocks in the combustion chamber due to ignition of the hypergolic propellants.

The main goal -- to improve the weaknesses of the Diplom thesis Erstellung eines FORTRAN-Programmes zur Simulation des Anfahrverhaltens eines Raketentriebwerks -- could be partially fulfilled. The next steps are to program the computer code, test, qualify, and adjust it to measurement data.

If the program is useable to calculate transient mass flows, additional models should be implemented such as an atomization model of the propellants in the combustion chamber, a more precise flow model through the injection model (using Method of Characteristics), as well as a Fourier Time Expansion Theory for the combustion instability analysis.

The estimation is that the expansion, programming, and qualification of such a program will take at least another 12 months of *Rocket Science Brain-Work*.

References

1 Anderson. J.D.. "Computational Fluid Dynamics," New York, McGraw-Hill. 1995

2 Barrére. M. et al., "Rocket Propulsion," Amsterdam. Elsevier Publishing. 1960

3 Carton. D.S., Maxwell. W.R. and Hurden. D., "Rocket Propulsion Technology Volume I." New York, Plenum Press. 1961

4 Chisholm. D., "Two-Phase Flow in Piplines and Heat Exchangers." Great Britian, Pitman Press. 1983

5 Fischer. J.L., "Combustion Engineers Handbook. Adapted from the Walther-Taschenbuch: translated into English," London. G.Newnes, 1961

6 Forman W.A., "Combustion Theory," London. Addison-Wesley. 1965

7 Gardiner. W.C., "Combustion Chemistry," New York. Springer-Verlag, 1984

8 Gaubatz. W.A. and Webber. W.T., "Calculation of the Ignition and Start Transient of Liquid Propellant Rocket Engines." Pasadena. McDonnell Douglas. 1970

9 Hagerty. R.P. et al., "Combustion and Propulsion." New York. Macmillan. 1963

10 Kakac. S. and Ishii. M.. "Advances in Two-Phase Flow and Heat Transfer Volume I," Bosten. Martinus Nijhoff Publishers. 1963

11 Kakac. S. and Ishii. M., "Advances in Two-Phase Flow and Heat Transfer Volume II." Bosten. Martinus Nijhoff Publishers. 1963

12 Kanmuri. A. et al., "Transient Analysis of LOX/LH2 Rocket Engine (LE-7)." Monterey, AIAA 25th Joint Propulsion Conference. 1989

13 Kit. B. and Evered. D.S., "Rocket Propellant Handbook." New York. Macmillan. 1960

14 Kluger. P. and Farrel. E.C., "Digital Computer Analysis of Transients in Liquid Rocket Engines." Sacramento. Aerojet-General Corp.. 1957

15 Melek-Pahayev, N.I., "Liquid-Propellant Engines," New York. Macmillan. 1962

16 Messerschmid, E., "Grundlagen der Raumfahrtsystem," Stuttgart, University Stuttgart. 1991

17 Moody, F.J., "Introduction to Unsteady Thermofluid Mechanics," New York. John Wiley & Sons. 1990

18 Pashaev. M. and Ivanovich, N. I., "Liquid-Propellant Engines," New York, Macmillan. 1962

19 Penner, S.S. and Ducarme, J., "The Chemistry of Propellants," London. Pergamon Press. 1960

20 Prickett. R.P. et al., "Water Hammer in a Spacecraft Propellant Feed System." Boston. 24th Joint Propulsion Conference. 1988

21 Ring, E., "Rocket Propellant and Pressurization Systems," Englewood Cliffs. New York, Prentice-Hall. 1964

22 Rogers, G.F.C. and Mayhew, Y.R., "Engineering Thermodynamics," Hong Kong, Longman Group. 1980

23 Ruth, E.K. et al., "Advanced Liquid Rocket Engine Transient Model." Orlando. AIAA. 26th Joint Propulsion Conference. 1990

24 Schmidt. G., "Dokumentation zur Vorlesung Technik der Fluessigkeits-Raketentriebwerke." Munich. Daimler Benz Aerospace and University Munich. 1996

25 Strunz. R., "Dimplomarbeit: Erstellung eines FORTRAN-Programmes zur Simulation des Anfahrverhaltens eines Raketentriebwerks." Munich. Daimler Benz Aerospace. 1996

26 Sutton. G.P., "Rocket Propulsion Elements." New York. John Wiley & Sons. 1992

27 Wallis. G.B., "One-Dimensional Two-Phase Flow," New York, McGraw-Hill. 1969

28 Wiech, R.E. and Strauss, R.F., "Fundamentals of Rocket Propulsion," New York. Reinhold Publishing, 1960

29 Wilkins, R.L., "Theoretical Evaluation of Chemical Propellants." New York. Prentice-Hall. 1960

30 Yang, V. and Anderson, W., "Liquid Rocket Engine Combustion Instability," AIAA Volume 169. 1995

Appendix 1: Test Facility Dimension

The complete geometric dimension of the test facility can be seen at the technical drawing of the *Deutsche Forschungs- und Versuchsanstalt fuer Luft- und Raumfahrt e.V.* no. 244.31/0-2. The following figures show some dimensions.

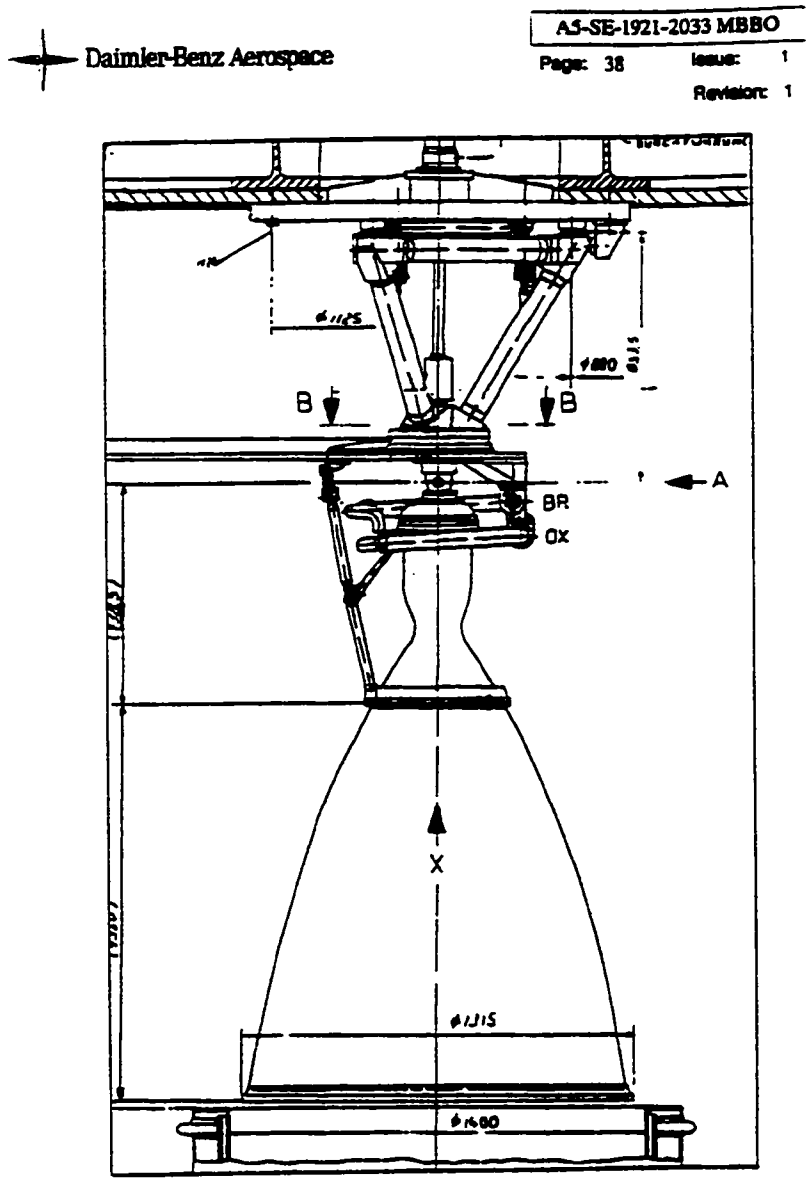

Figure A1.1: Rocket Engine Mounted in the Test Bed[25]

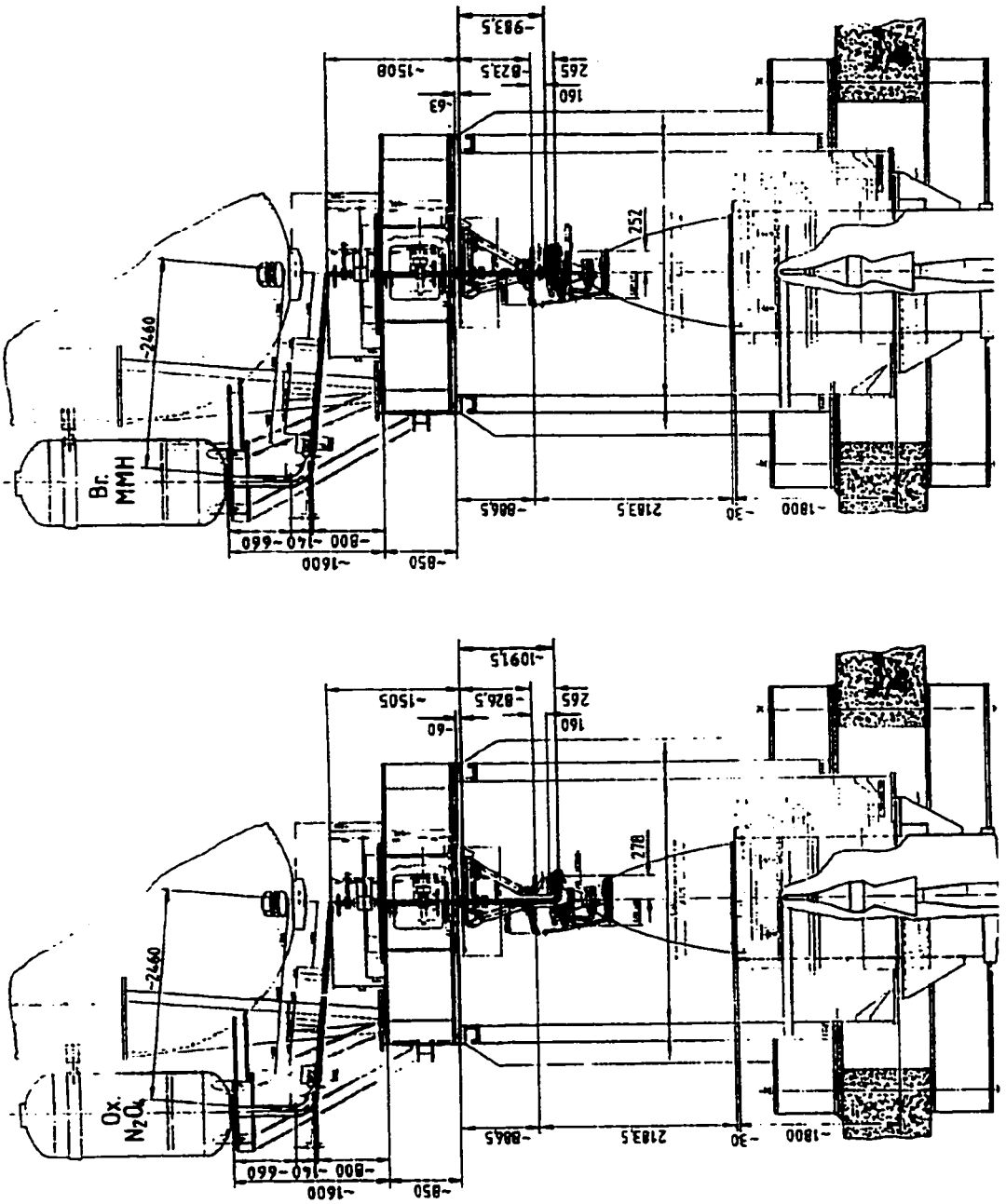

Figure A1.2 (cont'd): Rocket Engine Mounted in the Test Bed[25]

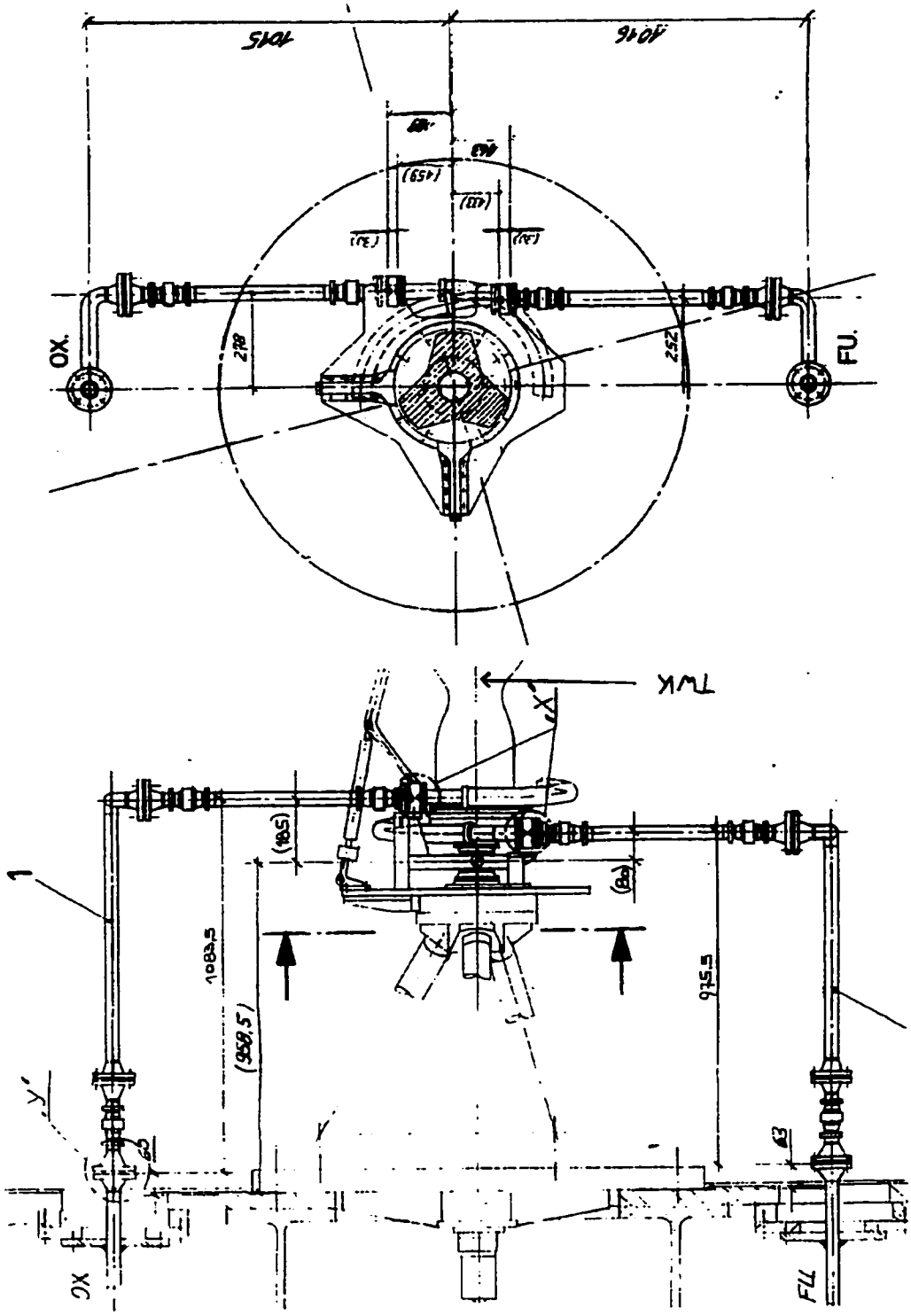

Figure A1.3 (cont'd): Rocket Engine Mounted in the Test Bed[25]

Appendix 2: Performance Data, Geometric Dimensions, and Miscellanies

Performance Data	
Characteristic Velocity	1681 m/s
Combustion Chamber Pressure	10.3 bar
Combustion Efficiency	0.980
Exit Velocity	3168 m/s
Fuel Mass Flow / ignition	5.75 kg/s
Fuel Mass Flow / steady state	2.876 kg/s
Impulse Efficiency	0.926
Injection Element Area (oxygen, fuel)	335.89 mm^2, 264.00 mm^2
Injection Velocity (oxygen, fuel)	12 m/s, 14 m/s
Lateral Forces at ignition	5 kN
Mass Flow Ratio	2.05
Maximum Combustion Chamber Pressure at Ignition (stable combustion)	20 bar
Maximum Nozzle Temperature	1393 K
Maximum Thrust at ignition	50 kN
Nozzle Efficiency	0.945
Oxygen Mass Flow / ignition	8.25 kg/s
Oxygen Mass Flow / steady state	5.896 kg/s
Pressure Loss Calibration Orifice	1.47 bar
Pressure Loss Cooling Channel (fuel)	1.50 bar
Pressure Loss Feed Line (oxygen, fuel)	1.10 bar, 0.50 bar
Pressure Loss Injector (oxygen, fuel)	6.14 bar, 3.63 bar
Propellant Temperature (oxygen, fuel)	293 K
Specific Impulse	323.2 s
Thrust in Vacuum	27.80 kN
Total Mass Flow / ignition	14 kg/s
Total Mass Flow / steady state	8.772 kg/s
Valve sequence	70 ms

Geometric Data	
Mass	122 kg
Dimension (length)	2183.5 mm
Injection Element (amount)	132
Injection System	Coaxial
Number of lateral holes through Sleeve (fuel)	4
Number of Openings at Post (fuel)	10
Nozzle Throat Diameter	136 mm
Cylindrical Combustion Chamber Diameter	210 mm
Nozzle Diameter at Manifold	428.7 mm
Amount of Cooling Channels	184
Width x Height of Cooling Channels Entrance	2.6 mm x 5 mm
Width x Height of Cooling Channels Exit	1.3 mm x 1.84 mm
Total geometric Volume Oxygen (empty sections)	1.3 l
Total geometric Volume Fuel (empty sections)	1.8 l

Miscellanies	
Stored Propellant	9700 kg
Duration of Mission	1100 s
Damping of LF-Oscillations	Pressure Loss at Injector
Damping of HF-Oscillations	Cavity Ring
Diameter of one Cavity Drill	8 mm
Total Area of Cavity Openings	1759.29 mm^2
Amount of Cavity Drills	35 (29 T1-mode: 6 T2-mode)
Re-ignition	yes

Appendix 3: Calculation of Property Data

The following calculation was done to obtain the ratio volumetry expansivity over specific heat at constant pressure for the two phase region of the two propellants:

Reference temperature and gas constants of the propellants

$t := 293 \qquad RN2O4 := 90.354 \qquad RMMH := 180$

Density of the propellants: Liquid Phase

$rhoN2O4(t) := 2066 - 1.979t - 482.6 \cdot 10^{-6} \cdot t \qquad rhoN2O4(293) = 1.486 \cdot 10^{3}$

$rhoMMH(t) := 1.15034 - 9.3949 \cdot 10^{-4} \cdot t \cdot 1000 \qquad rhoMMH(293) = 875.069$

Specific volumes of the liquid propellants

$$vN2O4(t) := \frac{1}{rhoN2O4(t)}$$

$$vMMH(t) := \frac{1}{rhoMMH(t)}$$

Specific enthalpy of the liquid propellants

$$hN2O4(t) := 0.000023364 \left[e^{\frac{t}{100}} \right]^6 - 0.003497105 \left[e^{\frac{t}{100}} \right]^5 + 0.1084437 \left[e^{\frac{t}{100}} \right]^4 + 7.687356 \left[e^{\frac{t}{100}} \right]^3 -$$

$$- 633.01598 \cdot \left[e^{\frac{t}{100}} \right]^2 + 21912.56 \cdot \left[e^{\frac{t}{100}} \right] - 465171.1568$$

$$hMMH(t) := 0.000000903139 t^5 - 0.0017139 t^4 + 1.27899 t^3 - 467.2491 t^2 + 86389.27 t - 5531192.2$$

Saturation Pressure

$$pN2O4(t) := 10^{9.82372 - \frac{2331.98}{t} + \frac{84567}{t^2}} \qquad pN2O4(t) = 707.637$$

$$pMMH(t) := 10^{9.181621 - \frac{1065.025088}{t} - \frac{158905.5445}{t^2}} \qquad pMMH(t) = 4.963 \cdot 10^{3}$$

Specific volumes of the gaseous propellants

$$vN2O4gas(t) := \frac{RN2O4 \cdot t}{pN2O4(t)} \qquad vN2O4gas(t) = 37.411$$

$$vMMHgas(t) := \frac{RMMH \cdot t}{pMMH(t)} \qquad vMMHgas(t) = 10.627$$

Specific enthalpy of the gaseous propellants

$$hN2O4gas(t) := 0.35288t^2 + 591.5763t - 13982.7468 \qquad hN2O4gas(t) = 1.896 \cdot 10^5$$

$$hMMHgas(t) := 1.374545t^2 + 857.3571t - 1664906.14 \qquad hMMHgas(t) = -1.296 \cdot 10^6$$

State Equations of the two-phase mixture

$$vN2O4fg := vN2O4gas(t) - vN2O4(t) \qquad vN2O4fg = 37.411$$

$$vMMHfg := vMMHgas(t) - vMMH(t) \qquad vMMHfg = 10.626$$

$$hN2O4fg := hN2O4gas(t) - hN2O4(t) \qquad hN2O4fg = 4.097 \cdot 10^5$$

$$hMMHfg := hMMHgas(t) - hMMH(t) \qquad hMMHfg = -2.453 \cdot 10^6$$

Mean density of the homogeneous mixture

$x := 0 .. 1$

$$rhomN2O4(x) := \frac{rhoN2O4(t) \cdot \frac{1}{vN2O4gas(t)}}{x \cdot rhoN2O4(t) + \frac{1}{vN2O4gas(t)} \cdot (1 - x)} \qquad rhomN2O4(0.5) = 0.053$$

$$rhoN2O4gas(t) := \frac{1}{vN2O4(t)}$$

$$rhomMMH(x) := \frac{rhoMMH(t) \cdot \frac{1}{vMMHgas(t)}}{x \cdot rhoMMH(t) + \frac{1}{vMMHgas(t)} \cdot (1 - x)} \qquad rhomMMH(.5) = 0.188$$

$$yN2O4(x) := rhomN2O4(x) \cdot \frac{vN2O4fg}{hN2O4fg} \qquad yN2O4(0) = 0.136$$

$$yMMH(x) := rhomMMH(x) \cdot \frac{vMMHfg}{hMMHfg} \qquad yMMH(0) = -3.79 \cdot 10^{-3}$$

Graphs of the relation volumetric expansivity over specific heat at constant pressure

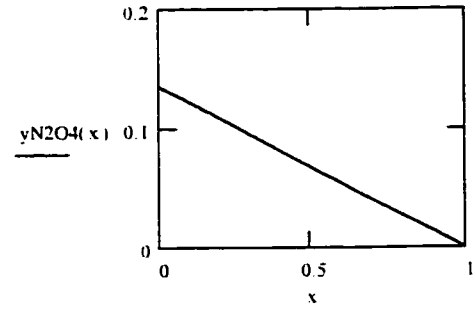

Oxygen

$yN2O4(0.5) = 4.882 \cdot 10^{-6}$

Figure A3.1: Expression 6-37 with respect to the Quality, Oxygen

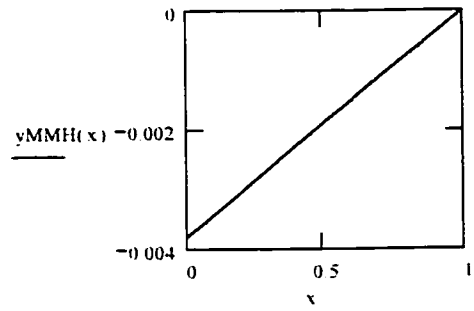

Fuel

$yMMH(0.5) = -8.15 \cdot 10^{-7}$

Figure A3.2: Expression 6-37 with respect to the Quality, Fuel

IMAGE EVALUATION TEST TARGET (QA-3)

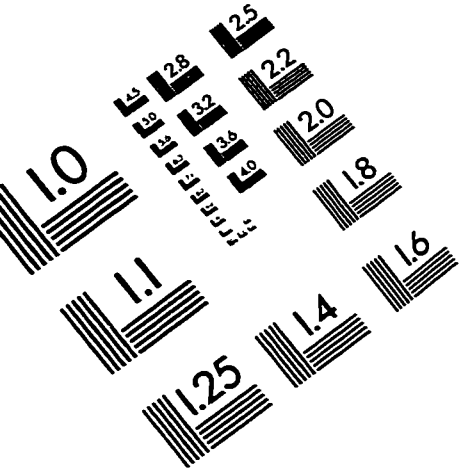

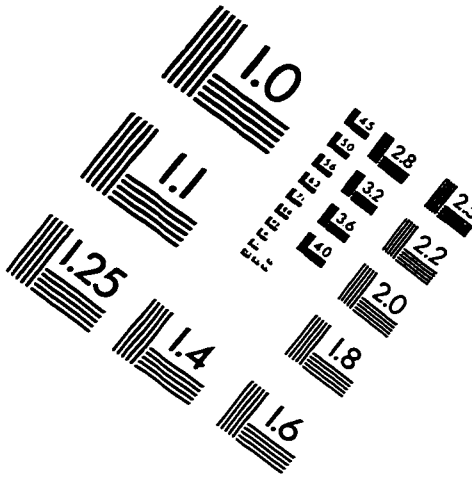

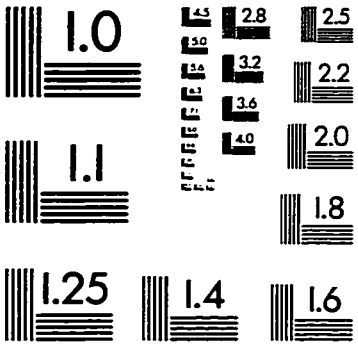

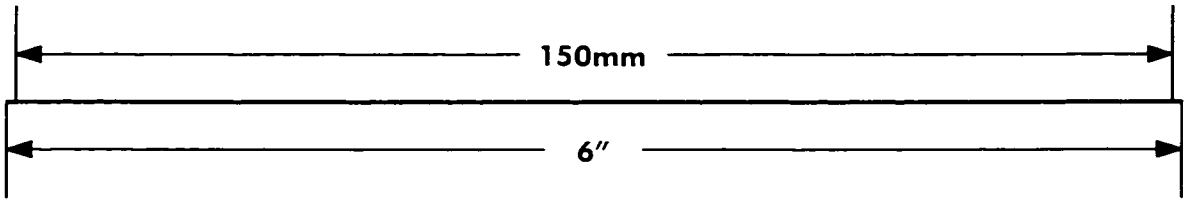

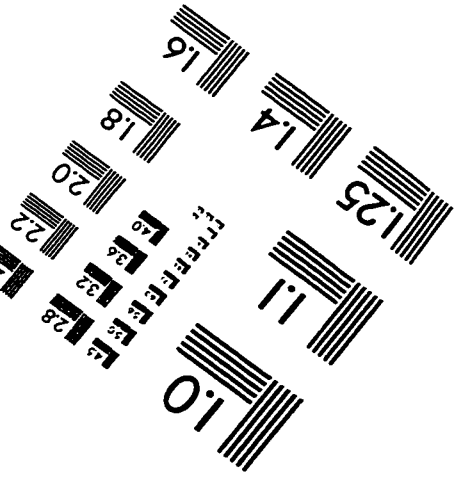

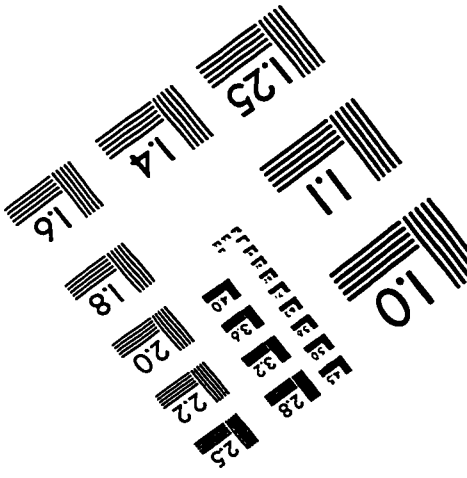

APPLIED IMAGE, Inc
1653 East Main Street
Rochester, NY 14609 USA
Phone: 716/482-0300
Fax: 716/288-5989